Project Code: MQP JRB 0501

Thermal Manikin Testing of Fire Fighter Ensembles

A Major Qualifying Project Report

Submitted to the University of

WORCESTER POLYTECHNIC INSTITUTE

In partial fulfillment of the requirements for the

Degree of Bachelor of Science

By:

_____
Andrew D. Ellison

_____
Timothy M. Groch

_____
Beth A. Higgins

_____
Mark T. Verrochi

Date: April 27, 2006

Approved: _____
Advisor, Professor Jonathan R. Barnett

Abstract

Fire testing criteria was developed for an existing fire fighter clothing evaluation facility designed by previous WPI projects. To accommodate full ensembles, a new manikin suspension system was constructed. Laboratory instrumentation was updated to facilitate refined data collection and allow for additional sensors provided by NCTRF. A series of calibration analyses were conducted on the instrumentation to compare with results from past experiments. Recommendations defining ensemble failure were compiled based on prototype testing of US Navy and Australian protective clothing.

Authorship Page

Section Number	Section Titles	Primary Author
-	Abstract	Group
-	Acknowledgements	Group
-	Authorship Page	Group
-	Table of Contents	Mark
-	List of Figures	Group
-	List of Tables	Group
-	Nomenclature	Group
-	Executive Summary	Tim
1	Introduction	Beth
2	Background	Group
2.1	Navy Clothing and Textile Research Facility	Andrew
2.2	Navy Fire Scenarios	Andrew
2.3	Test Facility	Andrew
2.4	Reproducing Real Fire Conditions	Andrew
2.5	Manikin Data Collection	Andrew
2.6	Fire Fighter Gear	Tim
2.7	Skin and Skin Burns	Beth
2.8	Current Test Methods	Mark
2.9	TPP and RPP Criteria	Beth
3	Methodology	Group
3.1	Updating Laboratory	Mark
3.2	Calibration Device	Group
3.3	Schmidt-Boelter Gauge	Andrew
3.4	Suspension System	Group
3.5	Prototype Testing	Beth
4	Results	Andrew
4.1	Calibration	Beth
4.2	Flame Edge Heat Fluxes	Andrew
4.3	Prototype Tests	Andrew
5	Conclusions	Group
5.1	Test Protocol	Andrew
5.2	Prototype Ensemble Test Evaluation	Mark
5.3	General Recommendations	Mark
6	References	Group
7	Appendices	Group
A	Heat Transfer through Fire Fighter Clothing	Tim
B	Sipe 2004 Sensor Energy Balance	Tim
C	Manikin Suspension Models	Tim
D	Suspension Calculations	Beth
E	Preliminary Tests	Andrew

Acknowledgements

Many people have assisted throughout the duration of this project. Thank you for all of your support and help along the way! The following is a list of people that have aided in the completion of this project:

1. Jonathan Barnett – Project Advisor
2. Harry Winer – Navy Contact
3. Country Fire Authority – Donator
4. Navy Clothing and Textile and Research Facility – Donor
5. Joel Sipe – Advisor on Manikin Testing
6. Kerry Dineen – Lab Assistant
7. Todd Sullivan – Lab Assistant
8. Jim Johnson – Calibration Device Constructor
9. Nathan Rosenblad and Adam Teti – Suspension System Construction Assistants
10. Michael O'Donnell – Suspension System Welder
11. Neil Whitehouse – Suspension System Constructor
12. Siamak Najafi – Computer Technician
13. Randy Robinson – Computer Technician
14. Garry Benoit (North East Region Sales Representative for SurvivAir) – Donor
15. John Merrill (Regional Manager Scott Health and Safety) – Donor
16. George Zinkus and Burt Davis (Massachusetts Fire Academy) – Donor

Table of Contents

Abstract ii
Authorship Page iii
Acknowledgements iv
Table of Contents v
List of Figures vii
List of Tables ix
Nomenclature x
Executive Summary xi
1 Introduction 1
2 Background 3
2.1 Navy Clothing and Textile Research Facility 3
2.2 Navy Fire Scenarios 3
2.3 Test Facility 4
2.4 Reproducing Real Fire Conditions 8
2.5 Manikin Data Collection 10
2.6 Fire Fighter Gear 11
2.6.1 NFPA 1971 12
2.6.2 Components 12
2.6.3 Heat Transfer through Fire Fighter Clothing 17
2.7 Skin and Skin Burns 21
2.7.1 Skin Layers 21
2.7.2 Types of Burns 22
2.7.3 Predicting Skin Burns 24
2.8 Current Test Methods 32
2.8.1 NFPA 2112 33
2.8.2 ASTM F 1930 33
2.8.3 Thermo-Man 35
2.8.4 Pyroman 35
2.8.5 University of Alberta Test 35
2.8.6 RALPH 36
2.8.7 Manikin Pit Test 37
2.9 TPP and RPP Criteria 37
2.9.1 Accuracy of the Testing 38
3 Methodology 39
3.1 Laboratory Preparation 39
3.2 Calibration Device 40
3.2.1 Designing mechanism 40
3.2.2 Brainstorming and Analyzing Design 41
3.2.3 Final Design Selection 41
3.3 Schmidt-Boelter Gauge 42
3.3.1 Calibrating the Schmidt-Boelter Gauge 42
3.3.2 Determining Heat Flux at Flame Edge 43
3.4 Suspension System 43

3.4.1 Original Design 44
3.4.2 Revising Mechanism 45
3.4.3 Analysis of Designs 45
3.4.4 Final Design Selection 47
3.5 Prototype Testing 48
4 Results 51
4.1 Calibration 51
4.2 Flame Edge Heat Fluxes 52
4.2.1 Schmidt-Boelter Gauge Calibration Factor 52
4.2.2 Heat Flux at Flame Edges 56
4.2.3 Heat Flux at Flame Edges 60
4.3 Prototype Tests 64
4.3.1 Australian Ensemble 1 65
4.3.2 Australian Ensemble 2 72
4.3.3 Navy Ensemble 78
5 Conclusions 86
5.1 Test Protocol 86
5.2 Prototype Ensemble Test Evaluation 88
5.3 General Recommendations 88
6 References 91
Appendix A: Heat Transfer through Fire Fighter Clothing 93
Appendix B: Sipe 2004 Sensor Energy Balance 98
Appendix C: Manikin Suspension Models 102
Appendix D: Suspension Calculations 113
Appendix E: Preliminary Tests 125

List of Figures

Figure 2-1 Alden Research Lab Facility 4
Figure 2-2: Copper Slug Sensor Energy Balance (Sipe, 39) 7
Figure 2-3: Burner Configurations (Woodward, 7-8) 9
Figure 2-4 Skin Layers (Sipe, 2004) 21
Figure 2-5 Stoll and Chianta Curve for Second Degree Burns (Sipe, 23) 31
Figure 2-6 Stoll and Chianta Total Energy Absorbed (Sipe, 23) 32
Figure 2-7 Instrumented Manikin in ASTM F 1930 Test Room (Sipe, 27) 34
Figure 3-1: Wiring the Manikin 39
Figure 3-2: Laboratory Computer Station 40
Figure 3-3: Front View of Calibration Device (Design A) 42
Figure 3-4: Existing Support Apparatus 44
Figure 3-5: Sway Bar Behind Manikin 44
Figure 3-6: Suspension System 48
Figure 3-7: Heat Flux Over Distance in Room 49
Figure 4-1: Calibration of New Sensors 51
Figure 4-2: Exposed Heat Flux at Doorway 53
Figure 4-3: Schmidt-Boelter Flux compared to Gardon Flux using Average Calibration Factor Excluding Negative Voltage Values 54
Figure 4-4: Schmidt-Boelter Flux compared to Gardon Flux using Average Calibration Factor Including Negative Voltage Values 54
Figure 4-5: Best Fit Curve 55
Figure 4-6: Calibration Curve for Schmidt Boelter Gauge 56
Figure 4-7: Run #1 at 1.94 MW 56
Figure 4-8: Run #2 at 1.94 MW 57
Figure 4-9: Run #3 at 1.94 MW 57
Figure 4-10: Run #1 at 1.04 MW 58
Figure 4-11: Run #2 at 1.04 MW 58
Figure 4-12: Fire Size of 0.87 MW 59
Figure 4-13: Fire Size of 0.69 MW 59
Figure 4-14: Run #1 at 1.94 MW 60
Figure 4-15: Run #2 at 1.94 MW 61
Figure 4-16: Run #3 at 1.94 MW 61
Figure 4-17: Run #1 at 1.04 MW 62
Figure 4-18: Run #2 at 1.04 MW 62
Figure 4-19: Fire Size of 0.87 MW 63
Figure 4-20: Fire Size of 0.69 MW 63
Figure 4-21: Australian Ensemble 1 Pre-Test 65
Figure 4-22: Australian Ensemble 1 Doorway Run 1 66
Figure 4-23: Australian Ensemble 1 Six Second Exposure Run 1 68
Figure 4-24: Australian Ensemble 1 Six Second Exposure Run 2 68
Figure 4-25: Australian Ensemble 1 Ten Second Exposure Run 1 69
Figure 4-26: Australian Ensemble 1 Ten Second Exposure Run 2 70
Figure 4-27: Australian Ensemble 1 Doorway Test Run 2 71

Figure 4-28: Australian Ensemble 1 Post-Test 72
Figure 4-29: Australian Ensemble 2 Pre-Test 73
Figure 4-30: Australian Ensemble 2 Doorway Run 1 74
Figure 4-31: Australian Ensemble 2 Six Second Exposure Run 1 75
Figure 4-32: Australian Ensemble 2 Ten Second Exposure Top Five Sensors 76
Figure 4-33: Australian Ensemble 2 Ten Second Exposure Second Five Sensors 76
Figure 4-34: Australian Ensemble 2 Skin Burn Locations 77
Figure 4-35: Australian Ensemble 2 Post-Test 78
Figure 4-36: Navy Ensemble Pre-Test 79
Figure 4-37: Navy Ensemble Doorway Run 1 80
Figure 4-38: Navy Ensemble Six Second Exposure Run 1 81
Figure 4-39: Navy Ensemble Six Second Exposure Run 2 81
Figure 4-40: Navy Ensemble Ten Second Exposure Run 1 82
Figure 4-41: Navy Ensemble Ten Second Exposure Run 2 83
Figure 4-42: Navy Ensemble Doorway Exposure Run 2 84
Figure 4-43: Navy Ensemble Post-Test 85

List of Tables

Table 2-1 Skin Properties (SFPE Guide, 10) 28
Table 2-2 Injury Parameter Values (SFPE Guide, 15) 29
Table 2-3 Activation Energy and Pre-Exponential Term (SFPE Guide, 16) 29
Table 2-4 Time to First and Second Degree Burns (SFPE Guide, 16) 30
Table 2-5 Stoll and Chianta (Sipe, 23) 31
Table 2-6 Thermal properties of Human Skin verses Colorceran (Sipe, 31) 36
Table 3-1: Fire Sizes 43
Table 4-1: Gardon Gauge Steady State Heat Fluxes in Doorway 52

Nomenclature

The following is a list of the abbreviations used and their meanings:

AISI – American Iron and Steel Institute
ASTM – American Society for Testing of Materials
CFA – Country Fire Authority
ISO – International Standards Organization
MQP – Major Qualifying Project
NCTRF – Navy Clothing and Textile Research Facility
NFPA – National Fire Protection Association
PBI – polybenzimidazole
PTFE – polytetrafluoroethylene
RALPH – Research Aim Longer Protection Against Heat
RPP – radiant protective performance
SCBA – self contained breathing apparatus
SFPE – Society of Fire Protection Engineers
TBA – total burn area
TBSA – total body surface area
THL – total heat loss
TPP – thermal protective performance
WPI – Worcester Polytechnic Institute

Executive Summary

Fire fighter ensembles are often the only source of protection for rescue workers in severe fire conditions. Garment testing plays a crucial role in predicting gear performance in a variety of thermal conditions. A majority of the current tests utilize only a small sample of material, which can not be used to indicate the behavior of an entire garment. In order to fully understand how well an ensemble will perform, a standardized test must be developed in which entire ensemble (helmet, self contained breathing apparatus (SCBA), jacket, gloves, pants, boots) is tested simultaneously.

A facility was constructed at Alden Research Laboratories in Holden, Massachusetts. This laboratory supported by the Navy Clothing and Textile Research Facility (NCTRF), and is maintained and operated by Worcester Polytechnic Institute (WPI) faculty and students. Past academic projects designed and constructed a modified International Standards Organization (ISO) 9705 room, with a motorized track capable of moving a thermally instrumented manikin through the burn room. Eight square propane sand burners located in the center of the room are able to produce fires of nearly 3.2 MW in size. The original manikin suspension allowed for the application of jackets, pants, gloves, and boots, but did not consider the testing of a helmet and SCBA.

In order to achieve full ensemble testing several aspects of the Holden fire lab needed to be updated. The first task was to update the laboratory's instrumentation. Eight new skin sensors were donated by the NCTRF and installed in addition to the existing 40 copper slug sensors in the manikin. The new sensors were located in areas which typically experience high heat fluxes.

The NCTRF also provided new data acquisition equipment from National Instruments to accommodate the additional sensors. This new equipment required the laboratory computer to be updated to the most recent version of LabView and Windows operating system.

The next step in preparing the lab involved calibrating all of the new thermal sensors. To achieve this, an apparatus was constructed to hold one of the new skin sensors, an old copper slug sensor, and two Gardon gauges. The device was an L-shaped design, with the front face containing four equally spaced holes for each sensor/gauge.

To accomplish full ensemble testing a new suspension for the manikin had to be engineered. The old mechanism was too narrow at the head of the manikin to allow for a helmet, and a vertical stabilizing bar at the manikin's back prohibited the addition of an SCBA unit. The new suspension had to be designed in order to support the manikin fully clothed in fire fighter turn-out gear. Minimal contact points to the manikin were desired to prevent interference during testing.

Before prototype testing began, analysis of the fire had to be conducted to determine what heat fluxes were being produced. The heat flux values were important to compare the collected data to work previously done at the laboratory. A Schmidt-Boelter gauge had been used by previous researchers to gather heat flux data, and was calibrated for use during this project. The gauge was then used to determine the heat flux at the edge of the flames. To do this, the gauge was placed 1.55 m (5ft) into the room, aligning with the front edge of the sand burners. The fire was then set and data was collected to determine the amount of energy produced.

Over ten different designs were considered for the new suspension but a bolted hook approach was chosen. The revised mechanism consists of only a head unit with enough clearance to allow testing with helmets. There is no longer a back piece, as sway is prevented by two secured bolts. The new suspension was installed and proved successful in several full ensemble tests.

With the laboratory ready for testing, a standardized procedure was required such that each test could be replicated for a variety of ensembles. It was determined that for each step in the testing procedure, the manikin would be exposed to a 1.5 MW fire; with runs increasing in severity. First, the manikin would be stationary in the doorway of the burn room and exposed to fire for 30 seconds. This would be a base line test and provide the lowest heat flux exposure of all of the runs. The manikin would then be run through the room at a speed of 0.27 m/s (comparable to six second Dupont Thermo-Man exposure), then repeated. The third test would expose the manikin to the most severe conditions, traversing through the room at 0.16 m/s (comparable to ten second Dupont Thermo-Man exposure), then repeated. The final exposure is a replicate of the doorway run and was done to explore the effects of ensemble deterioration due to fire exposure.

A failure criterion was developed in addition to the testing procedure. Ensembles failure depends on the percent of total body area (TBA) that incurs burns according to Henrique's burn integral. It was determined that if an ensemble permits over ten percent of the total body area to experience second degree burns during any test, the ensemble fails. At this level of injury, a victim must be transferred to a burn clinic for specialized treatment. First degree burns are considered insignificant for tests of this severity and will be ignored.

With the lab prepared, test procedures defined, and failure criteria determined; prototype testing was the next step. The first test was conducted on a traditional United States structural fire fighter suit comprised of a Neoprene 100% Nomex outer shell, Gortex-laminated 100% Nomex moisture barrier, and a 100% Nomex quill thermal liner. The second suit to be tested was a one piece garment donated by the United States Navy, consisting of a Kevlar/Polybenzimidazole (PBI) outer shell, Nomex moisture barrier, and a Kevlar batt thermal liner. The final tests involved two structural fire fighter suits donated by Country Fire Authority (CFA) of Victoria, Australia. The two suits are very different in material composition. The first is a more traditional suit constructed of a Nomex IIIA outer shell, a laminate to Nomex scrim moisture barrier, and a Sonatara E89 thermal barrier. The second Australian suit consists of a 100% Wool shell and a 100% cotton thermal liner and is the current protective clothing worn by fire fighters in Victoria. According to test results, all four ensembles met passing criteria.

1 Introduction

Thermal protective gear is vital to the safety of fire fighters and other personnel who face the threat of fire. However, the performance of thermal protective gear in extreme fire scenarios is not accurately predicted by current standard test methods. To date, the majority of testing consists of subjecting small samples of material to a thermal insult. The flux through the material is measured to determine if it was equivalent to the energy which would cause a second degree burn of human skin. Although useful for comparing products, these small scale tests cannot be extrapolated to accurately portray the behavior of a full fire fighter ensemble under extreme thermal conditions.

Larger scale tests consist of life sized manikins fitted with thermal sensors and fire fighter turnout gear subjected to a thermal insult. American Society for Testing of Materials (ASTM) has published standards to evaluate the results, but the tests do not accurately model fire ground activity. These tests are limited to garments and do not evaluate full ensembles (including helmet, gloves, boots, SCBA). The manikin is in a static position, while a person in a fire situation would be better modeled as a dynamic element. Also, the manikin is exposed to fire jets at prescribed locations, which is also unrealistic.

The United States Navy is concerned with personnel incurring injury during fire fighting or other activities on the fire ground in their facilities. To assess the effectiveness of current gear in protecting against thermal injury, they have expressed interest in developing a new method of testing and failure criteria. With this impetus, WPI students began designing a prototype testing facility. A modified ISO 9705 burn room was constructed in an off campus laboratory. Students developed a track system to support the

manikin and allow it to travel through the burn room at variable speeds. The manikin was equipped with copper slug sensors to determine heat flux felt at its surface. This project focused on updating the laboratory and developing a test procedure and failure criteria for full ensemble testing.

2 Background

2.1 Navy Clothing and Textile Research Facility

The Navy Clothing and Research Facility (NCTRF) is a department of the United States Naval Supply Systems Command, located in Natick, Massachusetts. The organization focuses their efforts on research and development of textiles and materials worn by our nation's military for a variety of scenarios from moisture protection in sailors' dry-suits to materials protecting soldiers from biomedical hazards. This facility's objectives also include the protection of military (and civilian) fire fighters from thermal injuries in fire conditions.

Currently the Navy is restricted to testing fire fighter turnout gear on bench-scale testing apparatus in their facility, leaving all full scale testing to the DuPont Thermo-Man manikin. After research was completed in conjunction with Worcester Polytechnic Institute, the NCTRF devoted funds to developing a full-scale thermal/flammability testing facility that could accurately recreate fires that may occur on board US Navy vessels. This facility is located in Holden, Massachusetts and is operated by WPI students and faculty.

2.2 Navy Fire Scenarios

In 1998, David LeBlanc conducted research to determine the types of fires that fire fighters would likely encounter on naval vessels and how they may differ from those experienced by land fire fighters. This research was done to determine if current test

methods accurately simulate shipboard fires, and if not, what modifications to the tests must be made.

LeBlanc analyzed possible fire scenarios in the engine room, berthing or supply areas, and on the deck using computer models and hand calculations. After thorough investigation of these scenarios he determined that the majority of fires on board naval vessels would be so severe that no protective clothing would survive (LeBlanc, 62). He focused his research on fires that were controllable; where fire fighters might find themselves working (LeBlanc, 62). His final conclusions determined that the clothing test methods in 1998 did not accurately reflect fire scenarios that might be experienced by fire fighters, and therefore testing methods should be revised (LeBlanc, 62).

2.3 Test Facility

A few years later, the NCTRF appropriated funds to sponsor a facility that would model these types of fires. This facility was built at Alden Research Labs in Holden, Massachusetts, and was designed/constructed by WPI students (Figure 2-1). The design was focused on producing a test facility that can accurately portray naval shipboard fires. During design, Fay considered the use of a robotic manikin in the future; although this concept was not a reality at the time of construction (Fay, 40).

Figure 2-1 Alden Research Lab Facility

The facility took shape as a modified ISO 9705 room. The modifications were necessary to allow an instrumented manikin to travel through the burn room, while a large enough fire was burning to produce the required fire conditions. The track system allows the manikin to be supported from the ceiling of the room, minimizing unwanted thermal interference by a support structure. Additional burners allows the typical fire size in an ISO 9705 room (approximately 200 kW) to increase to over 3 MW after adding a fuel vaporizer (Fay, 42). This was important because in current test methods fire fighter turnout gear is tested at heat fluxes near 84 kW/m^2 which requires a fire size of nearly 1.5 MW in this facility (Fay, 41, 75). The vaporizer is included to provide the fuel at a steady flow and pressure, which results in higher and more consistent heat release rates at the burners (Fay, 42).

Finally, a second doorway in the rear of the room allows for the manikin to completely pass through the burn room, without having to stop its motion. In order to allow for faster cooling of the burn room after fire tests were completed, the remainder of the short walls (around the doorways) are hinged at the room corners. This allows test personnel to provide more ventilation to the room and expedite the cooling process

The burners used in the lab are one foot square sand burners. They were fabricated in the WPI machine shop and their design is based on the ISO 9705 room burner configuration. In order to provide adequate fuel to these burners, four 100 lb propane tanks are stored on site. All four tanks are connected in parallel and provide fuel for the burn room simultaneously. The fuel flow is governed by a Teledyne Hastings HFC-308 digital mass flow controller (Barter et al, 46). The controller uses a laptop

running a user interface where laboratory personnel can dial exactly what flow rate is desired with near instantaneous results.

The flow controller allows the maximum actual fire size to reach 1.6 MW, although the controller has the potential to produce fires up to approximately 3 MW. An additional control panel with quarter turn valves is still used to turn on and off the flows to the individual burners, and to assist in controlled ignition.

In order to collect and evacuate all products of combustion from the burn room a ventilation system was constructed and a high-powered blower was rented. This system includes two ten foot square hoods centered above both doorways to the burn room.

A track and motor mechanism carries the manikin through the fire. A 0.75 horsepower variable frequency drive motor powers the track (Barter et al, 47). This mechanism allows the speed of the manikin to be dialed in on a controller, and limits the jerk that the manikin experiences while accelerating and decelerating.

The facility includes an instrumented manikin that arrived with sensors in place, but the majority of the sensors were broken and unusable (Sipe, 34). Sipe began researching new sensors for the manikin, based on the following design characteristics:

1. The sensors must be inexpensive
2. The sensors must be easy to fabricate or readily available for purchase.
3. The sensors need to be accurate within ±10% when reading incident fluxes.
4. The sensors must be durable, and able to withstand repeated tests.
5. The sensors should be comparable to human skin.
6. The sensors need to record incident heat fluxes of 0-20 kW/m^2 (Sipe, 36).

With these requirements, and due to budgetary constraints, Sipe determined that the best choice for sensors in the lab are copper slug sensors, although there are more accurate sensors available (Sipe, 104).

The sensors were designed as copper 110 alloy disks about the size of a penny set in thermoset polymers (Sipe, 38). The size was chosen to allow the slugs to fit in the old sensor's housings and therefore fit in the manikin. On the unexposed side of each sensor a bead thermocouple was glued. Inside the housing, a small air gap exists between the thermocouple and the back edge of the housing (see Figure 2-2). The thermocouple is wired to a National Instruments data acquisition board and temperature readings are monitored continuously. Finally, the incident faces of the copper slugs are painted black so the sensors act as black body absorbers (Sipe, 38-42).

The temperature reading from each thermocouple can be used to calculate the incident heat flux on the sensor using a simple energy balance. Figure 2-2 demonstrates the energy transfer through the device visually, and the derived energy balance equations can be found from Sipe's 2004 work and repeated in Appendix B. These calculations require differential equation calculations in order to determine the incident heat flux on the device.

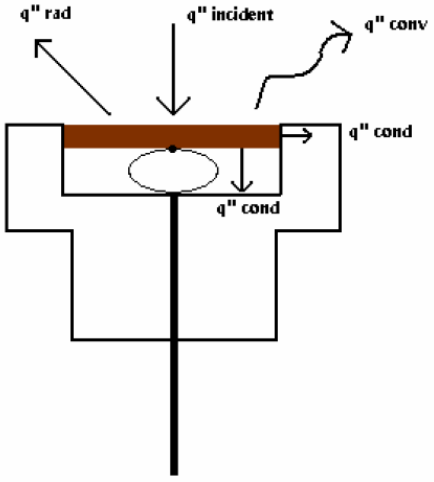

Figure 2-2: Copper Slug Sensor Energy Balance (Sipe, 39)

Forty sensors were manufactured and installed in various locations on the manikin (Sipe, 54). These locations were determined to provide the most body surface area

coverage. Sipe determined that the best balance between computer data acquisition limitations and calculation accuracy resulted in thermocouple sample readings being taken at 4 Hz (Sipe, 57).

2.4 Reproducing Real Fire Conditions

Based on the fires identified by LeBlanc in 1998, Fay ran various initial tests on the apparatus. These tests recorded baseline functions of the apparatus. It was determined that the original design and configuration (as of 2002) was capable of creating fires in excess of 2 MW (Fay, 79). Data was gathered on 1 MW fires to determine what fluxes an instrumented manikin would be exposed to in the facility at this burn rate. Fay determined that a 1 MW fire would produce heat fluxes of at least 80 kW/m^2 at a height ranging from 0.71 m to 1.1 m (Fay, 75). Fay also determined that this range can be widened by increasing the mass flow rate to the burners (Fay, 79).

Next, Woodward took over research in the laboratory. He focused his research on determining what be the effects of different burner configurations representing different fire scenarios. His scenarios can be seen in Figure 2-3 and included the following:

Configuration A: Original configuration designed to apply an even distribution of flames over the manikin's surface.
Configuration B: Provide "intense radiation" to the manikin, while limiting the flame impingement on the material.
Configuration C: Considered the worst possible scenario, this design created flashover conditions in the lower doorway after 90 seconds.
Configuration D: Used to represent wild fire scenarios with low flame heights, approximately waist high.

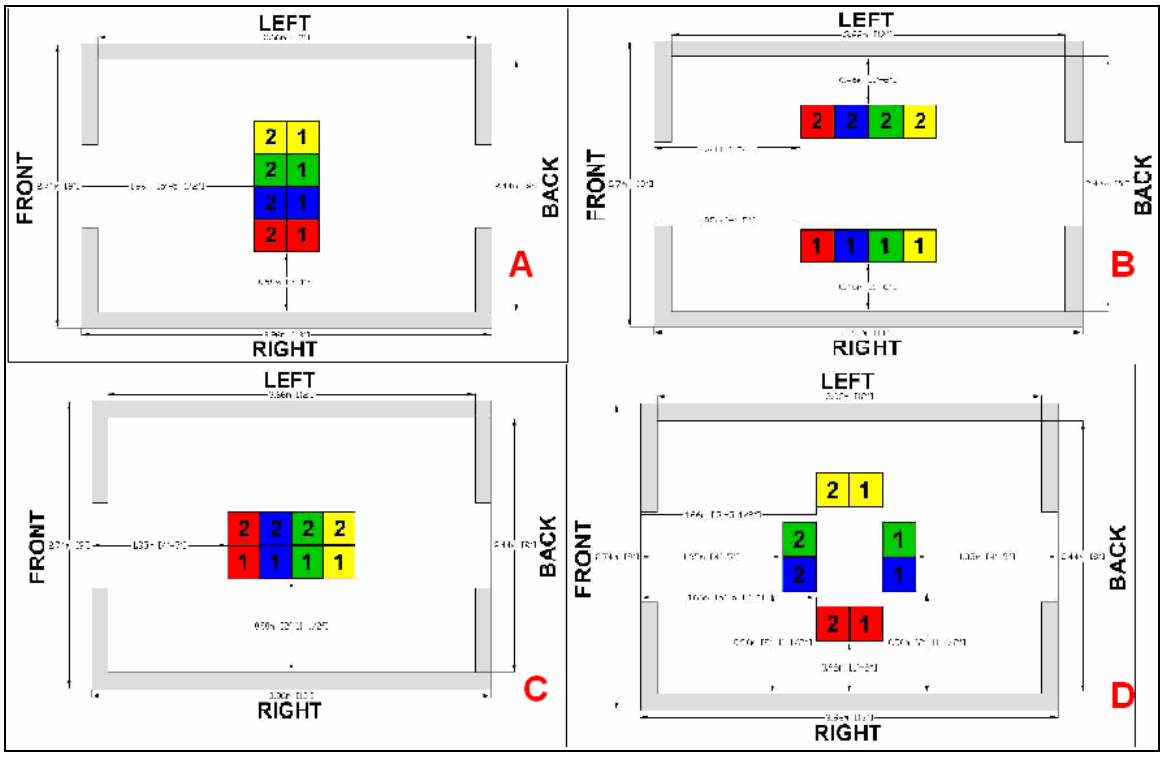

Figure 2-3: Burner Configurations (Woodward, 7-8)

Woodward constructed these various configurations and then measured the heat flux on the centerline of the flame using a Schmidt-Boelter gauge fixed to the end of a steel pipe (Woodward, 11). Because the Schmidt-Boelter gauge is a constant temperature referencing device, a water cooling system was designed within the pipe to deliver a constant temperature water source (Woodward, 12).

The next step for Woodward was to measure temperature at various locations within the burn room. He developed and constructed a makeshift thermocouple tree using steel piping and wooden support structures outside the burn rooms (Woodward, 14). He measured temperature at six different elevations within the room, and three different horizontal locations (Woodward, 14).

Both the heat flux and temperature data was recorded in the area where the manikin's sensors are expected to be during the tests. This is why thermocouple data was

only recorded within the door widths, and the heat flux measurement was designed to determine maximum incident heat flux on the clothing during the test.

After recording this data, Woodward compared the results for the different fire scenarios. In his final conclusions, he determined that configurations A and C had the potential to expose the suit to the 84 kW/m^2, with A producing the most repeatable results (Woodward, 56). He also noted that there is an issue when testing in cooler ambient conditions. When the ambient temperature approaches zero degrees Celsius, the pressure within the propane tanks drops too low to allow for appropriate fuel flow through the system, this then causes deviations in fire sizes (Woodward, 61).

2.5 Manikin Data Collection

Sipe used two different testing procedures to collect data. One method measured the heat flux upon the unclothed manikin outside of the fire room, located at eight and nine feet from the centerline of the burners to allow for the thermal shield (Sipe, 63). Gardon gauges, installed in the manikin's torso gave heat flux results with a close relationship to those of the sensors. The second method involved the manikin traversing through a 1.5 MW fire (comparable to Woodward's fire size) while outfitted with fire resistant clothing.

From the tests in the doorway, Sipe reported that the largest heat flux obtained was 6.3 kW/m^2 at eight feet and 4.5 kW/m^2 at nine feet (Sipe, 72). Since these flux values are so low, it was determined that this testing scenario would be best used to simulate fire conditions for non-fire fighting personnel such as people witnessing a fire.

From the tests through the fire, the manikin had maximum heat flux readings of between 40 and 50 kW/m^2 (bare-skinned, fast moving). These values are still much lower

than the Thermo-Man test. There was a possibility; however, that these low readings were due to the lag in the sensors calculating flux data, and the limited exposure time (Sipe, 85). Since the manikin was being exposed to the fire so quickly, the sensors may not have had enough time to accurately heat up to record precise readings. For the moving tests where the manikin was wearing PBI coveralls, the maximum heat fluxes recorded were of the order of 2.5 kW/m^2 (Sipe, 89). Finally, with the FR cotton coveralls, the manikin was exposed to approximately 73 kW/m^2 wearing FR cotton (Sipe, 93). This value, under "protective" clothing was surprising. It was determined that on the slowest speed setting, 0.55 ft/s, the manikin would have had first degree burns on 73% of its body (Sipe, 94). These results showed that the sensors can, in fact, be used to determine skin burn criteria under protective clothing.

After conducting this experimental work, Sipe determined that the sensors and manikin test procedures, are, in fact, appropriate for determining skin burn potential in fire scenarios for a manikin wearing fire protective garments.

2.6 Fire Fighter Gear

Fire fighters are exposed to extreme environments; subject to intense temperatures and other life threatening hazards. Often the only protection from the dangerously high heat flux exposures is the gear rescue workers wear. These garments must be able to provide a barrier that will protect the sensitive skin lying beneath it. Without proper equipment and technology, a fire fighter could sustain serious burns of life threatening injury.

2.6.1 NFPA 1971

National Fire Protection Association (NFPA) 1971 Standard on Protective Ensemble for Structural Fire Fighting 2000 Edition lists standards and specifies the minimal design, performance, and certification requirements for structural fire fighter ensembles. This code also describes the proper testing methods for protective gear; including coats, pants, jumpsuits, helmets, gloves, and footwear. For more information on such testing, see Section 2.8. The standard is considered for all new designs, manufacturing, and certifications of fire fighter clothing. The code does not apply to fire gear manufactured before or in accordance with previous NFPA standards. The most current edition of NFPA 1971 is the 2000 version which is scheduled for revision in 2006.

General requirements set by NFPA 1971 for fire fighter ensembles include requirements that all fabrics and stitching used in the clothing are flame resistant, and all protective materials must not melt or drip. The flame resistance should be a permanent quality of the garment, and must not be affected by everyday use or laundering. The specifications for material strength and shrinkage are also clearly defined in this standard (NFPA, 2000).

2.6.2 Components

Typical firefighting jackets and pants are usually comprised of three main layers. The exterior layer, or the outer shell, is exposed to most of the physical abuse and thermal insult. The middle layer is the moisture barrier, which protects the thermal liner. The thermal liner is in direct contact with the fire fighters' skin, and is the main protection from burns.

Outer Shell

The outer shell is the first layer of protection provided by the ensemble. The materials used in this layer are designed to come in direct contact with flame and heat, without degrading or burning. These materials must be durable in order to keep up with the extreme wear and tear associated with fire fighting. Outer shells are usually treated with water resistant finishes, but most of the moisture protection is provided by the middle layer. The following are examples of materials used in outer shell design.

Nomex® IIIA

Nomex® IIIA is a type of nylon material manufactured by DuPont and commonly used in shell construction. This material has very high tensile strength which protects against tearing and provides strong resistance to heat (degrading at 480ºC). Nomex® is also light and inexpensive as well as durable (DuPont, 2002).

Advance®

Advance® is a combination of Nomex® and Kevlar®, another fire resistant polymer manufactured by DuPont. Advance® is light material that offers higher thermal resistance (rated for 570°C), abrasion resistance, and water resistance than Nomex® alone. This fabric is affordable, and is longer lasting and more durable than most outer shell materials (DuPont, 2002).

Basofil®

Basofil® is a combination of 40% Basofil® and 60% Kevlar®. This is one of the newest outer shell fabrics, which, unlike most shell materials, is able to be manufactured

in just about any color. Basofil® performs well across a large range of heat fluxes, and will not fail until 590ºC. This material is heavy compared to other shell fabrics, but its thermal characteristics permit the use of lighter liner materials (DuPont, 2002).

Mellenia®

Mellenia® is a high-end outer shell fabric and is the newest technology currently available. This fabric maintains durability and thermal resistance (does not degrade at temperature in excess of 700°C), while being light weight and very flexible (Globe, 2006).

PBI®

PBI® has been used in outer shell construction for over a decade and is still one of the most widely used materials today. This fabric is able to withstand intense temperatures (withstands temperatures in excess of 700ºC) and physical abuse. PBI® is light weight and flexible, as well as cost effective (Globe, 2006).

Moisture Barriers

The moisture barrier is the middle layer that is often never seen by the user, but is perhaps the most important fabric in the construction. The main purpose of this layer is to keep the thermal liner dry, so that the insulating ability of the liner is not compromised by highly conductive moisture. This layer is comprised of materials that are water proof and breathable, allowing heat and moisture to escape, but not penetrate. The effectiveness of the moisture barrier is measured by the amount of energy allowed to pass through it, or the total heat loss (THL).

Microporous

Microporous barriers consist of tiny passages that allow air and moisture to pass through the material. This material is available in hydrophilic (water accepting), hydrophobic (water repelling), or in combination. Microporous barriers are constructed from both polytetrafluoroethylene (PTFE) and polyurethane bases.

Monolithic

Monolithic barriers have a continuous coating that does not permit the flow of air or water vapor. A breathable form of this material is available, allowing the transmission of fluids only by molecular diffusion. These barriers come with a neoprene coating which is not breathable compared to polyurethane based and polyester based.

Bi-Component

This technology combines both the monolithic and microporous forms and is considered superior to both because it combines the benefits of both materials.

Crosstech®-W.L. Gore

Crosstech® is a high grade polyurethane barrier. It is tough and durable; able to maintain superior performance after long term use and laundering. Crosstech® offers the highest thermal resistance of any moisture barrier; withstanding temperature of 260°C for five minutes (Globe, 2006).

RT7100-W.L. Gore

RT7100 is a less expensive version of the Crosstech® moisture barrier. This technology performs as well as high-end polyurethane barriers, but lacks thermal stability and long life (Globe, 2006).

Stedair 3000®-Stedfast

Stedair 3000® is the newest technology applied to moisture barriers. In addition to the normal moisture barrier properties, this layer protects against battery acid, chlorinated water, gasoline, and hydraulic fluids. These hazardous materials are commonly encountered by fire fighters during emergencies (Globe, 2006).

Thermal Liners

The thermal liner account for approximately 75% of the thermal protection provided by all three layers; and insulates the user from conduction, convection, and radiant heat. This layer must be able to provide thermal protection, comfort on the users' skin, and moisture management (Globe, 2006). Thermal liners are required by current standards to be permanently sewn-in or detachable by buttons (Southern Mills, 2006).

The thermal liner consists of two main components; a non-woven batting and the face cloth. The face cloth is the potion that comes in contact with the user's skin, and is typically constructed of a woven lining fabric such as Nomex® or fire retardant cotton. This material is quilted or laminated to a non-woven thermal insulator. The thermal resistance is provided by the insulators fibers and the air gaps within the batting. Most thermal battings are constructed of Nomex®/Kevlar® blends (WFR, 2006).

Caldura®-S. L. Platinum

Caldura® is a lightweight thermal liner including a Nomex® face cloth. This liner allows free movement, excellent air permeability, and dries faster than any other thermal liners (Globe, 2006).

Synergy®- 2-Layer Basofil® Quilt

This thermal liner is constructed of two layers of Basofil® quilt for maximum thermal protection. This material is lightweight, flexible, and highly insulative (Globe, 2006).

Aralite® Quilt

Aralite® Quilt utilizes manipulated Kevlar® fibers to produce a lightweight thermal liner with excellent performance. This technology is inexpensive and superior to most thermal liners (Globe, 2006).

2.6.3 Heat Transfer through Fire Fighter Clothing

Heat transfer analysis of fire fighter clothing is necessary to understand the protective properties of ensemble materials. Radiation is the primary mode of heat transfer in a fire scenario, but energy can enter the clothing by localized flame contact exposures. These types of thermal insults can cause heat stresses and/or thermal decay of ensemble components. Skin burns are the most severe result of radiant heat transfer, and the insulative properties of turnout gear are the only source of protection for rescue workers. (Mell and Lawson, 10)

This phenomenon must be carefully modeled in order to predict clothing performance in real world fire situations. In most cases, skin burns occur when little to no deterioration of the protective material is present. Damage to the clothing will certainly result in diminished performance, but less obvious factors can also greatly affect heat transfer through the equipment (Mell and Lawson, 1). Perspiration and water contained within a garment act as conductors of heat, and are also capable of storing energy within the layers of clothing. Scalding or steam burns can occur when trapped moisture becomes heated and begins to evaporate. If gear is compressed against the skin, burns may result because the insulative protection provided by air gaps within the materials is removed. (Mell and Lawson, 3)

The National Institute of Standards and Technology (NIST) developed two tests to predict heat transfer through fire fighter gear. The first test utilizes an apparatus that exposes material specimens to radiant heat and direct flame contact. Thermocouples are placed on and within the testing samples, and temperatures are recorded continuously throughout the experiment. The second tool used by NIST involves an analytical computer model that outputs specific information on the energy transfer occurring through the clothing. The details and calculations for heat transfer through protective clothing can be found in Appendix D. (Mell and Lawson, 3)

Manufacturers

There are many manufactures of fire fighter clothing located through the world. Three major producers of high end fire garments are Globe Manufacturing Company, Fire-Dex, and Lion Apparel Incorporated.

Globe Manufacturing Company is a major producer of fire fighter clothing. Globe began in 1887, and today is one of the leading fire gear producers in the world. Globe was the first company to patent a three layer suit comprised of an outer shell, moisture barrier, and thermal liner. This layout is still the core design for fire suits being manufactured around the world (Globe, 2006).

Fire-Dex began as a manufacturer of welding gloves, and then evolved into a producer of fire fighter protective clothing. Fire-Dex is one the four largest manufacturers of fire gear in the United States, having filled single orders of up to 19,000 jackets; the largest sale on record. Fire-Dex manufactures a wide variety of protective clothing such as custom turnout gear; aluminized proximity gear, emergency response uniforms, and NFPA approved hoods and gloves (Fire-Dex, 2006).

Lion Apparel has been in business for over 100 years, producing clothing for safety personnel worldwide. This company supplies protective clothing to the United States Army Corps of Engineers, United States Marine Corps, and the German Armed Forces (Lion Apparel Incorporated, 2006).

Structural Firefighting

Structural firefighting is the most common form of fighting. Fire fighters must face many fire scenarios within different types of structures such as two story homes, high rises, and commercial properties. Also, fire fighters run the risk of being exposed to hazardous materials such as flammable liquid spills and explosions. The primary purpose of structural fire fighters is to conduct search and rescue operation in a burning construction and to control and suppress the fire. Other responsibilities of a structural fire

fighter involve hazardous materials incident management, motor vehicle accident extrication, and occasional brush fire management.

All these emergency situations require that a structural fire firefighter's protective clothing be durable, comfortable, and water resistant. A fire fighter's primary tool is water; whether sprayed from hoses, vehicles, or structural protection systems exposing them to large amounts of moisture daily. Any protective clothing must repel moisture from the fire fighter's skin, in order to prevent skin burns. Also, the clothing must protect against a variety of dangers including radiant heat, flame exposure, and limited hazardous materials exposure. Structural fire fighters wear the protective clothing described in Section 2.6.2.

Wildland Fire Fighting

Wildland fire fighters manage fires that take place outside, often in the forest or brush. These types of rescue workers often encounter very large fires, which can spread at great velocities. These firefighters must work long shifts (measured in days or weeks, not hours such as structural firefighters) in dry, hot weather conditions. The difference between wildfire fighters and their structural counterparts is that wildfire fighters are not exposed directly to fire conditions under normal circumstances, but the risk of such condition does exist. Wildland fire fighters wear clothing that is made up of only the outer shell to protect against limited radiant and flame impingement, as well as to allow the wearer to maintain cool temperatures. This clothing is described in Section 2.6.2.

2.7 Skin and Skin Burns

2.7.1 Skin Layers

The skin is the single largest organ of the human body acting as a protective barrier against bacteria and disease as well as a cooling and insulating mechanism for the body. The skin is typically broken down into three main layers: the epidermis, dermis, and subcutaneous tissue (as shown in Figure 2-4).

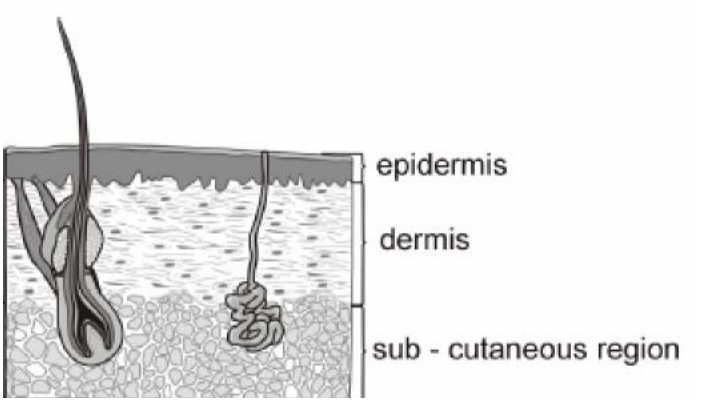

Figure 2-4 Skin Layers (Sipe, 2004)

The epidermis is the topmost layer of the skin and is typically between 75 and 150 μm in depth. The basal layer of the epidermis is responsible for producing new cells to replace the dead cells outer layer.

Below the epidermis, the dermis is between one and four millimeters thick and contains the vascular, nervous, lymphatic structures, and the hair follicles (SFPE Guide 2). Generally, when thermal damage extends beyond the hair follicle depth, cells can no longer be regenerated. (SFPE Guide, 3)

The final layer is subcutaneous tissue composed mostly of fat and connective tissue, but also blood vessels and nerves. The fat plays an important role in regulating the temperature of the body by acting as an insulator.

2.7.2 Types of Burns

Skin burns are evaluated by ranking the level to which the skin has been damaged. Several scales exist to evaluate skin burns and the most common is to rank by first, second, or third degree.

Superficial (First Degree)

First degree burns are appropriately the most superficial. The thermal damage in this case only affects the epidermis. The physical signs of a first degree burns include redness and some pain, but no blistering. The epidermis will flake and peel as it heals and the dead cells are replaced with those generated in the basal layer.

Partial Thickness (Second Degree)

A second degree burn occurs when the epidermis is destroyed at the burn location. A superficial second degree burn does not damage the dermis. If the dermis is damaged, the trauma is considered a deep second degree burn. Physically, the skin will appear red, blistered, moist, and will be painful. A pale white color will appear under the blisters if the burn is deep.

Full Thickness (Third Degree)

Third degree burns occur when both the epidermis and dermis suffer complete necrosis. This burn extends below the hair follicle depth. Damage may also penetrate the subcutaneous tissue. The skin is unable regenerate on its own, and will appear gray in color, charred, and have a leathery texture. The victim will often have no feeling at the burn site.

Fourth Degree and Beyond

Although it is common to discuss first, second, and third degree burns exclusively, the rating system does extend to a sixth degree. Fourth degree burns are those which require skin grafts to heal the patient. Fifth degree burns are those in which the muscle is damaged. Sixth degree burns damage the bone.

Rating System Inadequacies

The degree rating scale is criticized for lacking a direct correlation between the initial appearance of the skin and the actual depth of injury, which is the most reliable indicator of burn severity. The appearance of the skin can be misleading in certain circumstances and the burn degree can be misdiagnosed. (SFPE Guide, 4)

University of Rochester Grading System

In an attempt to rectify this rating issue, an alternate system was developed by the University of Rochester. The ratings run from 0-5 based on the appearance and the depth of the burn, but was later modified to a rating of 0-10 which also accounted for changes in the cells to classify the damage. Although this guide is more thorough, the traditional degree rating is more widely accepted and will be used. (SFPE Guide 4)

Medical Community Ratings

If a burn victim sustains a serious enough burn, they must be transferred to a specialized treatment facility called the burn unit. The attending medical staff will make the determination whether to send the victim to the burn unit based on the following criteria:

- "Partial thickness burns greater than 10% total body surface area (TBSA)
- Burns that involve the face, hands, feet, genitalia, perineum, or major joints
- Third-degree burns in any age group
- Electrical burns, including lightning injury
- Chemical burns, Inhalation injury
- Burn injury in patients with preexisting medical disorders that could complicate management, prolong recovery, or affect mortality
- Any patients with burns and concomitant trauma (such as fractures) in which the burn injury poses the greatest risk of morbidity or mortality. In such cases, if the trauma poses the greater immediate risk, the patient may be initially stabilized in a trauma center before being transferred to a burn unit. Physician judgment will be necessary in such situations and should be in concert with the regional medical control plan and triage protocols.
- Burned children in hospitals without qualified personnel or equipment for the care of children
- Burn injury in patients who will require special social, emotional, or long-term rehabilitative intervention" (American Burn Association, 1999)

Percentage of total body area (TBA) is calculated using the 'rule of nines.' In this system, each of the following is 9% TBA on an adult: head, front chest, front stomach, front of leg, back of leg, arm, top of back, and back abdomen. Genitals are 1% TBA. (eMedicine, 2005)

2.7.3 Predicting Skin Burns

Normal human skin maintains temperature around 32.5˚C and begins to burn when it is raised above 44˚C. The following methods consider radiation as the only thermal insult and neglects conduction or convection. They model skin based on the assumption that it is under a constant thermal insult, is opaque, has a 32.5˚C starting temperature, and is a semi-infinite solid. (SFPE Guide, 7)

Time to Pain

Pain is often the first indicator that skin damage is occurring. The human skin has pain receptors at a depth of approximately 0.1 mm, varying by individual and by location

on the body. Experimental data have determined that, on average, “threshold pain” occurs when the temperature at the pain receptors reaches 45˚C and instantaneous destruction of the skin occurs at a temperature of 72˚C Time is therefore a serious factor in the degree of damage from thermal radiation. (SFPE Guide, 8)

Skin continues to incur damage even as it is cooling. In low level thermal exposures, up to 10% of skin damage occurs while the skin is cooling. In high level thermal exposures 35% of the damage may occur during the cooling period. (SFPE Guide, 12)

These considerations are very important when discussing fire fighters. By the time a fire fighter feels pain in a fire situation, he/she is likely to be in a high temperature environment. The time it takes to remove himself from the fire, remove the thermal protective gear, and cool his skin could be enough to result in serious injury. The time to pain can be calculated using Equation 1. The time to pain is completely dependent on the heat flux, with the minimum heat flux needed to feel any pain of 1.7 kW/m^2. (SFPE Guide, 8)

$$t_p = \left(\frac{35000}{\dot{q}''} \right)^{1.33}$$ **(Equation 1)**

For a heat flux of 6 kW/m^2 or less, a factor of safety of two is used (meaning multiply (1) by 0.5) and for a flux of more than 6 kW/m^2, the factor of safety is four.

Time to Blister

Blisters occur during superficial second-degree burns when the epidermis separates from the dermis at the basal layer, around 80μm below skin’s surface.

Experimental data has also determined how long it takes for blisters to form (see Equation 2 where tb is time to blister).

$$t_b = 300\left(\frac{\dot{q}''}{1000}\right)^{-1.46}$$ **(Equation 2)**

The recommended factor of safety for predicting the time to blister is 1.5 and is based on the available experimental data. (SFPE Guide, 9)

Skin Temperature over Time

There are four algorithms for measuring skin temperature over time when the thermal insult is a "square wave pulse of radiant energy" (SFPE Guide, 12). The first model, Equation 3, assumes skin is a single layer, opaque, semi-infinite solid and ignores sweating and other complex skin properties. It does not take into account cooling and will only predict the time to pain (time when the temperature at 80μm is 44ºC). Table 2-1 shows the variables from these equations, their meaning, and their values.

$$T = T_o + \frac{\dot{q}''_r}{k}\left[\frac{2\sqrt{\alpha t}}{\sqrt{\pi}}\exp\left(-\frac{x^2}{4\alpha t}\right) - x\,erfc\left(\frac{x}{2\sqrt{\alpha t}}\right)\right]$$ **(Equation 3)**

At the skin's surface, Equation 3 reduces to Equation 4.

$$T_s = T_o + \frac{2\dot{q}''_r\sqrt{t}}{\sqrt{\pi k\rho c}}$$ **(Equation 4)**

The recommended factor of safety for this model is 2. (SFPE Guide, 12)

As mentioned previously, cooling time plays a major role in predicting burns. The following three algorithms all account for cooling time. The first algorithm is Equation 5.

$$T = T_o + \frac{2\dot{q}''_r}{\sqrt{k\rho c}} + \left[\sqrt{\tau}\, ierfc\left(\frac{x}{2\sqrt{\alpha t}} \right) - \sqrt{t-\tau}\, ierfc\left(\frac{x}{2\sqrt{\alpha(t-\tau)}} \right) S(t) \right]$$

(Equation 5)

Through manipulation using the error function and its integral, Equation 6, Equation 5 can be manipulated into Equation 7, becoming the third algorithm.

$$erfc\beta = 1 - erf\beta$$

$$ierfc\beta = \frac{1}{\sqrt{\pi}} e^{-\beta^2} - \beta erfc\beta$$

(Equation 6)

$$T(t_2) = T_o + \left[T(t_1) - T_o \right] \sqrt{\frac{t_1}{t_1}} + \frac{\left[\dot{q}''_r(t_2) + \dot{q}''_r(t_2) \right](t_2 - t_1)}{2\sqrt{\frac{k\rho c t_2}{\pi}}}$$

(Equation 7)

Despite addressing the cooling effect of thermal insult on the skin, Equation 7 is not recommended for use in predicting skin burns because it does not take depth into account. This algorithm can only predict surface temperatures. Since we know that second degree burns, and thus blisters, begin when the temperature at 80μm reaches 44ºC, depth is crucial for predicting burns. The preceding equations also ignore the fact that the thermal conductivity of the skin is different during heating than it is during cooling. Far from being useless, however, the surface temperature-time models are used in equations predicting epidermal injury. (SFPE guide 13)

Table 2-1 Skin Properties (SFPE Guide, 10)

Property	Symbol	Value	Units
Thermal Conductivity (heating)	k_h	0.5878	W/m-K
Thermal Conductivity (cooling)	k_c	0.4518	W/m-K
Volumetric Heat Capacity	ρc	4,186,800	J/m^3-K
Activation Energy (44°C ≤ T ≤ 50°C)	ΔE	7.78×10^8	J/kmol
Activation Energy (T > 50°C)	ΔE	3.27×10^8	J/kmol
Pre-Exponential (44°C ≤ T ≤ 50°C)	P	2.185×10^{124}	1/s
Pre-Exponential (T > 50°C)	P	1.823×10^{51}	1/s
Epidermal Thickness (Bayer Layer Depth)	x_b	80	μm
Pain Receptor Depth	x_p	100	μm
Initial Skin Temperature	T_0	32.5	°C

Epidermal Thermal Damage Models

Henrique's Damage Integral

This model predicts the rate of injury to the epidermis based on an experimentally determined activation energy ΔE and pre-exponential term P. Equation 8 is Henrique's damage integral.

$$\frac{d\Omega}{dt} = P\exp\left(\frac{-\Delta E}{RT}\right) \quad \textbf{(Equation 8)}$$

An injury parameter, Ω, is obtained by integrating Equation 8 to get Equation 9:

$$\Omega = \int_0^t P\exp\left(\frac{-\Delta E}{RT}\right)dt \quad \textbf{(Equation 9)}$$

where:
Ω = quantitative measure of burn damage
P = pre-exponential term determined from experimental data, s^{-1}
e = natural exponential = 2.7183
E = the activation energy for skin, J/mol (see Table 2-1)
R = the universal gas constant, 8.315 J/kmol * K
T = absolute temperature at the appropriate skin layer, K
t = the time for which the skin is above 44 °C.

This parameter can then be easily translated into injury level using Table 2-2. (SFPE Guide, 15)

Table 2-2 Injury Parameter Values (SFPE Guide, 15)

Injury Parameter Value (Ω)	Level of Injury
0.53	First Degree Burn
1.0	Superficial Second Degree Burn

In using this same burn integral, scientists have determined many different values for the activation energy and pre-exponential term. Table 2-3 shows these values.

Table 2-3 Activation Energy and Pre-Exponential Term (SFPE Guide, 16)

Model	Temperature Range °C	Activation Energy, ΔE j/kmol	Pre-Exponential, P 1/sec
Weaver and Stoll	44≤T≤50	$7.78*10^{8}$	$2.185*10^{124}$
	T>50	$3.25*10^{8}$	$1.83*10^{51}$
Fugitt	44≤T≤55	$6.97*10^{8}$	$3.1*10^{98}$
	T>55	$2.96*10^{8}$	$5.0*10^{45}$
Takata	44≤T≤50	$4.18*10^{8}$	$4.322*10^{64}$
	T>50	$6.69*10^{8}$	$9.389*10^{104}$
Wu	44≤T≤53	$6.27*10^{8}$	$3.1*10^{98}$
	T>53	$6.27*10^{8}-5.10*10^{5}(T-53)$	$3.1*10^{98}$
Henriques	All Temps	$6.27*10^{8}$	$3.1*10^{98}$
Diller and Klutke	44≤T≤52	$6.04*10^{8}$	$1.3*10^{95}$
Mehta and Wong	All Temps	$4.68*10^{8}$	$1.43*10^{72}$
Torvi and Dale	44≤T≤50	$7.82*10^{8}$	$2.185*10^{124}$
	T>50	$3.27*10^{8}$	$1.83*10^{51}$

With these varying parameters, the times to reach first or second degree burns (Ω = 0.53 and 1 respectively) also vary as shown in Table 2-4.

Table 2-4 Time to First and Second Degree Burns (SFPE Guide, 16)

Irradiance	Weaver & Stoll	Fugitt	Takata	Wu	Henriques	Diller & Klutke	Mehta & Wong
kW/m^2	Sec	Sec	Sec	Sec	Sec	Sec	Sec
Ω = 0.53							
4	43	65	68	62	63	59	58
7	17	26	25	24	24	23	23
10	9.7	15	14	13	13	13	13
15	5.4	7.8	6.8	6.5	6.7	6.5	6.7
20	3.4	5.1	4.1	3.8	4.1	3.7	3.9
30	1.9	2.7	2.1	1.9	2.1	2.0	2.0
40	1.2	1.7	1.4	1.2	1.2	1.2	1.6
50	0.9	1.2	0.9	0.9	0.9	0.9	0.9
Ω = 1.0							
4	47	72	72	66	69	64	64
7	19	29	27	24	26	25	25
10	11	17	15	13	14	13	14
15	5.9	8.7	7.2	6.2	6.7	6.6	7.4
20	3.8	5.6	4.4	3.9	4.3	4.2	4.7
30	2.1	3	2.2	2.1	2.2	2.2	2.6
40	1.4	1.9	1.5	1.2	1.4	1.4	1.5
50	0.9	1.4	1	0.9	0.9	0.9	1.1

For prediction of second degree burns, the values of Weaver and Stoll are the most accurate when compared with experimental data. (SFPE Guide, 17)

Stoll and Chianta Curve

Stoll and Chianta developed a method to predict time to second degree burns based on experimental observations. Charting the temperature rise with heat flux of a copper slug, according to ASTM E 457-96, Stoll and Chianta created a simplified means of determining whether a second degree burn would occur (Sipe, 22). When the Stoll and Chianta curve (see Figure 2-5) is overlaid with the results of any copper slug subjected to a square wave thermal insult, the intersection point is where a second degree burn would occur (Sipe, 22). The values of this curve are in Table 2-5. The total energy absorbed is seen in Figure 2-6.

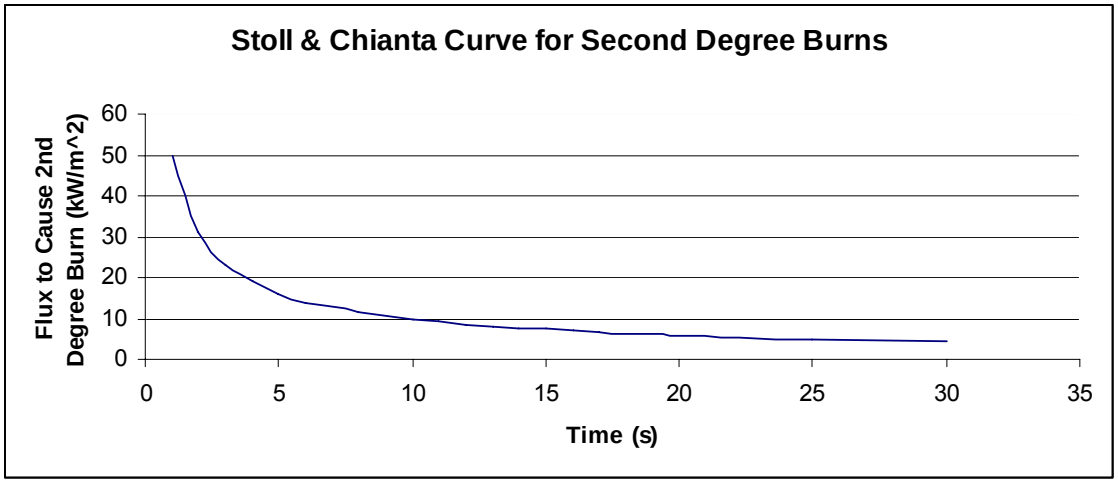

Figure 2-5 Stoll and Chianta Curve for Second Degree Burns (Sipe, 23)

Time	Heat Flux to Cause 2nd Deg Burn		Total Energy Absorbed		Calorimeter Equivalent Temp Rise	
	cal/cm^2*s	kW/m^2	cal/cm^2	kJ/m^2	Def F	Deg C
1	1.2	50	1.20	50	16.0	8.9
2	0.73	31	1.46	61	19.5	10.8
3	0.55	23	1.65	69	22.0	12.2
4	0.45	19	1.80	75	24.0	13.3
5	0.38	16	1.90	80	25.3	14.1
6	0.34	14	2.04	85	27.2	15.1
7	0.30	13	2.10	88	28.0	15.5
8	0.274	11.5	2.19	92	29.2	16.2
9	0.252	10.6	2.27	95	30.2	16.8
10	0.233	9.8	2.33	98	31.1	17.3
11	0.219	9.2	2.41	101	32.1	17.8
12	0.205	8.6	2.46	103	32.8	18.2
13	0.194	8.1	2.52	106	33.6	18.7
14	0.184	7.7	2.58	108	34.3	19.1
15	0.177	7.4	2.66	111	35.4	19.7
16	0.168	7.0	2.69	113	35.8	19.8
17	0.160	6.7	2.72	114	36.3	20.2
18	0.154	6.4	2.77	116	37.0	20.6
19	0.148	6.2	2.81	118	37.5	20.8
20	0.143	6.0	2.86	120	38.1	21.2
25	0.122	5.1	3.05	128	40.7	22.6
30	0.107	4.5	3.21	134	42.8	23.8

Table 2-5 Stoll and Chianta (Sipe, 23)

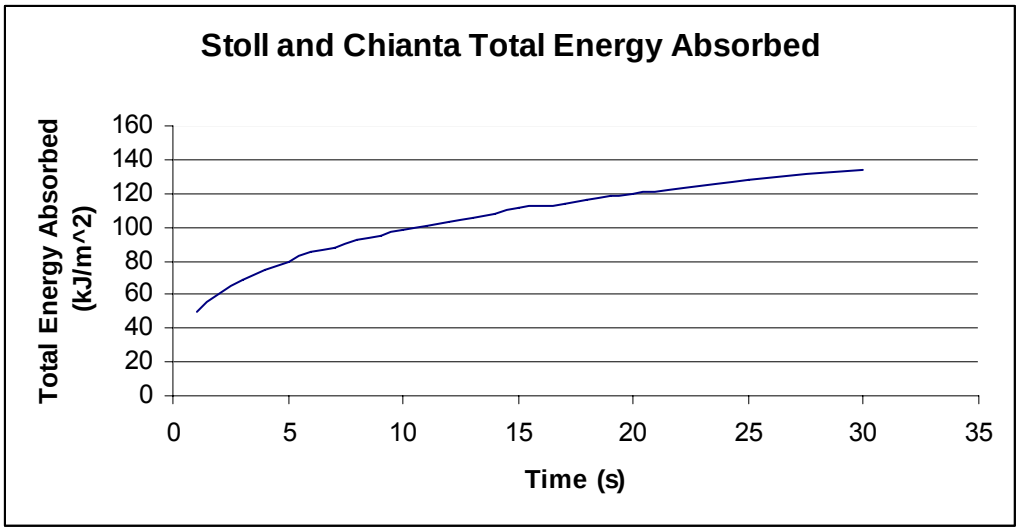

Figure 2-6 Stoll and Chianta Total Energy Absorbed (Sipe, 23)

2.8 Current Test Methods

Evaluating the thermal performance of clothing can be broken down into two categories. These two types consist of small scale tests and large scale tests. Small scale tests (also sometimes referred to as bench test scale) are completed using partial samples of garments for testing. Small scale test methods for fire fighter clothing are outlined in detail in many standards including NFPA 1971 Standard on Protective Ensemble for Structural Fire Fighting 2000 Edition and NFPA 1977 Standard on Protective Clothing and Equipment for Wildland Fire Fighting 2005 Edition.

Small scale testing is an inexpensive way to assess the fabric's level of protection; however, the test has many disadvantages. Materials are located in an apparatus and oriented in a manner that is not representative of normal application of the equipment. The level of protection of an entire piece of clothing constructed form the fabrics tested can not be extrapolated from testing. This is because in each small scale test, materials are tested statically and dry, which are not accurate representations of garments in real fire scenarios.

Large scale tests involve dressing a life size manikin with fire fighter clothing and exposing the manikin to a fire environment. An entire ensemble can be tested rather than just a small piece of material. Since the focus is being placed on full ensemble testing, a series of existing large scale tests are reviewed. The existing tests that are discussed include NFPA 2112, ASTM F 1930, Thermo-Man, Pyroman, University of Alberta Test, Manikin Pit Test, RALPH, and the Robotic Manikin.

2.8.1 NFPA 2112

One standard that the NFPA published addressing a manikin test is NFPA 2112 Standard on Flame-Resistant Garments for Protection of Industrial Personnel against Flash Fire 2001 Edition (NFPA 2112). Chapter 8.5 of this standard discusses a manikin test in compliance with ASTM F 1930 (see Section 2.8.2). The manikin test is to occur in accordance with ASTM F 1930 using an exposed heat flux of 84 kW/m^2 with an exposure time of three seconds. The percent of total body burn is reported as the body burn rating (for three specimens) and the average predicted body burn rating is then used to determine pass/fail performance for garment fabrics (NFPA 2112).

2.8.2 ASTM F 1930

The ASTM Standard Test Method for Evaluation of Flame Resistant Clothing for Protection against Flash Fire Simulations using an Instrumental Manikin, ASTM F 1930, describes a simulated flashover environment around a manikin. The manikin is composed of a thermally stable, flame resistant, non-metallic material. It has 100 heat flux sensors which are located throughout the body (except the hands and feet). The heat flux sensors must be able to measure and withstand a heat flux from zero to 167 kW/m^2, which is the

maximum heat flux exposed to the manikin if not dressed in fire protective clothing (ASTM F 1930).

Figure 2-7 shows the manikin in the test room specified in ASTM F 1930. The chamber is 7.0 feet by 7.0 feet by 8.0 feet and the manikin is located in the center to obtain a uniform heat flux across his body. The induced air combustion industrial style propane burners shown in the picture (six of the eight visible) are located at the height of the manikin's hips and knees in all four corners of the room produce a simulation of a flash fire. The fuel from these burners must provide a uniform heat flux of at least 84 kW/m^2 over a minimum exposure time of five seconds (Sipe, 27).

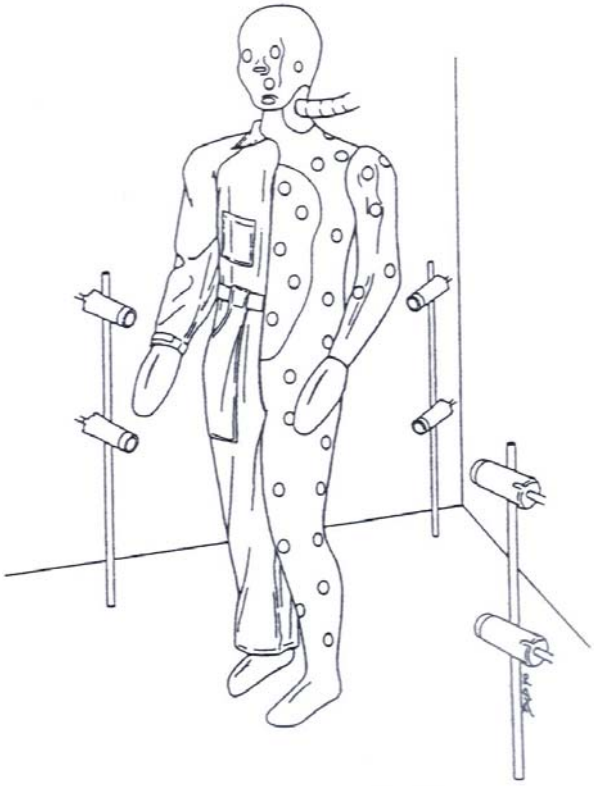

Figure 2-7 Instrumented Manikin in ASTM F 1930 Test Room (Sipe, 27)

From this test, the total percentage of second and third degree burns are recorded using Henrique's burn integral. The standard deviation of each sensor is also calculated to determine the uniformity of the heat flux. After the test, a map of a person can be

generated to show the degree of burn faced by each section of the body using the correlated data from the skin burn results.

2.8.3 Thermo-Man

The DuPont Thermo-Man test is very similar to ASTM F 1930. The manikin is six feet, one inch tall with 122 heat sensors used to measure protective performance of clothing under realistic flash fire conditions. The primary use of this manikin is to evaluate the extent of thermal protection properties of DuPont garments, specifically Nomex (Sipe, 23).

2.8.4 Pyroman

The Center for Research on Textile Protection and Comfort at North Carolina State University conducts a manikin test similar to that of the DuPont Thermo-Man test. The total heat flux is obtained from transducers located on the manikin with and without protective clothing. Heat transferred through the test material is measured and used to predict skin response and burn damage (Sipe, 29).

2.8.5 University of Alberta Test

The University of Alberta uses a fiberglass manikin for their tests. The manikin consists of 110 skin simulant sensors made of an inorganic material known as Colorceran. This material (commonly found product used for making chemistry lab benches) is made from calcium, aluminum, silicate, asbestos fibers, and a binder. Table 2-6 shows the material properties of Colorceran compared to human skin. The material does not have similar density, thermal conductivity, or specific heat values as skin.

However, the product of those three values (the thermal diffusivity) does have a close value to that of skin (Sipe, 30).

Table 2-6 Thermal properties of Human Skin verses Colorceran (Sipe, 31)

Property	Human Skin		Skin Simulant
	Epidermis	Dermis	
k (W/m*K)	0.255	0.523	0.97
ρ (kg/m^3)	1200	1200	1877
c (J/kg*K)	3598	3222	1205
kρc (J^2/m^4*°C^2*s)	1.1*10^6	2.0 *10^6	2.2*10^6
√ kρc (J/m^2*°C*s$^{1/2}$)	1050	1414	1483

The sensors of this manikin model the heat flux into the Colorceran and temperatures are measured by flat thermocouples attached by an epoxy-phenolic adhesive to the surface of the manikin. Once the sensors are installed on the manikin, the entire manikin is painted with black, high temperature paint. Heat flux can be calculated because the temperature at the skin surface and the properties of the skin simulant are known. Burn damage to the skin is predicted from this test using the Henriques burn damage integral (Sipe, 31).

2.8.6 RALPH

Research Aim Longer Protection Against Heat (RALPH) is a heat sensing manikin test developed at Fire Technology Services in Altrincham, Cheshire, England. RALPH is used to evaluate the heat transfer performance of full size garment systems when subjected to flash fire conditions. A ‘sister’ manikin Sophie was also developed at Fire Technology Services and commissioned in 2005. Both manikins test personal protection equipment ensembles.

RALPH has a total of 56 sensors on the torso, legs, and arms (representing 80 percent of the manikin body) which monitor the temperature on the manikin surface during testing. These temperatures can be used to determine burn predictions that occur

through the clothing. During a test, the manikin is exposed to two burner setups to represent flash fire conditions on the manikin with a mean heat flux level of 80 kW/m2 (Healey and Eaton).

2.8.7 Manikin Pit Test

The NCTRF modified the ASTM F 1930 test by placing the manikin on a boom and dynamically moving the manikin through a fire. This modification is known as the manikin pit test. In this test, heat exposure is created by burning a Heptane pool fire that is capable of up to 84 kW/m^2. The manikin is propelled along a track at a calculated velocity that results in a desired exposure time. The data obtained during this test can be used to observe the development of skin burns as a function of time (Fay, 17).

2.9 TPP and RPP Criteria

The NFPA requires that fire fighter gear meet a minimum thermal resistance rating. For structural fire fighters, this resistance is a Thermal Protective Performance (TPP) rating and for Wildland Firefighting is a Radiant Protective Performance (RPP) rating (NFPA 1971).

Based on the Stoll and Chianta curve, these tests deal with a 6" by 6"samples (3" by 10" for Wildland gear) from a fire fighter ensemble be exposed to radiative heat (NFPA 1971). The structural gear is exposed to 83 kW/m^2 and Wildland gear is exposed to 21 kW/m^2 (NFPA 1971) from a constant heat source. A copper calorimeter is placed next to the fabric and temperature measurements taken. These measurements are then compared to the Stoll and Chianta curve to determine where they cross (NFPA 1971).

The time to burn value is then multiplied by the incident heat flux to obtain the total energy absorbed and determine the TPP or RPP value (NFPA 1971). The TPP must be 1450 kJ/m^2 or greater to be acceptable for a structural ensemble and the RPP must not be less than 290 kJ/m^2 to be approved as Wildland firefighting gear (NFPA 1971).

2.9.1 Accuracy of the Testing

There are several issues with the existing testing. First is that the sensors have much different properties than human skin (Gagnon, 2). The testing ignores the effect of water on or absorbed in the suit and the compression caused by a fire fighter's movement, both of which increases the heat transfer. The test also does not take into effect the clothing layer cooling while still on the skin. The predictions are based on a constant square wave incident heat pulse on bare skin (Gagnon, 18). The result of these assumptions and neglecting may be that second degree burns occur earlier than the current tests predict.

3 Methodology

3.1 Laboratory Preparation

Before data collection could begin, the lab needed to be updated for testing. This involved cleaning the facility, repairing older equipment, and implementing the new equipment from the United States Navy. The following paragraphs are an overview of the steps taken to make the lab ready for testing.

Once the lab was organized, maintenance on the equipment was required. The sensors on the manikin were tested to ensure they were functioning properly and any wiring problems were repaired. Poor connections were soldered or secured with electrical clips. The new sensors, provided by the United States Navy, were wired from the computer to the manikin similar to the existing sensors (Figure 3-1).

Figure 3-1: Wiring the Manikin

Another issue that had to be addressed was the piping system used to provide the propane to the burners from the tanks. Many leaks were found and were repaired before propane could be used in the system. Some of the connections required additional Teflon tape to provide for a tighter seal and prevent leaks from occurring.

The NCTRF provided more recent additions of current hardware to be used with the LabView program for collecting data. To accommodate the hardware update, LabView 7.1 and Windows XP were installed. The virtual instrument program (VI) in LabView had to be rewritten to work with all the upgrades. Once all hardware and software issues were mitigated, the computer station was ready for data collection (see Figure 3-2).

Figure 3-2: Laboratory Computer Station

3.2 Calibration Device

Test apparatus for comparing skin sensors, copper slug sensors, and two Gardon gauges (one water-cooled) needed to be designed to compare heat flux values obtained from each sensor.

3.2.1 Designing mechanism

Design process steps were completed to define a mechanism that would hold the gauges and sensors in place. A list of performance specifications catalog the requirements of the part. Brainstorming determined many possibilities for design and each idea was analyzed. Once those steps were finished, a final selection was chosen for design. The following is a list of the necessary requirements for design of the calibration device:

1) Holder must not melt or burn under given radiant heat flux
2) Holder must be stationary
3) Holder cannot block or interfere with sensor faces
4) Holder must allow for wired connections to value-calculating device.
5) Holder must hold both sensors and the Gardon Gauge
6) Sensors must be close together without interfering with one another
7) Holder must be self supporting, or mounted/clamped in place
8) Holder must hold sensors in same orientation as on manikin in fire fighter ensemble test.
9) Holder must have low conductivity
10) Relatively inexpensive material.

3.2.2 Brainstorming and Analyzing Design

After outlining the performance specifications, brainstorm ideas were collected. The first idea, Design A, was an L-shaped piece with four holes drilled into its vertical face for holding the sensors/gauges. This design would require a small quantity of material and could be easily manufactured. One disadvantage is that the backsides of the sensors/gauges are not well protected by the encasement. Design B was an upside down U-shaped design with holes located on one of the vertical faces. This design would require more material to construct but would be self-supporting and provide some protection for the sensors/gauges. A cube option was design C, which featured a fully protected encasement of the sensors and wires. This option would require the most material. The final idea, Design D, was an A-shaped design that would require about as much material as Design A, but would be more difficult to manufacture. All designs were expected to be located at edge of fire room with sensors parallel to the door opening.

3.2.3 Final Design Selection

It was determined that sensor protection would not be a major factor during testing as radiation from fire to sensors/gauges would be minimal (except on their faces).

Design A was chosen because it required the least amount of materials to build, and could be easily manufactured. The built calibration device can be seen in Figure 3-3.

Figure 3-3: Front View of Calibration Device (Design A)

3.3 Schmidt-Boelter Gauge

In order to compare the data gathered during this project to previous data collected in the facility, the amount of heat flux emitted at the flame edges was collected. Woodward had designed and conducted research with a Schmidt-Boelter gauge enclosed in the end of a long steel pipe (see Section 2.4). This gauge was held in the flame while data was gathered and recorded. For the current project, similar research was needed. However, the calibration factor of the Schmidt-Boelter gauge was unavailable, and it would be too time consuming to reconstruct the device to include a new gauge. It was determined that the most beneficial step was to determine the calibration factor based on known heat fluxes. After the calibration factor had been defined, it would be possible to use the device as is.

3.3.1 Calibrating the Schmidt-Boelter Gauge

The calibration of the Schmidt-Boelter gauge was completed by comparing its voltage output to the heat flux absorbed by a previously calibrated Gardon gauge. The two gauges were positioned at a height of 0.8 m (2.6 ft) from the room floor and at a distance of 1.85 m (6 ft) from the center of the burners. The gauges were placed equidistant from the room's centerline to use the fire's symmetry. Once this setup was

complete, the burners were ignited, and data was gathered from both devices simultaneously. The measured voltage from the Schmidt-Boelter gauge and heat flux from the Gardon gauge were compared, and an appropriate calibration factor was determined. This value was based on the multiplication factor between the two readings.

3.3.2 Determining Heat Flux at Flame Edge

After calibrating the Schmidt-Boelter, the next step in the data gathering process was to determine the heat flux at the flames edges. This process included moving the Schmidt-Boelter gauge a distance of 1.55 m (5 ft) further into the room so that the gauge aligned vertically with the edge of the burners. The fire was then increased to predetermined increments (see Table 3-1) and the steady state heat flux absorbed by the Schmidt-Boelter gauge was recorded.

Table 3-1: Fire Sizes

Flow Controller	Fire Size
45%	1.56 MW
40%	1.39 MW
35%	1.22 MW
30%	1.04 MW
25%	.87 MW
20%	.69 MW
15%	.53 MW

3.4 Suspension System

A new suspension system was designed to support the manikin fully clothed in fire fighter turnout gear (consisting of jacket, pants, gloves, boots and helmet) and a self-contained breathing apparatus (SCBA) while also withstanding fire sizes of greater than 1.5 MW. The design of this mechanism had to minimize the contact points on the

clothing/manikin, prevent radiation shielding during the test, and maintain the manikin in a stable vertical position to maintain consistent view factors.

3.4.1 Original Design

The original mechanism was designed to support a manikin and a partial ensemble; including jacket, pants, gloves, and boots. Figure 3-4 was apparatus formerly used to support the manikin. Figure 3-5 shows the stabilizing bar and side rear view of that hanger mechanism (pictures were taken with the manikin in a lower position so the entire existing support mechanism could be clearly viewed). The manikin has a metal rod through its head which rested on two hooks from the support mechanism during testing.

Figure 3-4: Existing Support Apparatus

Figure 3-5: Sway Bar Behind Manikin

In order to complete a full ensemble test, a helmet and breathing apparatus must be placed on the manikin. The original support system was inadequate because the U-shaped hanger element attaching to the bar in the manikin's head was too narrow to accommodate a helmet. Also, the vertical stabilizing rod prevented the addition of an SCBA.

3.4.2 Revising Mechanism

The original system had to be redesigned not only to allow space for additional gear, but also to support the extra weight. The manikin weighs approximately seventy pounds and would need to be outfitted with at least fifty additional pounds of fire fighter clothing. Heat flux sensors are located in specific locations throughout the surface of the manikin, and must not be compromised through shielding or contact by the revised support mechanism. Additional design considerations include that the manikin must fit (loosely) through a doorway 30 inches wide and not physically contact the burner system at the burn room floor. The following is a list of performance specifications:

1) Mechanism must not melt or burn under given radiant heat, nor deform in any way.
2) Mechanism must support the weight of the manikin and ensemble during fire tests.
3) Mechanism cannot block or interfere with sensors or fire fighter ensemble parts.
4) Mechanism must attach to the existing track mount.
5) Mechanism and manikin must be able to pass through burn room without hitting the doorframe or burners (on the floor).
6) Manikin must be easily removed and/or lowered from support mechanism for maintenance.
7) Mechanism must include provision to keep wiring out of direct flame impingement.
8) Mechanism must be able to be built using available tools and materials in WPI machinist laboratories.

3.4.3 Analysis of Designs

Three final models were chosen from ten proposed (drawing can be found in Appendix C). The three designs would be made of one-inch square American Iron and Steel Institute (AISI) 1020 hollow tube steel, which would provide sufficient support for the manikin. This material was selected because it was similar to the previous suspension design. The joints would be fixed together by arc welding. The filler material would be a

steel alloy of at least E60XX rating, to provide sufficient strength. This material would supply maximum shear strength and resistance to fatigue fractures in the welds.

All three of the final models share the same design for the headpiece, which is very similar to the original mechanism, except elongated. The original headpiece was extended both horizontally and vertically to provide sufficient room for helmet applications. Two-inch square hooks replaced the original semicircles to increase the surface of the welds between the hooks and the vertical members. Four 0.25-inch bolts were used to support the mechanism; two of which connected the suspension to the track, and the other two securing the manikin to the head piece via the bar in its neck.

1) Square Head – Straight Rear Bar: The manikin would suspend from the revised head unit, with a straight bar in the back to prevent sway. The bar would push directly on the SCBA bottle, securing the manikin while in motion (see MODEL 10 in Appendix C).
2) Square Head – U-shaped Back: This design option focused on fitting many differently sized SCBA bottles. In addition to the revised headpiece, a U-shaped bar would support the back of the manikin to prevent sway. The bar would loop around the bottles, pushing on the belt of the SCBA unit beside the tank valve (see MODEL 1 in Appendix C).
3) Bolted Hooks: This model relied on the revised head unit to both suspend the manikin and prevent sway. Two bolts would secure the manikin into the square hooks, creating a solid unit. This design would provide additional levels of stability and support. This design simplifies the previous two designs by removing the rear bar of the support mechanism, and securing the manikin to the head

support. This simplification allowed for fewer limitations on fire fighter clothing being tested (see MODEL 6 in Appendix C).

3.4.4 Final Design Selection

The final model selected for machining was the bolted hook design, the modified headpiece with bolted hooks. This suspension underwent a stress analysis to ensure it could support the seventy pound manikin and over fifty pounds of turnout gear for this project and in the future. The new head piece allows for the use of helmets during testing and the elimination of the sway bar clears the back of the manikin for SCBA applications. Swinging of the manikin is now prevented by two steel bolts, securing the manikin to the square hook of the suspension.

This model was the most practical choice for a new suspension, causing virtually no contact points on the gear or the manikin. This modification allows for tests to be conducted with no radiation shielding from the suspension, while supporting and maintaining the manikin in the vertical position. The dimensions of the design allows the manikin to pass through the 30” wide doorway, and clear the sand burners on the floor of the burn room; meeting all of the performance specifications.

The modified suspension (Figure 3-6) was machined at WPI machine shops, and constructed of one-inch square AISI 1020 hollow steel tube. The material was welded together by arc welds, utilizing a steel filler material of at least E60XX rating. This formed a unit able to withstand the stresses caused (see Appendix D) by the manikin and the testing process. The design of this unit also allowed for great durability, maintaining structural integrity for the extended life of the mechanism. The modified suspension has

been successfully used in several full ensemble tests, proving to be an appropriate design for this application.

Figure 3-6: Suspension System

3.5 Prototype Testing

As no dynamic full fire fighter ensemble test exists, the procedure for carrying out such a test was not available. Therefore, it was necessary to create the procedure for this test. In order to have some method of evaluating the validity of the procedure and its results, parallel exposures to existing ensemble tests were included. Dupont's well-known Thermo-Man test was used as a guide and tool for comparison. Dupont exposes Thermo-Man to a heat flux of 84 kW/m^2 for durations of six and ten seconds to simulate a flash fire environment. Thermo-Man is stationary for the duration of the test.

To expose our manikin to a comparable heat flux and time frame, fluxes throughout the room had to be determined. The fire size was measured to be approximately 1.5 MW with a heat flux of 84 kW/m^2 over the burners. The flux at the doorway was determined to be 17 kW/m^2 and it was assumed that heat flux increased linearly from the door to the burner edge. Due to the manikin moving through the room, individual sensors are only exposed to radiation for the time in which they face the

flames. For example, sensors on the front of the manikin are only exposed to significant radiant heat during the manikin's approach to the fire and in the flames.

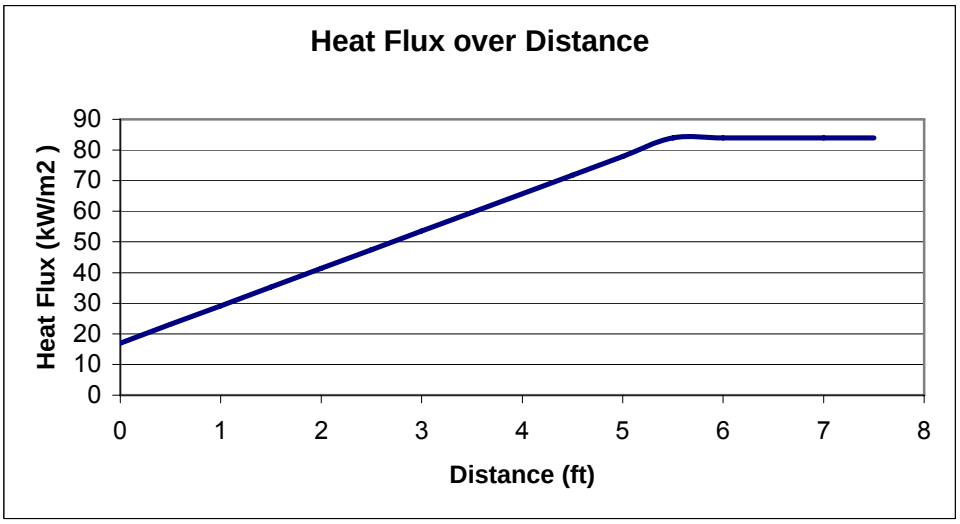

Figure 3-7: Heat Flux Over Distance in Room

The slope of this line, 12.18 kW/(m^{2}ft), was determined using the known distance to the burners (5.5 ft). The area under this curve, or the integral, is used to determine the total heat flux exposure over the distance traveled.

$$y = \int_{0}^{5.5} (12.18x + 17)dx + \int_{5.5}^{7.5} 84dx$$

Solving for this integral, y = 445.7 (ft)*kW/m^2. To match 84 kW/m^2 in six seconds, the total exposure must be 508 kJ/m^2. If y = 445.7 (ft)*kW/m^2, y divided by the velocity in ft/s will yield the exposure in kJ/ m^2.

$$504\frac{kJ}{m^2} = 445.7\,ft\frac{kW}{m^2} / r(\frac{ft}{s})$$
$$r = 445.7\,ft\frac{kW}{m^2} / 504\frac{kJ}{m^2}$$
$$r = 0.88\,ft/s$$

For an eight second exposure

$$672\frac{kJ}{m^2} = 445.7\,ft\frac{kW}{m^2} / r(\frac{ft}{s})$$
$$r = 445.7\,ft\frac{kW}{m^2} / 672\frac{kJ}{m^2}$$
$$r = 0.66\,ft/s$$

For a ten second exposure

$$840\frac{kJ}{m^2} = 445.7\,ft\frac{kW}{m^2} / r(\frac{ft}{s})$$
$$r = 445.7\,ft\frac{kW}{m^2} / 840\frac{kJ}{m^2}$$
$$r = 0.53\,ft/s$$

The above calculations give velocities of 0.27m/s (0.88 ft/s), 0.20 m/s (0.66 ft/s), and 0.16 m/s (0.53 ft/s) for six, eight, and ten seconds respectively. Thermo-Man uses only the six and ten second exposures. The eight-second exposure is for use in comparing our testing of Australian fire fighting gear to the testing performed in England on RALPH.

4 Results

4.1 Calibration

The calibration device was created to compare newly acquired sensors to the previously calibrated copper slug sensors and two Gardon gauges. The new sensors, as seen below in Figure 4-1, have a reaction consistent with that of the copper slug sensors. However, the magnitude of the reaction differs greatly. Since the material properties and internal dimensions of these sensors are unavailable, the response cannot be entirely understood at this time.

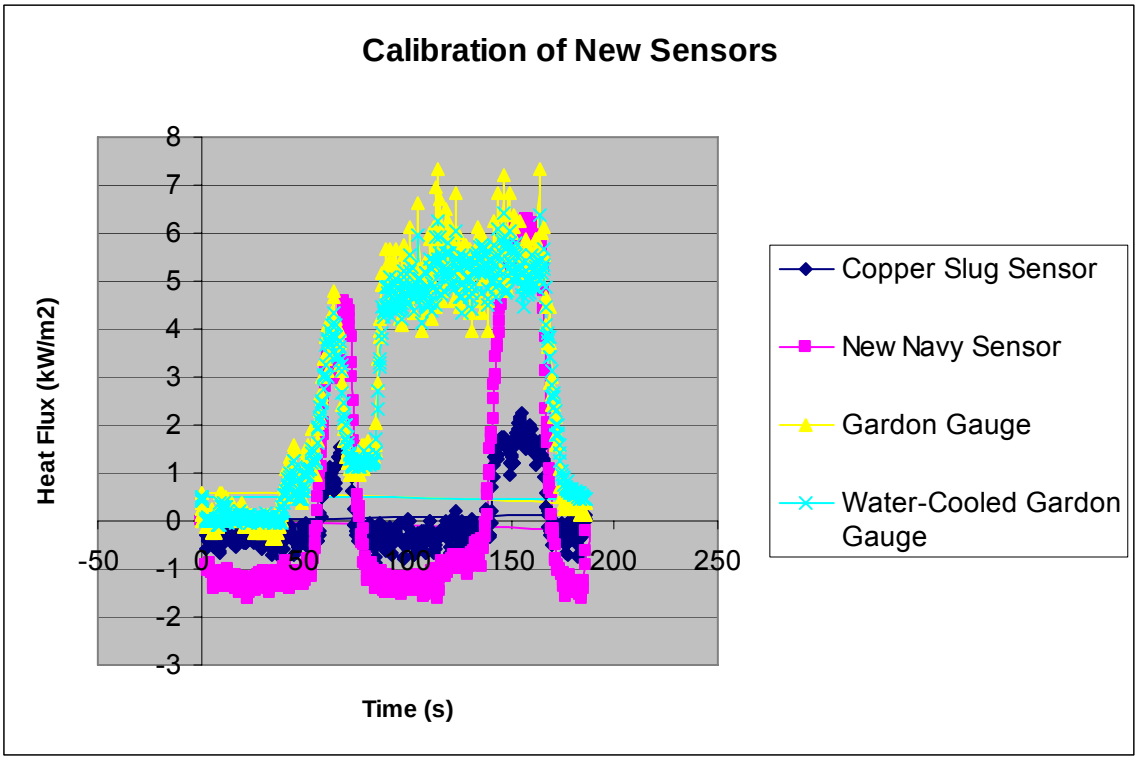

Figure 4-1: Calibration of New Sensors

4.2 Flame Edge Heat Fluxes

4.2.1 Schmidt-Boelter Gauge Calibration Factor

Figure 4-1 demonstrates the heat flux that both the Gardon gauge and the Schmidt-Boelter gauge were exposed to at 1.85 m (6 ft) from the fire centerline. The data in Figure 4-1 and Table 4-1 was collected by the Gardon Gauge after the fire reached steady state.

Table 4-1: Gardon Gauge Steady State Heat Fluxes in Doorway

		Gardon
Flow Percentage	**Fire Size**	**Doorway Flux (kW/m^2)**
30%	1.04 MW	8.5
25%	.87 MW	8
20%	.69 MW	6.5
15%	.53 MW	5
35%	1.22 MW	9
40%	1.39 MW	12
45%	1.56 MW	12.5

The 45% flow rate correlates directly to Sipe's data about the incident heat flux on the manikin in the doorway. Sipe had values nearing 17 kW/m^2 at this location for a 1.5 MW fire, much higher than the 12.5 kW/m^2 measured (Sipe, 72).

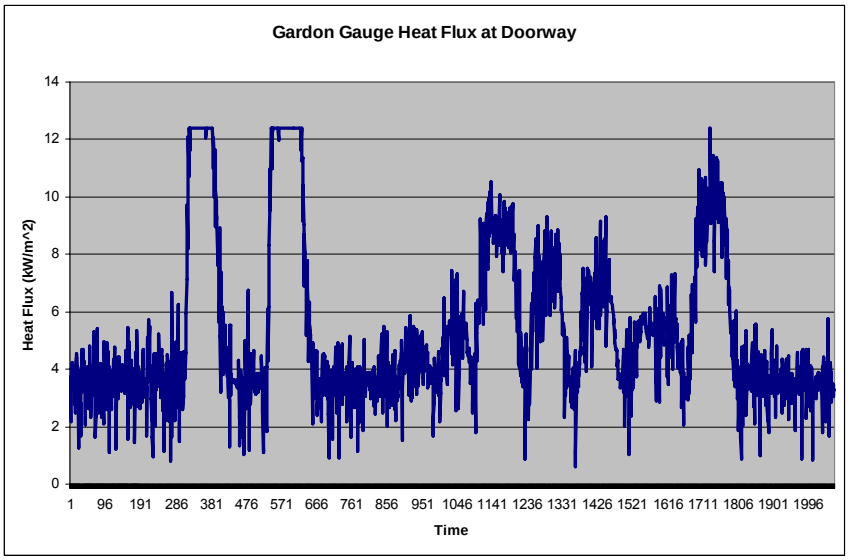

Figure 4-2: Exposed Heat Flux at Doorway

Once this data was collected, it was noticed that there were many outliers in the voltage reading from the Schmidt-Boelter gauge. To compensate for this, all negative voltages (indicating negative heat fluxes) were removed from the data, and an average was taken over the approximately 2000 time steps. When using this value of 18950 $kW/m^2/V$ to calculate the heat flux and comparing the results to the flux read by the Gardon gauge (see Figure 4-2), it was noted that the value appeared high. The team then considered the average factor when including the negative voltages, defining a value of 6400 $kW/m^2/V$ (see Figure 4-3). The results using this factor appeared too low. In order to deduce the correct factor, the value was altered, incrementally, until the heat flux curves read by both gauges aligned visually (see Figure 4-4).

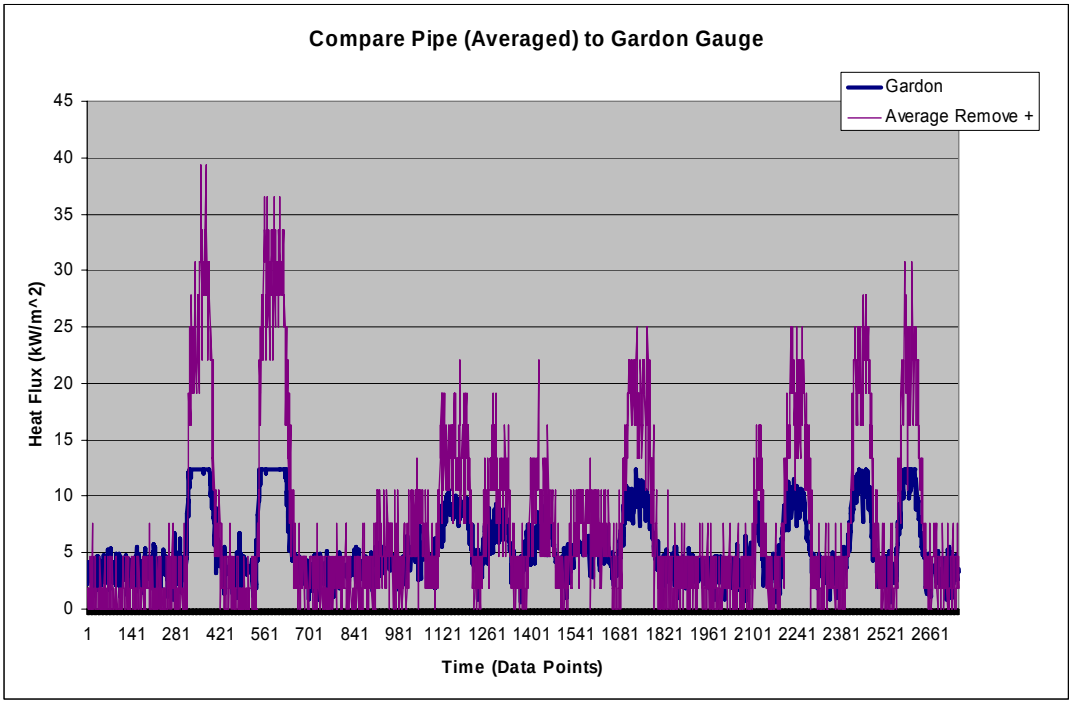

Figure 4-3: Schmidt-Boelter Flux compared to Gardon Flux using Average Calibration Factor Excluding Negative Voltage Values

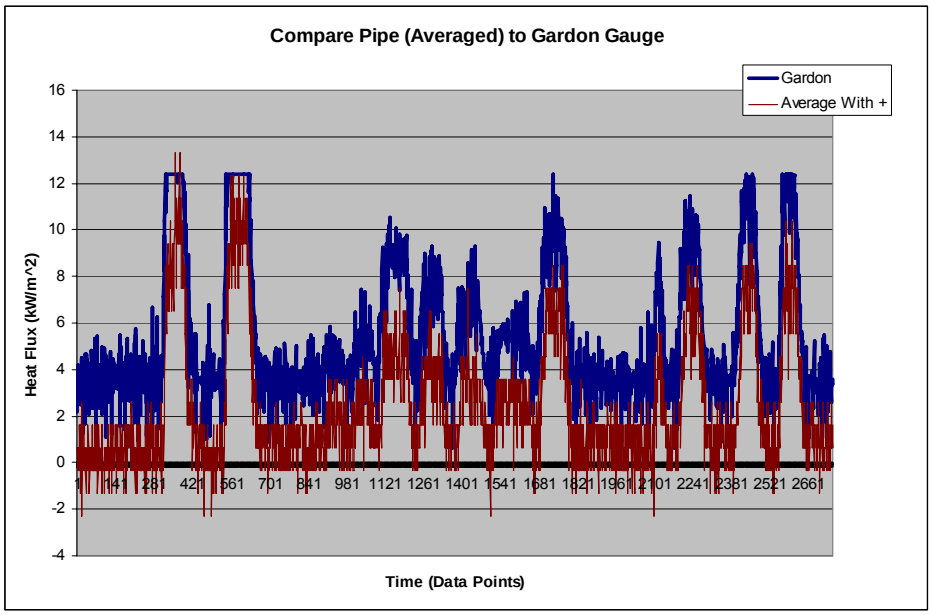

Figure 4-4: Schmidt-Boelter Flux compared to Gardon Flux using Average Calibration Factor Including Negative Voltage Values

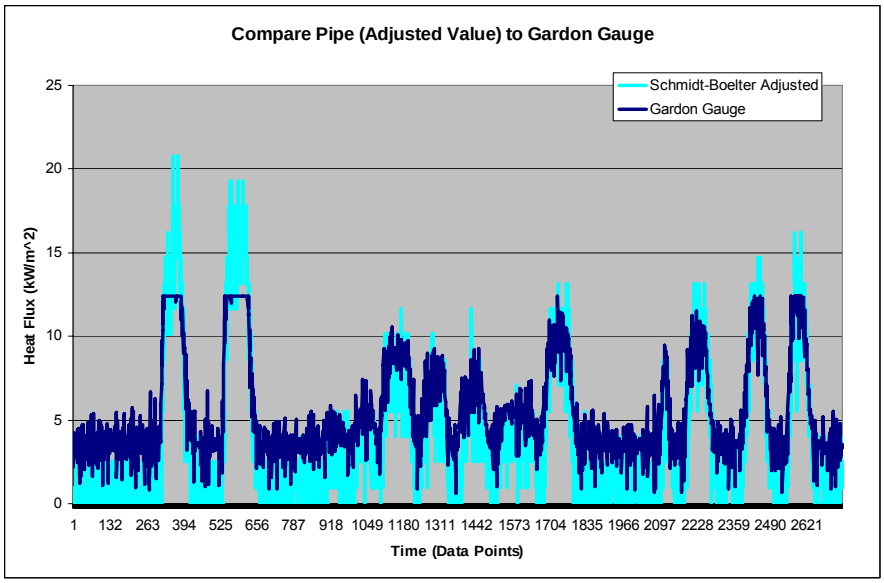

Figure 4-5: Best Fit Curve

Figure 4-5demonstrates the fit of the Gardon gauge's results to those of the Schmidt-Boelter gauge as calculated using an adjusted value of 10,000 $kW/m^2/V$. It is important to note, that even at these low heat flux values, there is evidence that the Schmidt-Boelter gauge is calibrated as more of a logarithmic curve than linear. This can be seen in Figure 4-5 where the Schmidt-Boelter gauge reads lower values than the Gardon gauge at low fluxes (after data point 787), and slightly higher values at higher heat fluxes (before data point 787). However, due to the large interference in the data recorded and the limitations of the Gardon gauge with respect to effects of high fluxes, the nearest approximation that can be made. This value gives a calibration curve as seen in Figure 4-6.

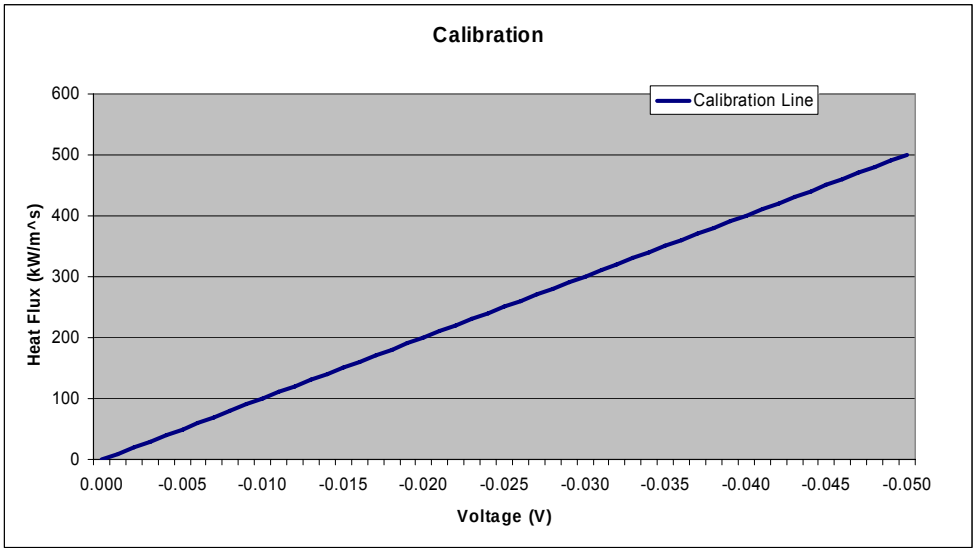

Figure 4-6: Calibration Curve for Schmidt Boelter Gauge

4.2.2 Heat Flux at Flame Edges

Using this newly determined calibration factor for the Schmidt-Boelter gauge, estimates were made of the heat fluxes at the edge of the flames in the compartment. Data was collected at four propane flow rates. The data collected is displayed in Figure 4-14, Figure 4-15, Figure 4-16, Figure 4-17, Figure 4-18, Figure 4-19, and Figure 4-20.

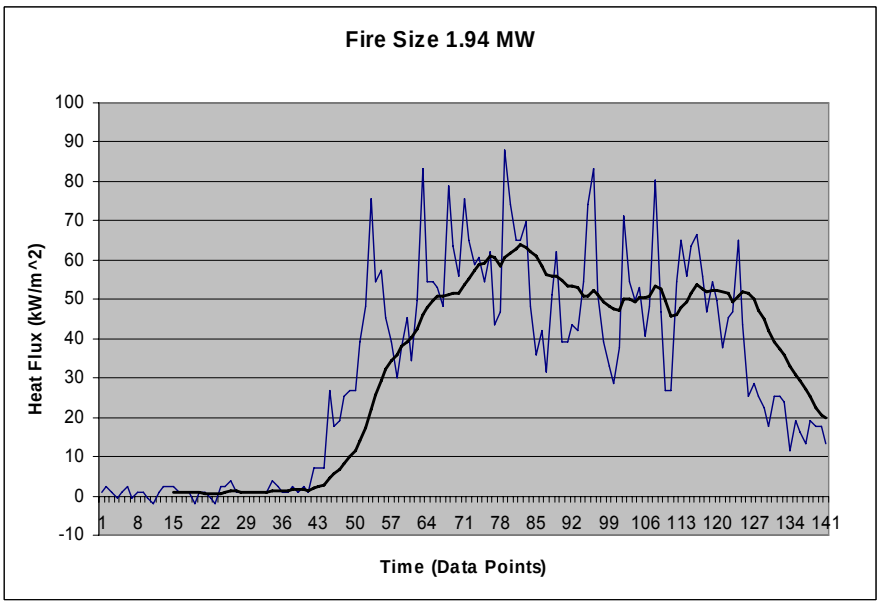

Figure 4-7: Run #1 at 1.94 MW

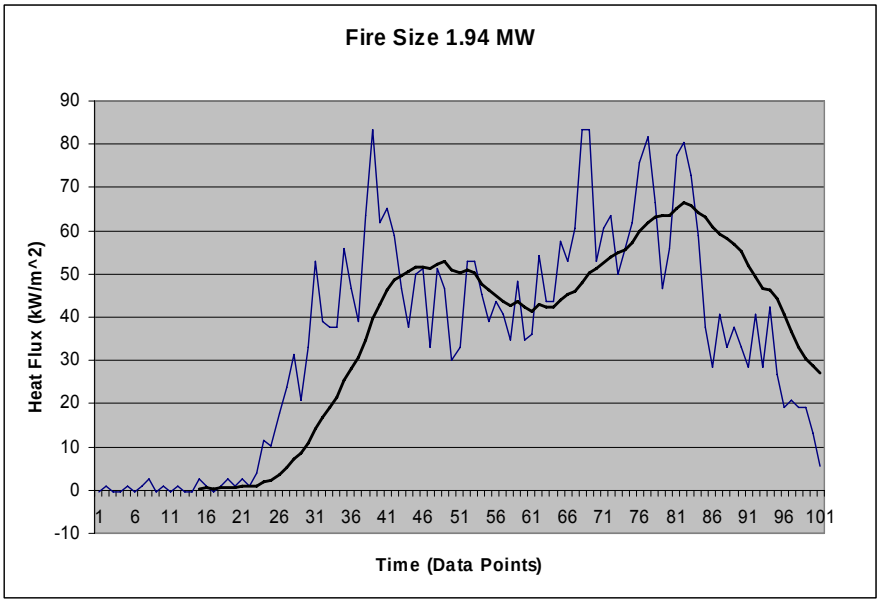

Figure 4-8: Run #2 at 1.94 MW

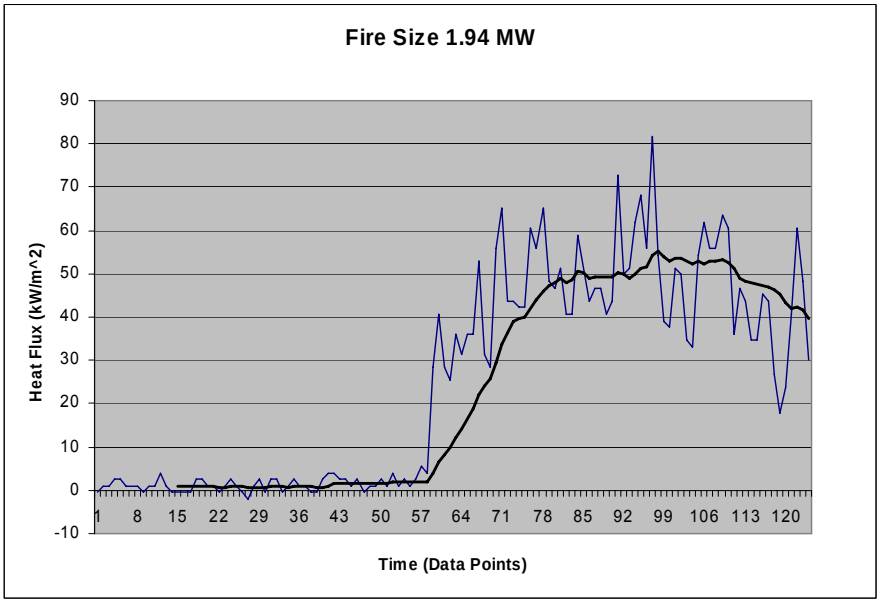

Figure 4-9: Run #3 at 1.94 MW

The data collected from a 1.9 MW fire (Figure 4-14, Figure 4-15, and Figure 4-16) portrays somewhat self-consistent values for the heat flux at the flame edge of approximately 55 kW/m^2. For the first two runs, it was noticed that the Schmidt-Boelter gauge may have been misaligned and pointed slightly towards the ceiling. This was corrected for the third run, but appeared to have little impact on the absorbed energy. It is

important to note that for an approximate 1.5 MW fire size, Woodward (75) collected data closer to the order of 80 kW/m^2 at the flame centers. This is an indication that the calibration of the Schmidt-Boelter gauge may be incorrect at high heat fluxes. Woodward's fire size estimates were based on visual flame heights; a methodology that allows for high error rates.

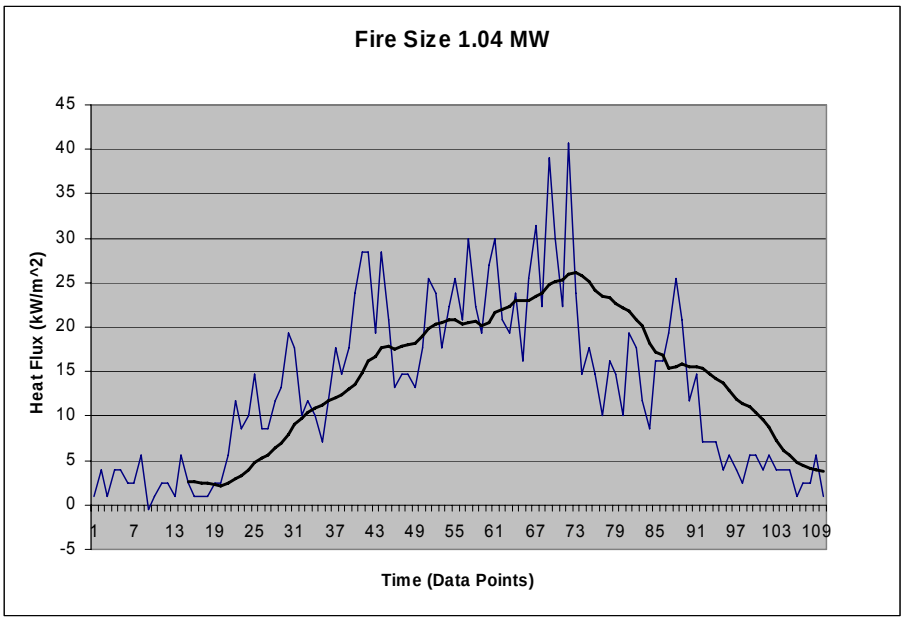

Figure 4-10: Run #1 at 1.04 MW

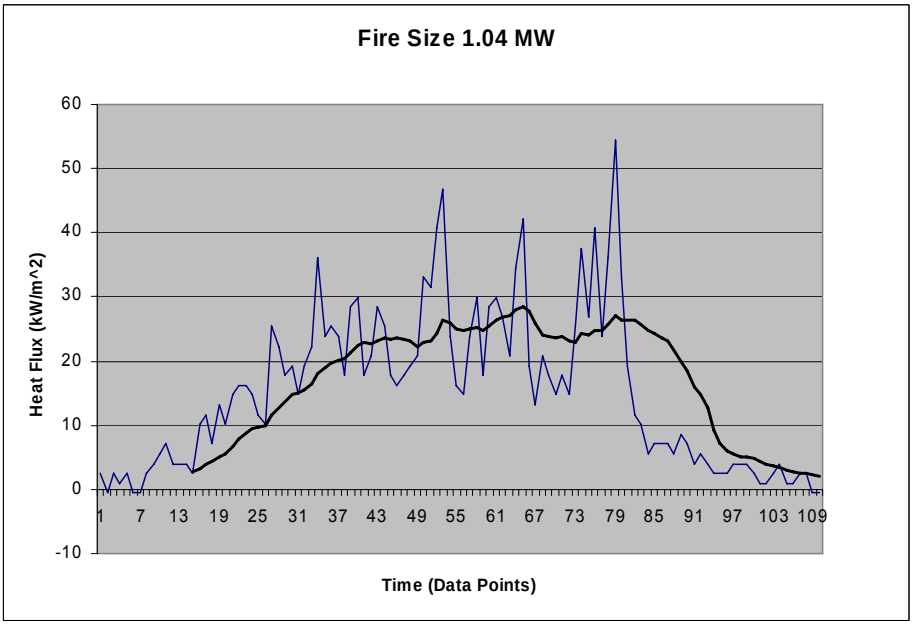

Figure 4-11: Run #2 at 1.04 MW

Figure 4-17 and Figure 4-18 demonstrate consistent results also, approximately 25 kW/m^2 for both test runs. This also demonstrates that the Schmidt-Boelter gauge is capable of making repeatable readings.

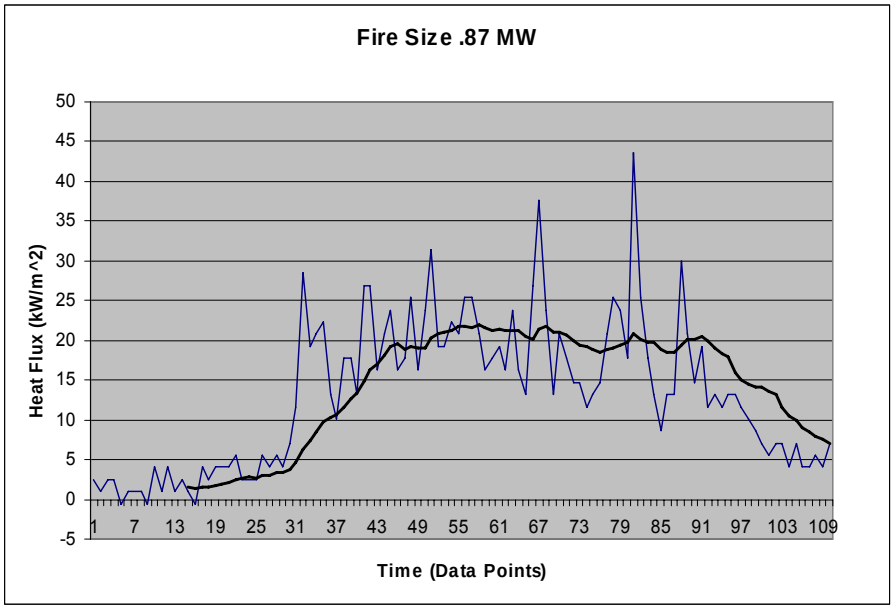

Figure 4-12: Fire Size of 0.87 MW

Flowing at 25% of the flow meter's capacity, a fire of 0.87 kW was produced, which emitted approximately 22 kW/m^2 at the flame edge.

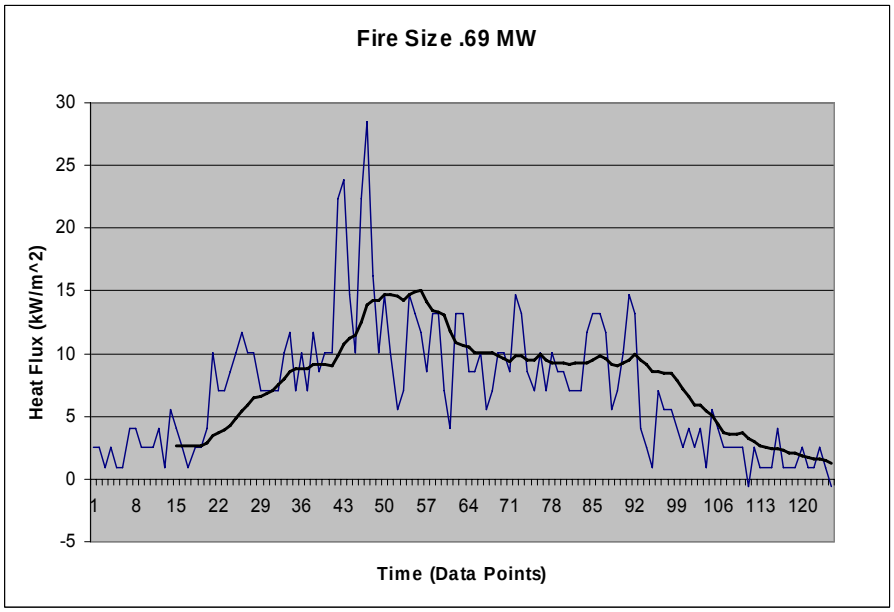

Figure 4-13: Fire Size of 0.69 MW

With the flow meter set to 20% capacity, a fire of 0.69 MW was produced at the burners. The heat flux at the edge of these flames was calculated to be approximately 15 kW/m^2.

Although the Schmidt-Boelter gauge's quantitative calibration is questionable, these results demonstrate that the burn room provides equivalent energy emissions for consistent fire sizes. This proves that any manikin tests using the apparatus should provide repeatable results.

4.2.3 Heat Flux at Flame Edges

Using this newly determined calibration factor for the Schmidt-Boelter gauge, estimates were made of the heat fluxes at the edge of the flames in the compartment. Data was collected at four propane flow rates. The data collected is displayed in Figure 4-14, Figure 4-15, Figure 4-16, Figure 4-17, Figure 4-18, Figure 4-19, and Figure 4-20.

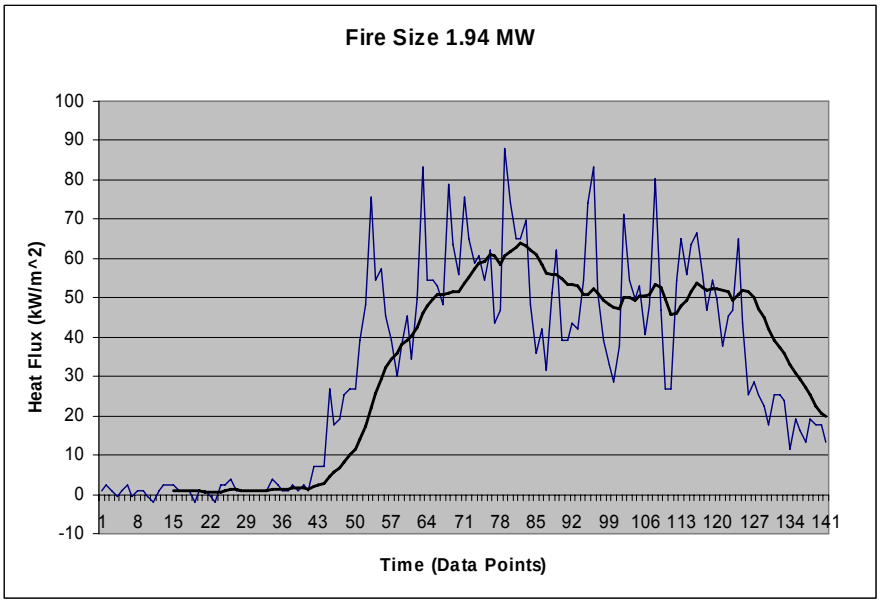

Figure 4-14: Run #1 at 1.94 MW

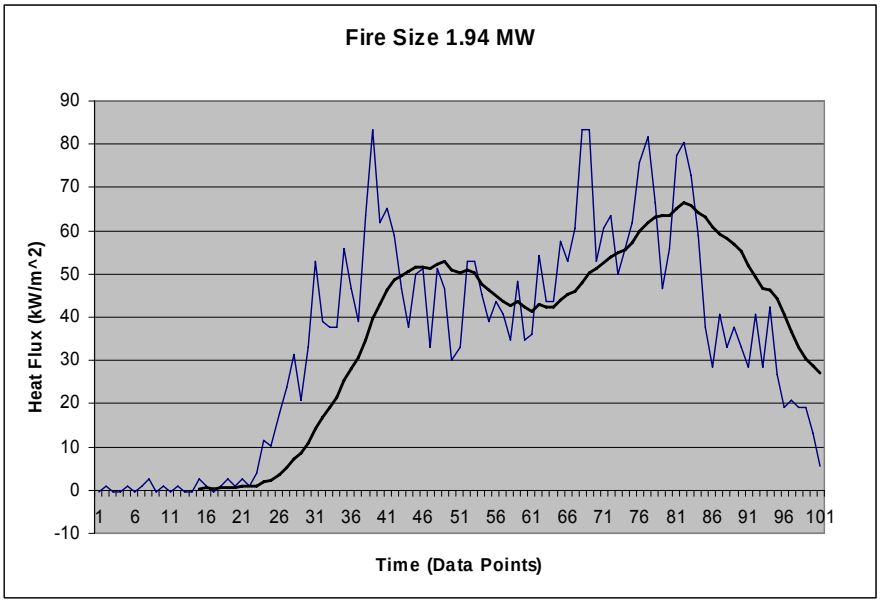

Figure 4-15: Run #2 at 1.94 MW

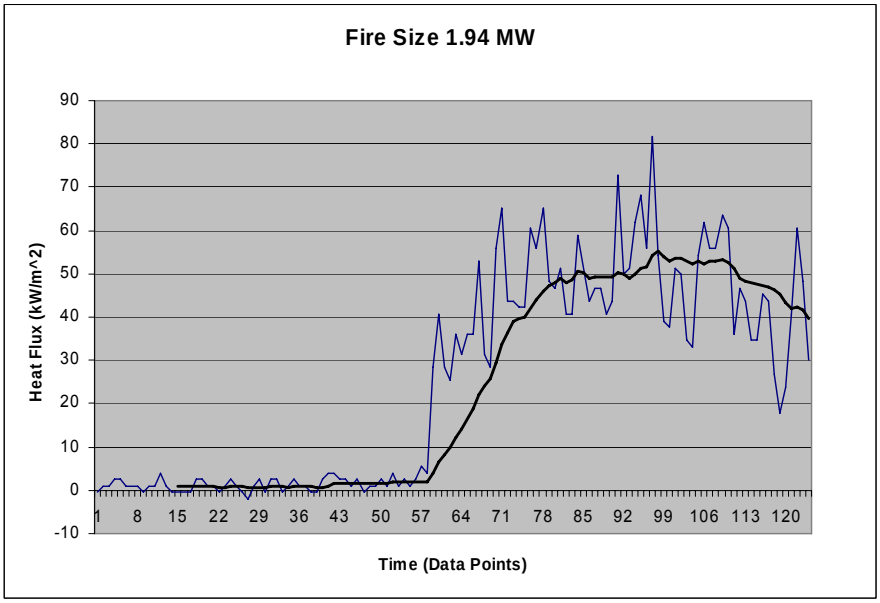

Figure 4-16: Run #3 at 1.94 MW

The data collected from a 1.9 MW fire (Figure 4-14, Figure 4-15, and Figure 4-16) portrays somewhat self-consistent values for the heat flux at the flame edge of approximately 55 kW/m^2. For the first two runs, it was noticed that the Schmidt-Boelter gauge may have been misaligned and pointed slightly towards the ceiling. This was corrected for the third run, but appeared to have little impact on the absorbed energy. It is

important to note that for an approximate 1.5 MW fire size, Woodward (75) collected data closer to the order of 80 kW/m^2 at the flame centers. This is an indication that the calibration of the Schmidt-Boelter gauge may be incorrect at high heat fluxes. Woodward's fire size estimates were based on visual flame heights; a methodology that allows for high error rates.

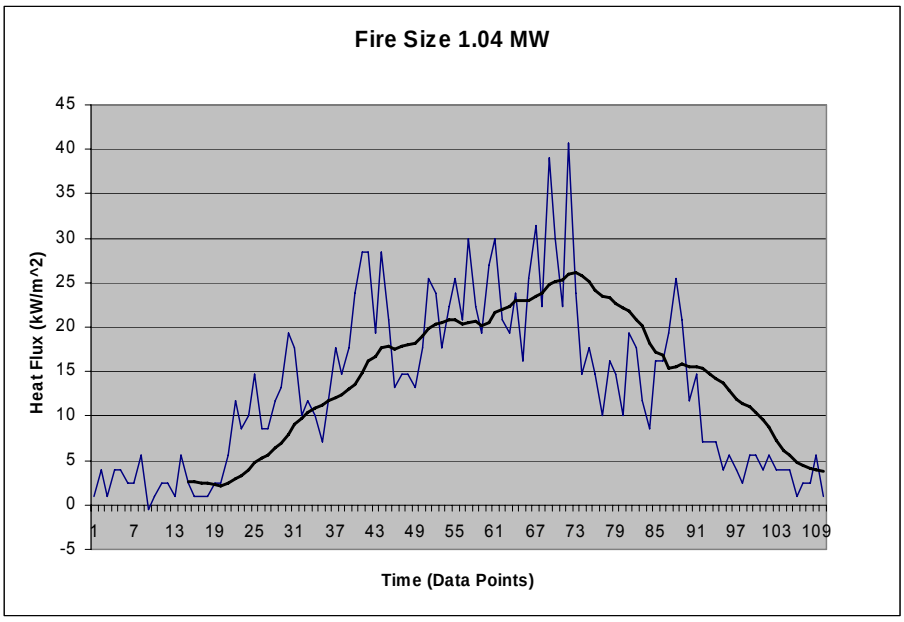

Figure 4-17: Run #1 at 1.04 MW

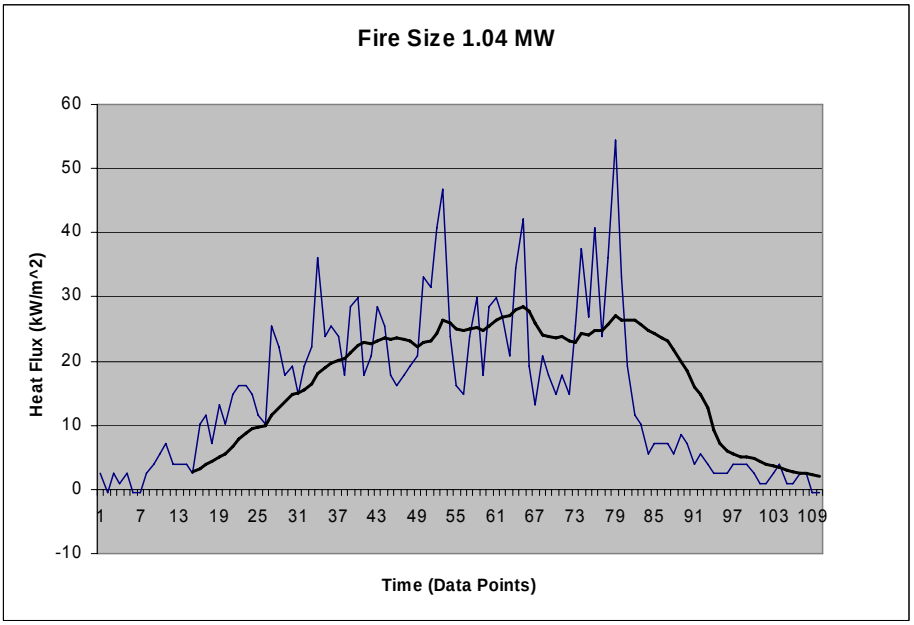

Figure 4-18: Run #2 at 1.04 MW

Figure 4-17 and Figure 4-18 demonstrate consistent results also, approximately 25 kW/m^2 for both test runs. This also demonstrates that the Schmidt-Boelter gauge is capable of making repeatable readings.

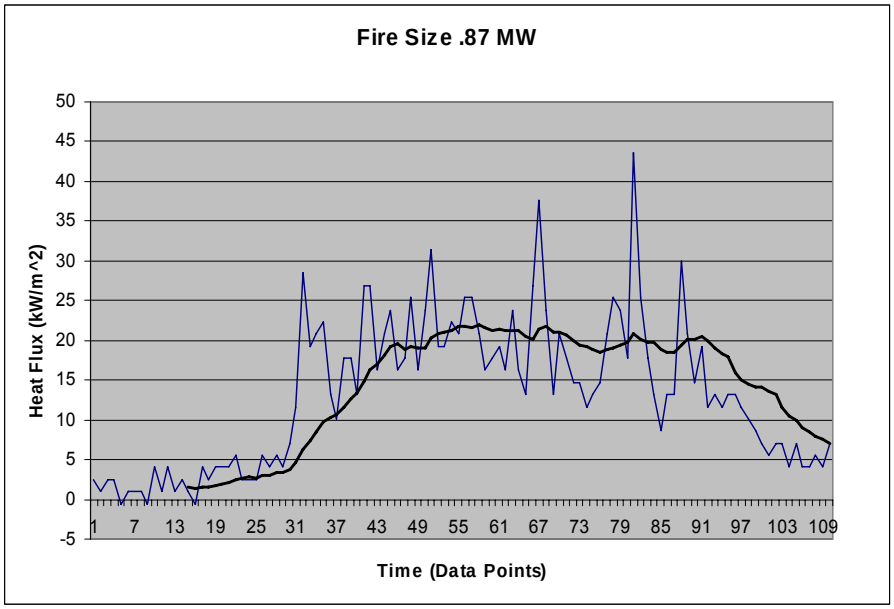

Figure 4-19: Fire Size of 0.87 MW

Flowing at 25% of the flow meter's capacity, a fire of 0.87 kW was produced, which emitted approximately 22 kW/m^2 at the flame edge.

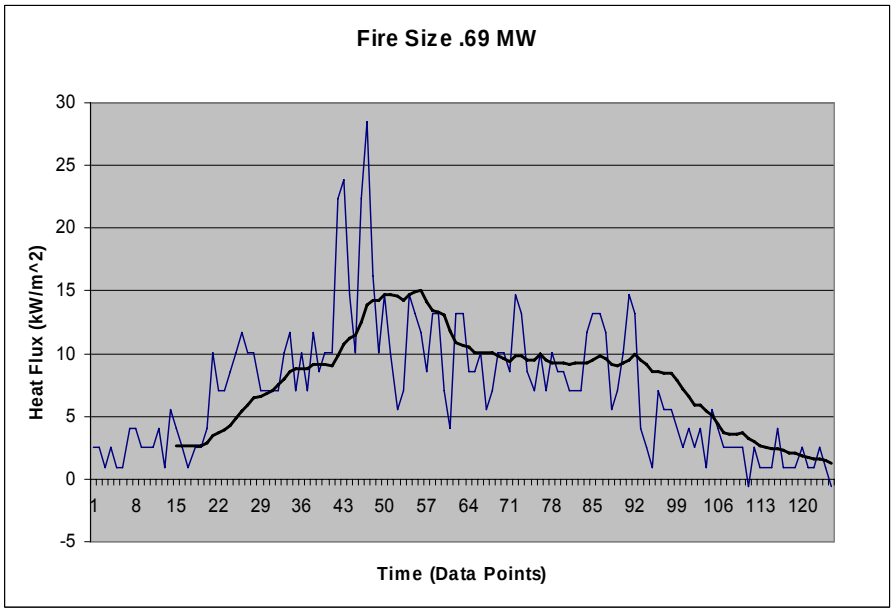

Figure 4-20: Fire Size of 0.69 MW

With the flow meter set to 20% capacity, a fire of 0.69 MW was produced at the burners. The heat flux at the edge of these flames was calculated to be approximately 15 kW/m^2.

Although the Schmidt-Boelter gauge's quantitative calibration is questionable, these results demonstrate that the burn room provides equivalent energy emissions for consistent fire sizes. This proves that any manikin tests using the apparatus should provide repeatable results.

4.3 Prototype Tests

In order to practice running tests on fire fighter ensembles, data was gathered on three ensembles at various exposures. This provided an opportunity to observe what affects the laboratory would have on the ensembles, as well as perfect the laboratory techniques before exposing the ensembles to comparable energy as the ASTM F 1930 test. The results from these lesser exposures can be seen in Appendix E of this report.

The data-gathering process continued with testing of ensembles at exposures that are comparable to current test methods. At these extreme exposures, there is a high risk of exposing the manikin to energy capable of causing skin burns through the gear. Each ensemble was tested at three speed settings (and therefore thermal exposures). The first test was conducted with the manikin stationary in the doorway for 30 seconds. During the next two tests, the manikin was moved through the flames at a speed of 0.27 m/s, followed by two additional speed runs at 0.16 m/s. These speed settings provided comparable exposures to the ASTM F 1930 test at exposure times of six and ten seconds, respectively. Finally, the manikin was exposed to a doorway test a final time to determine

if any noticeable degradation had occurred to the protective clothing. The results from these tests are listed in the following sections.

4.3.1 Australian Ensemble 1

The first ensemble evaluated at these higher energy exposures was the new Australian fire fighter ensemble. This ensemble consisted of an Australian structural helmet, green gloves, Australian boots and a green three layer suit. Also, the ensemble was completed with a Scott self-contained breathing apparatus. The protective suit itself consisted of a Nomex 3A outer shell, Laminate to Nomex scrim moisture barrier, Sonatara E89 Thermal Barrier. Figure 4-21 demonstrates the manikin clothed in preparation for testing.

Figure 4-21: Australian Ensemble 1 Pre-Test

The first test conducted on this ensemble involved holding the manikin in the doorway plane for 30 seconds, a calculated exposure of 504 kJ/m^2, comparable to the ASTM F 1930 six-second exposure, without any flame impingement. Using the temperature of the thermocouples in the manikin's sensors, the incident radiative flux was calculated. This value was then used to calculate an expected basal layer temperature, which then lead to the derivation of the exposed skin burn parameter using Henrique's Burn Integral. The five most severely affected sensors' data is recorded in Figure 4-22. Remembering that a second degree burn occurs at parameter values greater than 1.0, it can be stated that no sensors were exposed to enough energy to cause burns. Actually, the top sensors recorded almost one ten-thousandth of the second degree burn parameter during this exposure.

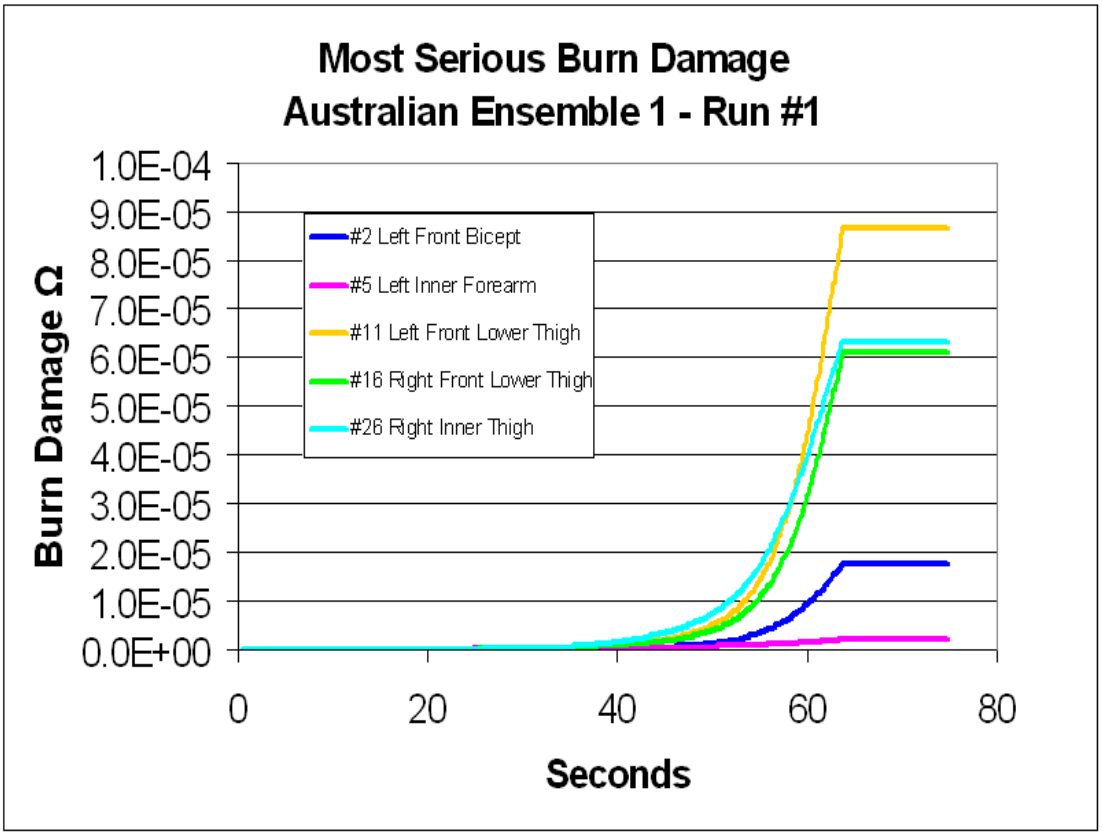

Figure 4-22: Australian Ensemble 1 Doorway Run 1

After cooling the manikin's sensors back to ambient conditions, the manikin was then tested twice at the same energy exposure, but while traversing the room. Although the incident energy on the manikin's sensors was not expected to increase during these runs, these tests introduced flame impingement to the protective clothing, as well as providing exposure rates of over 80 kW/m^2 at the burner centerline. Figure 4-23 and Figure 4-24 demonstrate the first and second runs at the speed of 0.27 m/s. As is demonstrated by these burn parameter calculations, once again, the Australian Ensembles were not exposed to any second degree burns. Also, it can be noted that the burn parameters are of comparable magnitude to the calculated values in the doorway (Figure 4-22). The difference between the calculated values for these two runs is due to unknown changes to the laboratory set up. Possibilities include changes in wind direction, or a burner being slightly clogged during the first test. However, the differences between the skin burn parameters can be considered negligible.

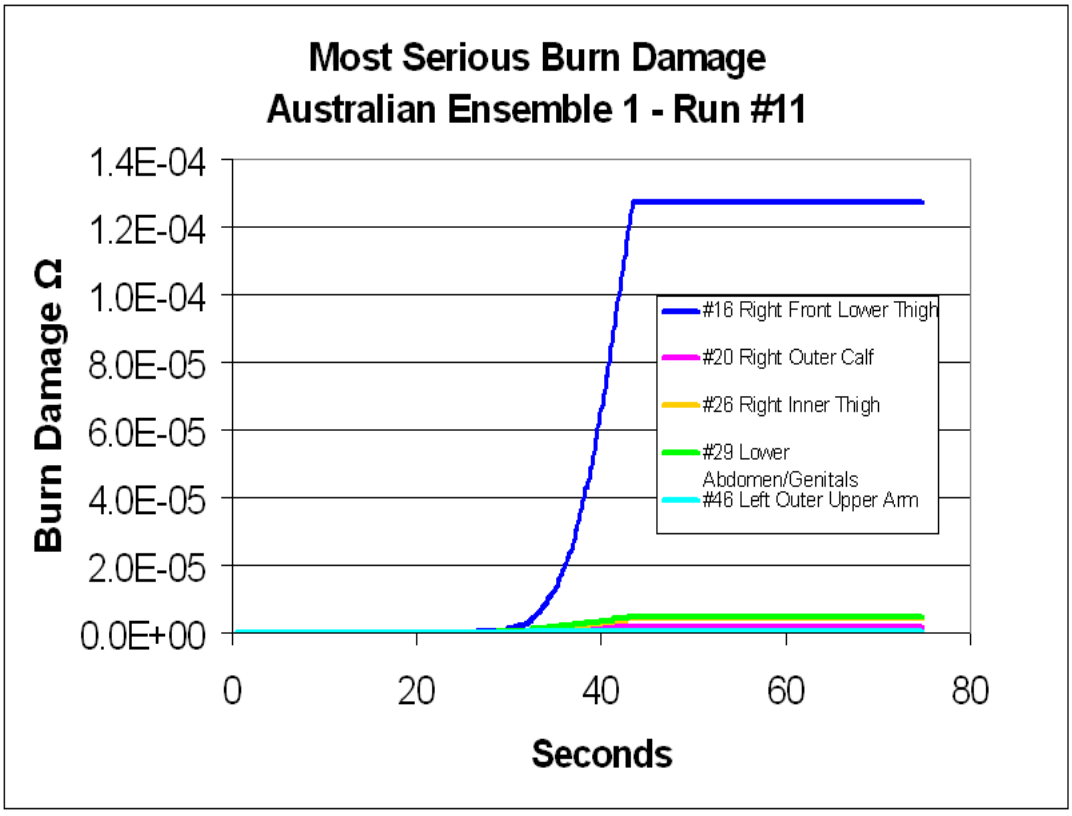

Figure 4-23: Australian Ensemble 1 Six Second Exposure Run 1

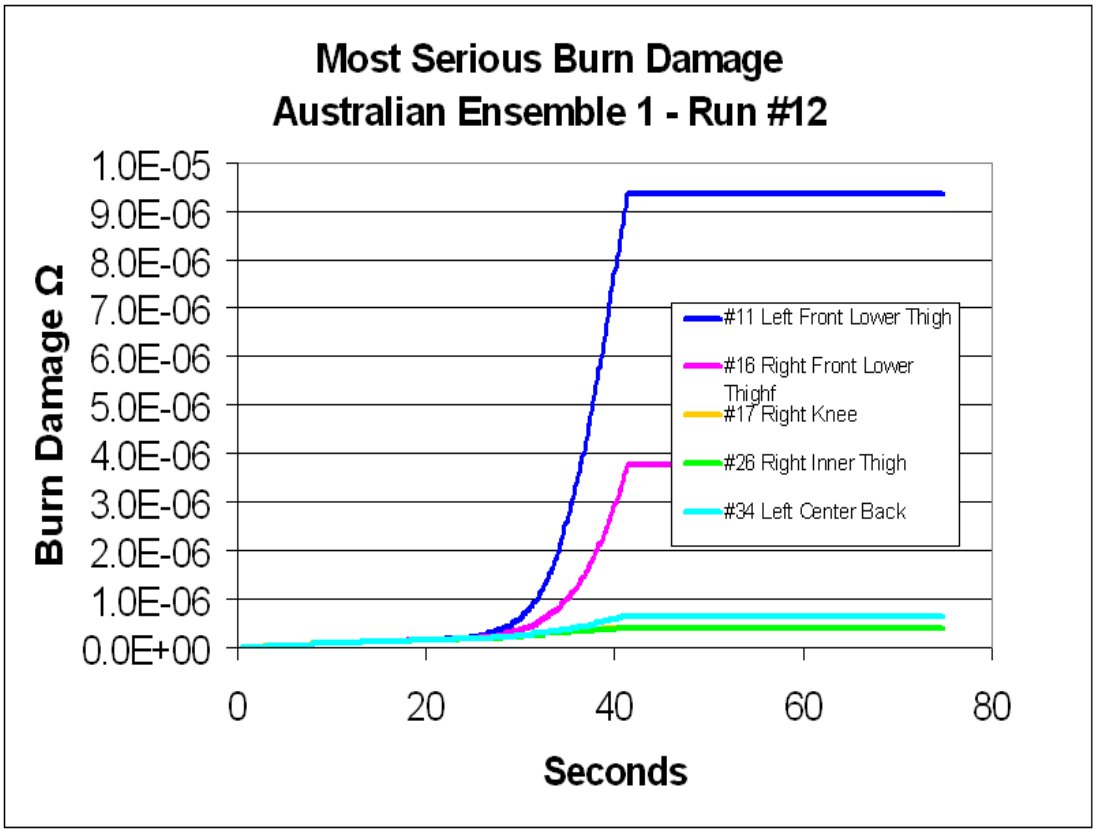

Figure 4-24: Australian Ensemble 1 Six Second Exposure Run 2

Next, the ensemble was exposed to two additional runs at a slower speed of 0.16 m/s, equivalent to the ASTM F 1930 ten second exposure, or 840 kJ/m^2. Here, it was expected that the manikins' sensors would be exposed to more energy, and therefore the skin burn parameter calculations should reveal higher burn parameters. The collected data can be seen in Figure 4-25 and Figure 4-26, representing the first and second tests respectively. These results demonstrate consistently higher burn parameters; however, these values are still well below the threshold of 1.0 for a second degree burn. Based on these results, it can be determined that the manikin was not exposed to any second degree burns at the tests highest energy exposure level.

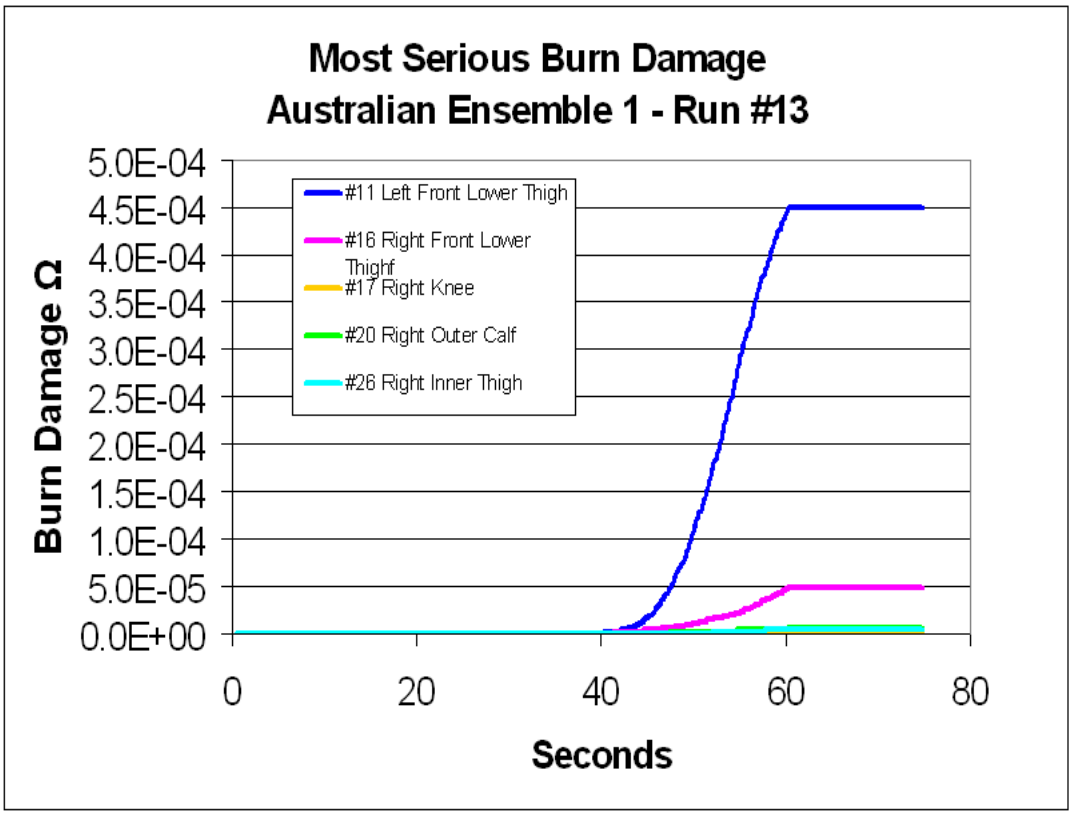

Figure 4-25: Australian Ensemble 1 Ten Second Exposure Run 1

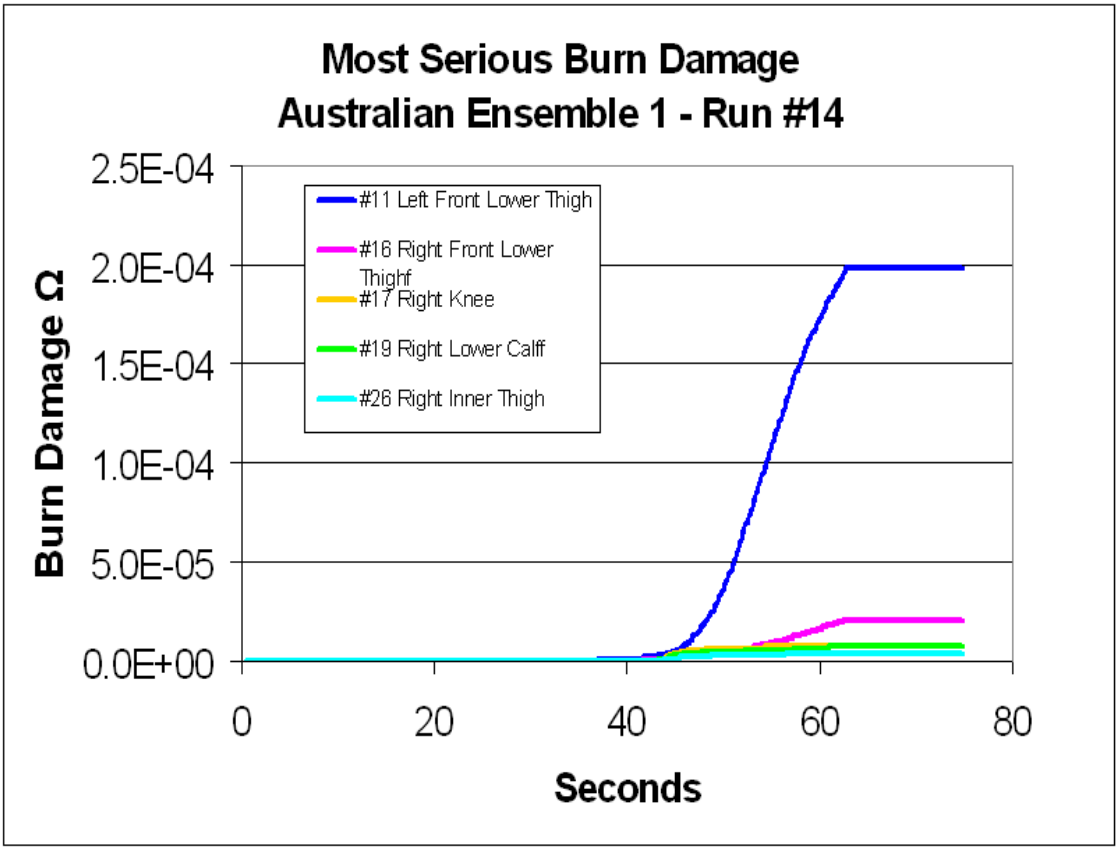

Figure 4-26: Australian Ensemble 1 Ten Second Exposure Run 2

Finally, the doorway test was repeated again for the first Australian Ensemble, returning the results listed in Figure 4-27. Comparing these results to those gathered during the initial doorway test (Figure 4-22) it can be shown that the ensemble did not degrade very much after such large energy exposures, returning relatively similar values for the burn parameters of the most affected sensors.

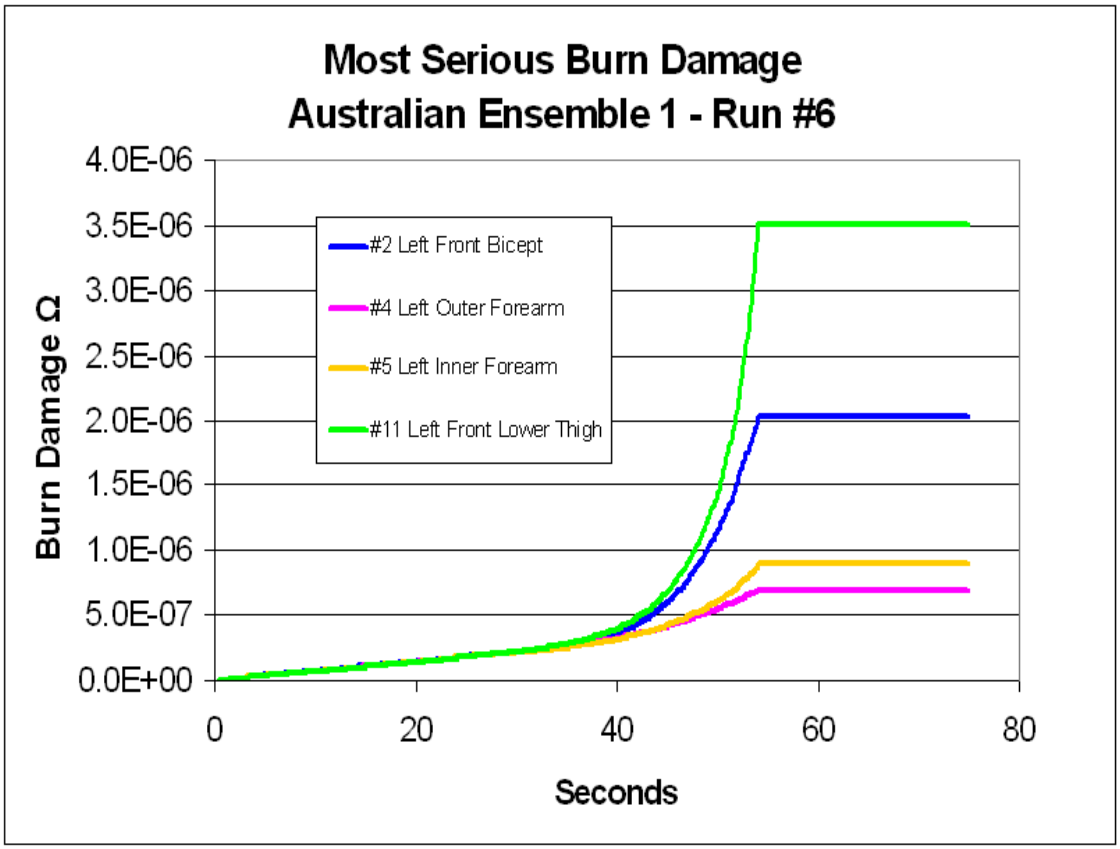

Figure 4-27: Australian Ensemble 1 Doorway Test Run 2

After the ensemble had been tested, it had charring on the undersides of the arms, the lower back, and especially on the font legs. The boots maintained their support and structure, while the helmet appeared sooty, with no damage to it. Finally, the gloves were slightly discolored on the bottom sides, but maintained their integrity. The final condition of the ensemble can be seen in Figure 4-28.

Figure 4-28: Australian Ensemble 1 Post-Test

4.3.2 Australian Ensemble 2

The next ensemble to be tested in the laboratory was the original Australian structural ensemble comprised of a wool coat and fire resistant cotton pants. The remainder of the tested ensemble consisted of the same gloves, helmet, SCBA, and boots that were tested on the first Australian ensemble. The coat was constructed of a 100% Wool Shell, and a 100% Cotton Thermal Liner while the pants were made out of fire resistant cotton. The outfitted manikin can be seen in Figure 4-29.

Figure 4-29: Australian Ensemble 2 Pre-Test

As was done with the other Australian ensemble, the first test for this set of clothing was conducted by moving the manikin into the doorway plane for thirty seconds, exposing it to 504 kJ/m^2. The burn parameter results from this test can be seen in Figure 4-30. Here, it can be noted that the skin burns are much higher than the three layer Australian ensemble had for the same exposure. The difference is nearly three orders of magnitude, indicating that this ensemble provides much less protection than the newer set of clothing. However, for this exposure, the manikins' sensors still recorded burn parameter values of less than one hundredth the threshold for second degree burns.

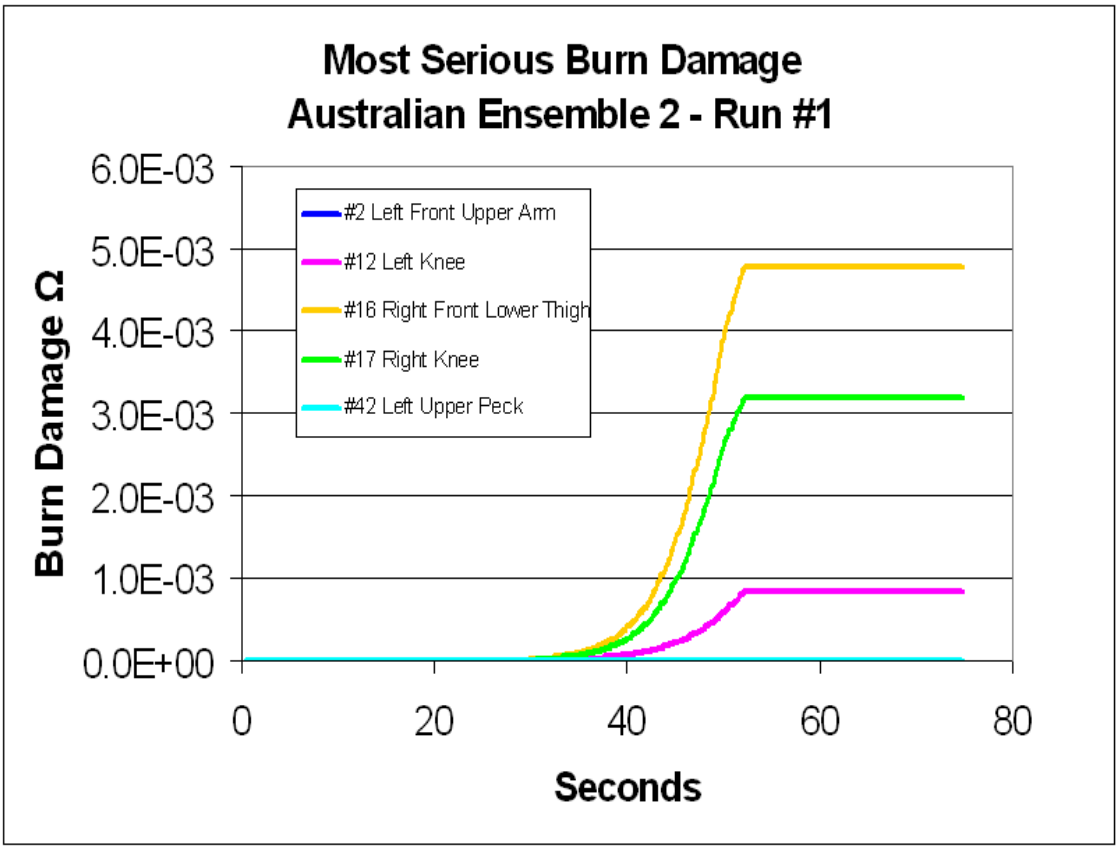

Figure 4-30: Australian Ensemble 2 Doorway Run 1

The 504 kJ/m^2 was only conducted once for this ensemble due to the observed deterioration of the clothing after one test. The burn parameters for the top five sensors can be seen in Figure 4-31. As would be expected, the burn parameter magnitudes did not increase significantly, as the energy exposure did not change; however, the ensemble did appear to be degrading rapidly during the test. Therefore, it was elected that the second run at the six second exposure be abandoned, and the ten second exposure run be completed in order to ensure that data was collected at all exposures.

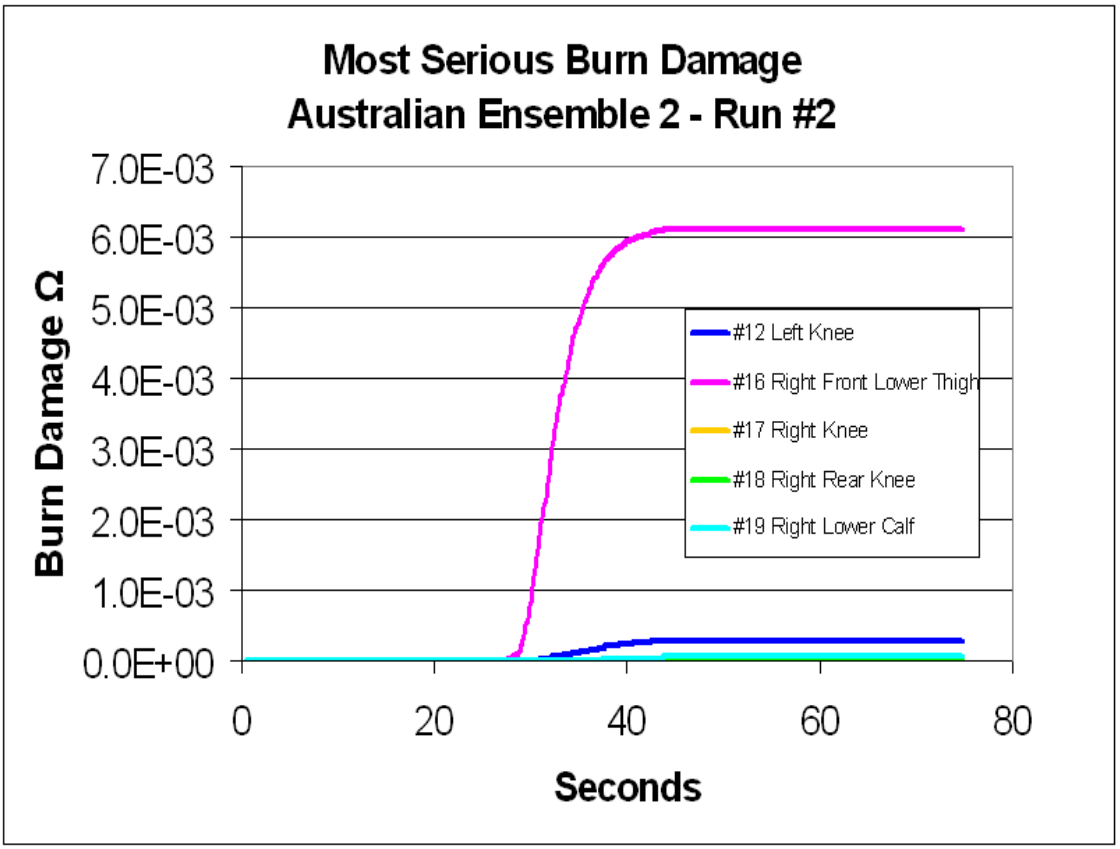

Figure 4-31: Australian Ensemble 2 Six Second Exposure Run 1

The final exposure for the second Australian ensemble was at a speed of 0.16 m/s, an effective energy exposure of 840 kJ/m^2. This test resulted in the near disintegration of the fire resistant cotton pants, and singing of the wool coat, and was therefore declared the final test for the ensemble. The skin burn calculation results for the top ten (separated by top five, and next five) sensors are shown in Figure 4-32 and Figure 4-33. All the sensors listed on these charts recorded skin burn parameters above 1.0, and therefore registered as second degree burns. The skin burn parameters were no longer calculated after the top ten sensors, because these sensors represent over twenty percent of the body area, more than double the tests failing criteria for skin burns.

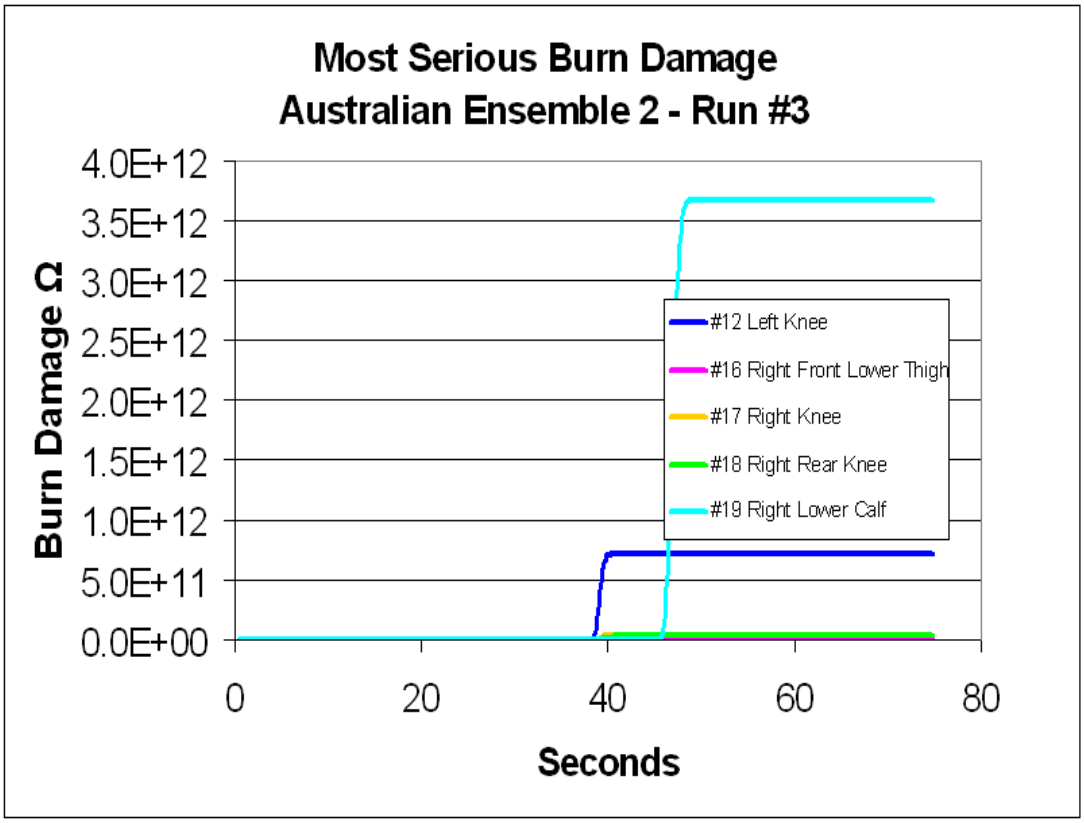

Figure 4-32: Australian Ensemble 2 Ten Second Exposure Top Five Sensors

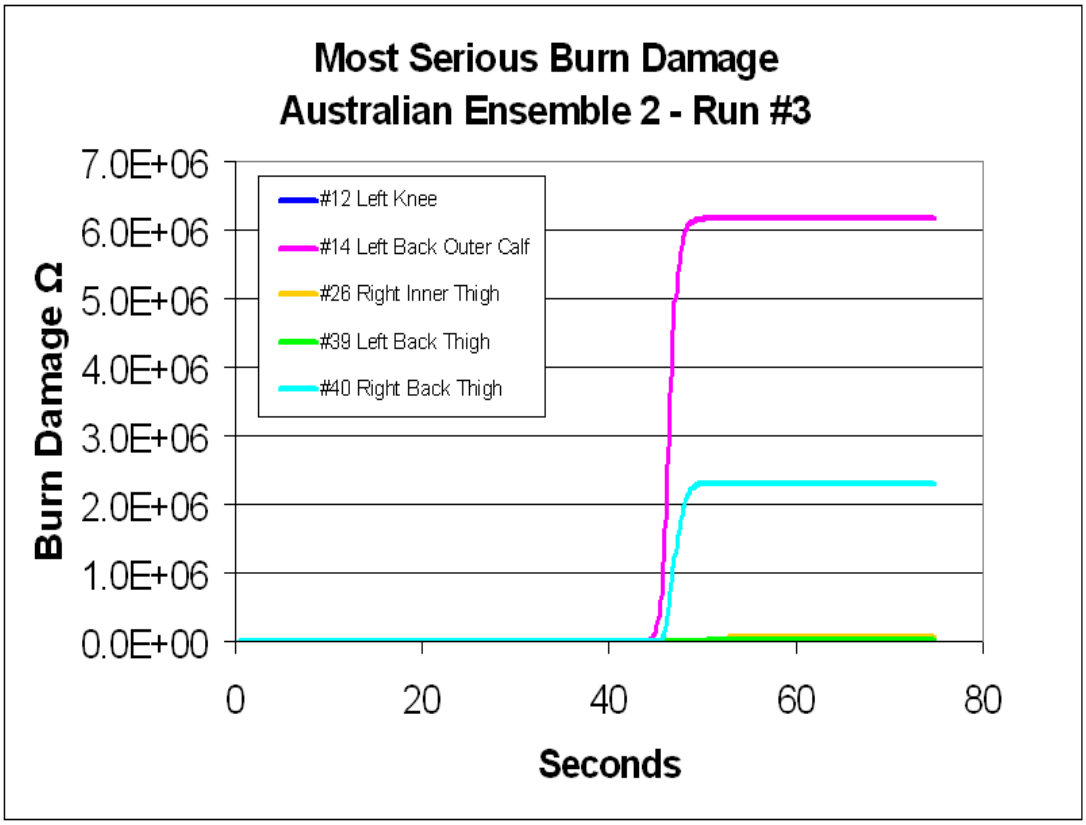

Figure 4-33: Australian Ensemble 2 Ten Second Exposure Second Five Sensors

The locations of the top ten sensors acquiring skin burns can be seen in Figure 4-34. Each of the top ten burned sensors are located on the manikin's legs, which would be expected since the pants disintegrated during the test. Also, it is important to note that it does not appear that any of the sensors that were protected by the wool coat would have failed, although burn parameter calculations were not conducted on those sensors. Overall, it can be stated that over twenty percent of the body would have experienced skin burn injuries if exposed to a fire of this magnitude, wearing this ensemble.

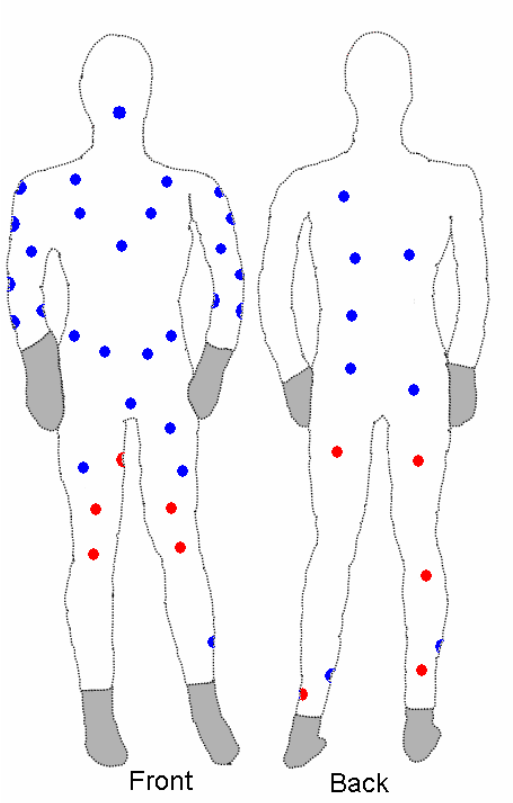

Figure 4-34: Australian Ensemble 2 Skin Burn Locations

After these tests, the Australian ensemble was very deteriorated, especially the pants. The fire resistant cotton was almost completely destroyed around the thighs and calves of the manikin, while the coat was singed slightly, but seemed to maintain its integrity. A photograph of the ensemble after the testing was complete can be seen in

Figure 4-35. The dustpan in this picture contains pieces of the pants that had fallen off during the fire. As the picture depicts, the pants lost their integrity, and did not pass the ensemble test.

Figure 4-35: Australian Ensemble 2 Post-Test

4.3.3 Navy Ensemble

The Navy ensemble consisted of the United States Navy's First Attack fire suit, a Navy helmet and gloves, as well as a Scott SCBA and regular rubber boots. The suit is constructed of a Kevlar/PBI Outer Shell, Nomex Moisture Barrier, and a Kevlar Batt Thermal Liner. The ensemble can be seen as tested in Figure 4-36, without the navy helmet and gloves, and rubber boots.

Figure 4-36: Navy Ensemble Pre-Test

The Navy Ensemble tested during these prototype tests was exposed to the same energy during the runs as the first Australian Ensemble. The first exposure, at the doorway for thirty seconds, resulted in skin burn parameters listed in Figure 4-37. The sensors exposed to the highest energy during this test recorded skin burn parameters nearly one ten-thousandth of the threshold for second degree burns. At this exposure, it seems that the navy suit performs very well.

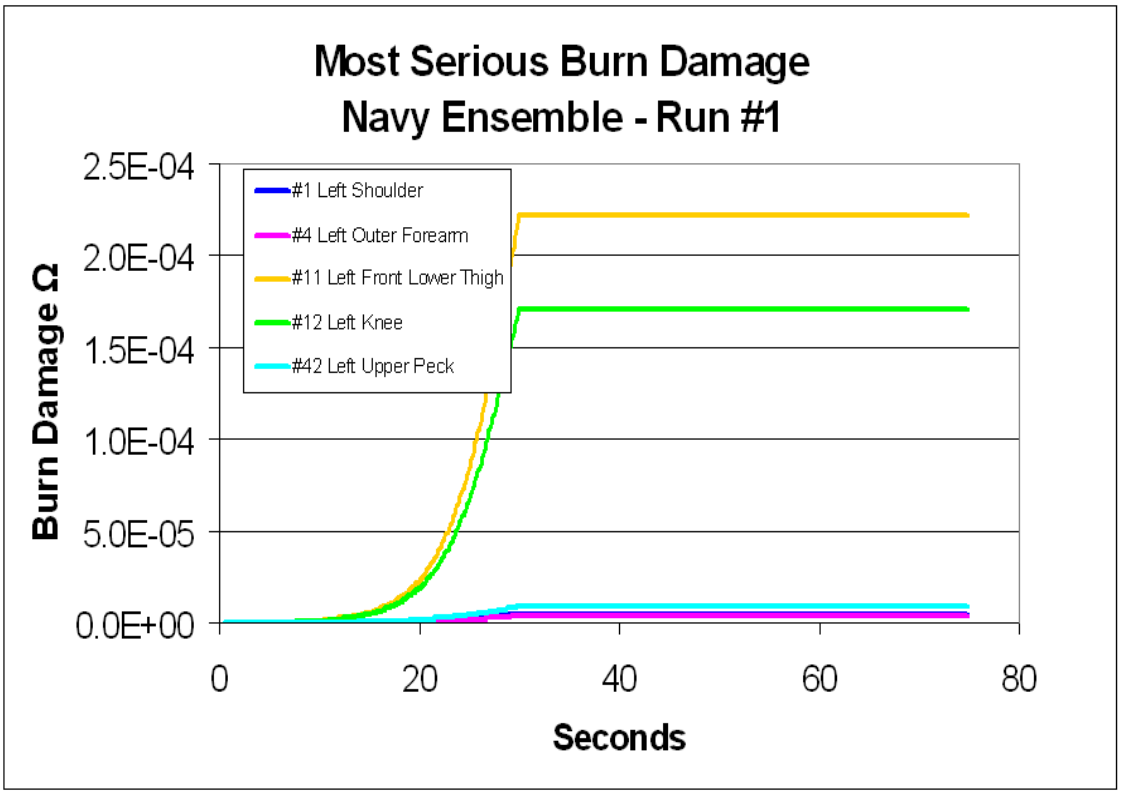

Figure 4-37: Navy Ensemble Doorway Run 1

The next tests conducted on the Navy Ensemble included two test runs at the 504 kJ/m^2 exposure, while traversing the manikin through the burn room at a speed of 0.27 m/s. The burn parameters that were calculated based of the sensors exposed to the highest incident heat flux are recorded in Figure 4-38 and Figure 4-31. After reviewing the calculation results, there were no skin burns at this exposure as well, with burn parameters of similar magnitude to the doorway test, multiple orders of magnitude lower than 1.0, the threshold for second degree burns.

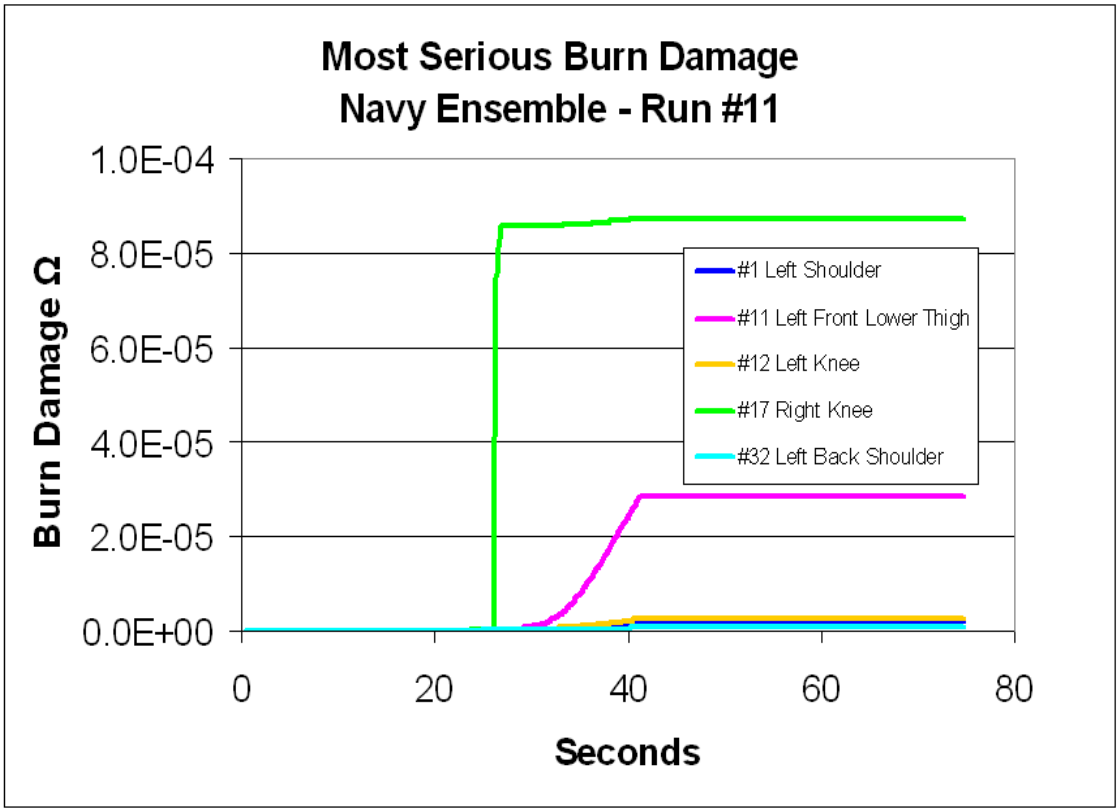

Figure 4-38: Navy Ensemble Six Second Exposure Run 1

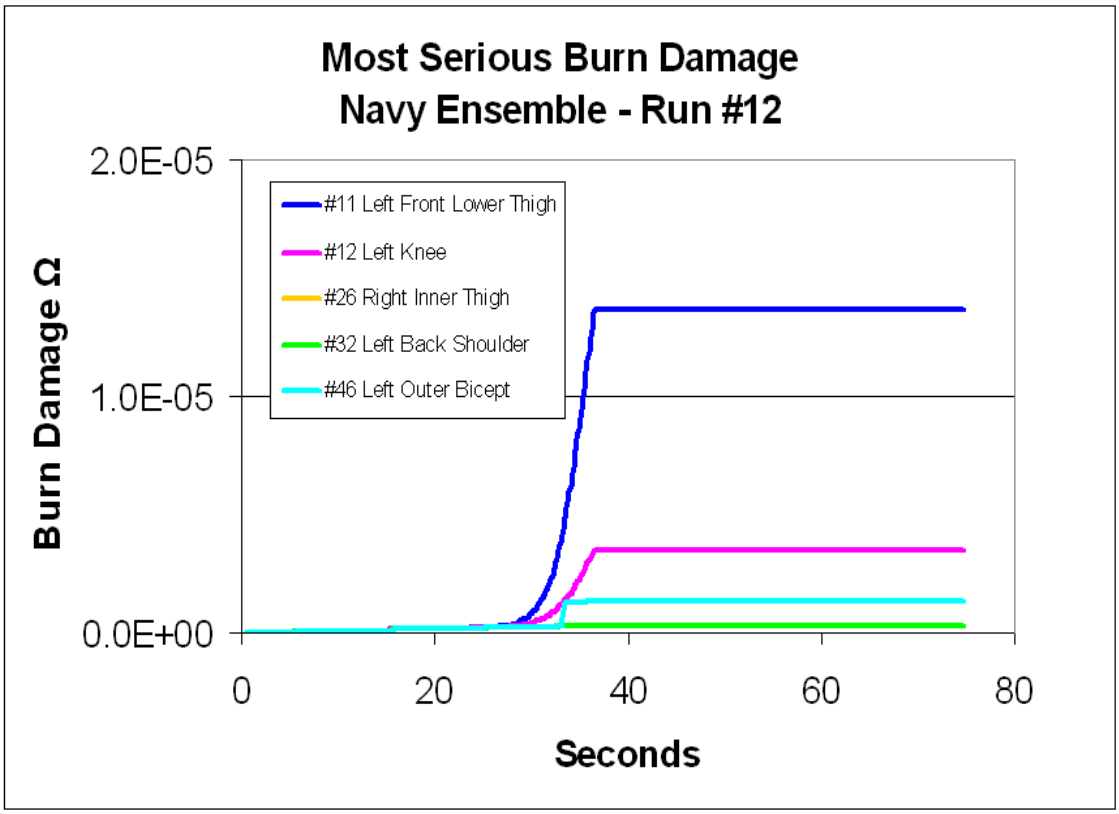

Figure 4-39: Navy Ensemble Six Second Exposure Run 2

The Navy Ensemble was then exposed to 840 kJ/m^2 by traversing the burn room at a speed of 0.16 m/s. These runs are comparable to the ASTM F 1930 test at an exposure time of ten seconds. The burn parameters for these runs, see in Figure 4-40 and Figure 4-41, were higher than the previous tests, but still almost two orders of magnitude below the burn threshold. No sensors on the manikin were exposed to enough energy to cause a skin burn under the navy ensemble.

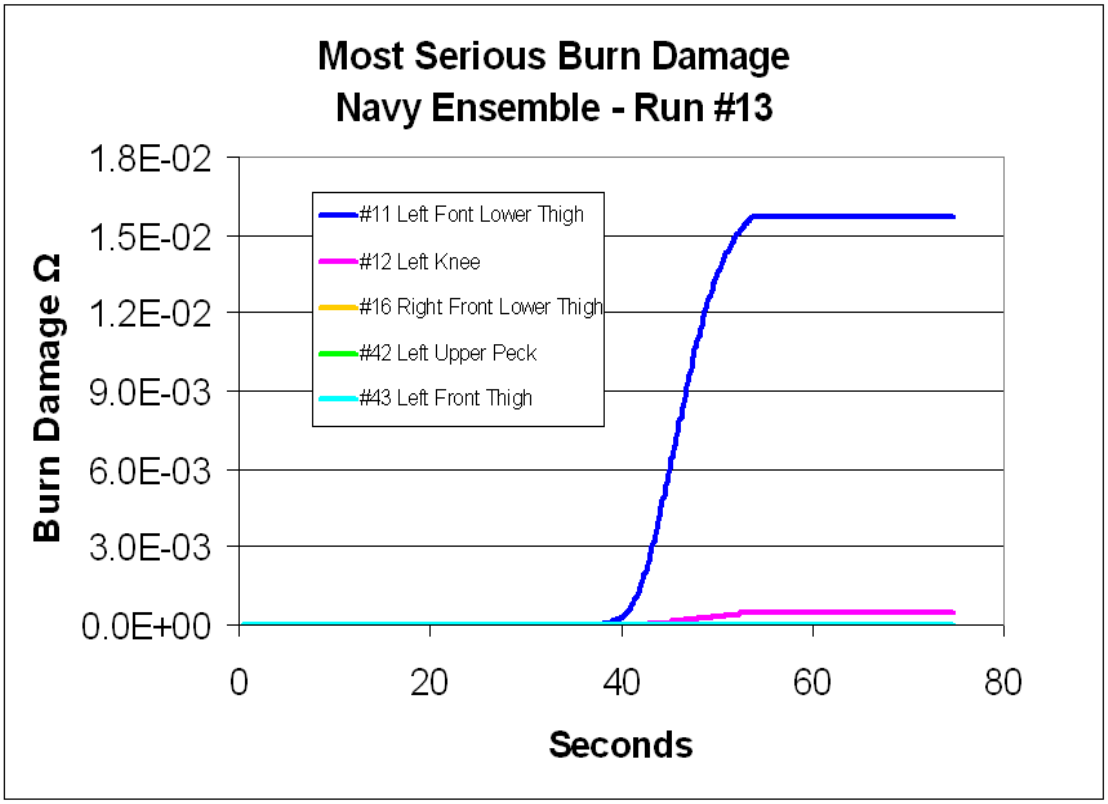

Figure 4-40: Navy Ensemble Ten Second Exposure Run 1

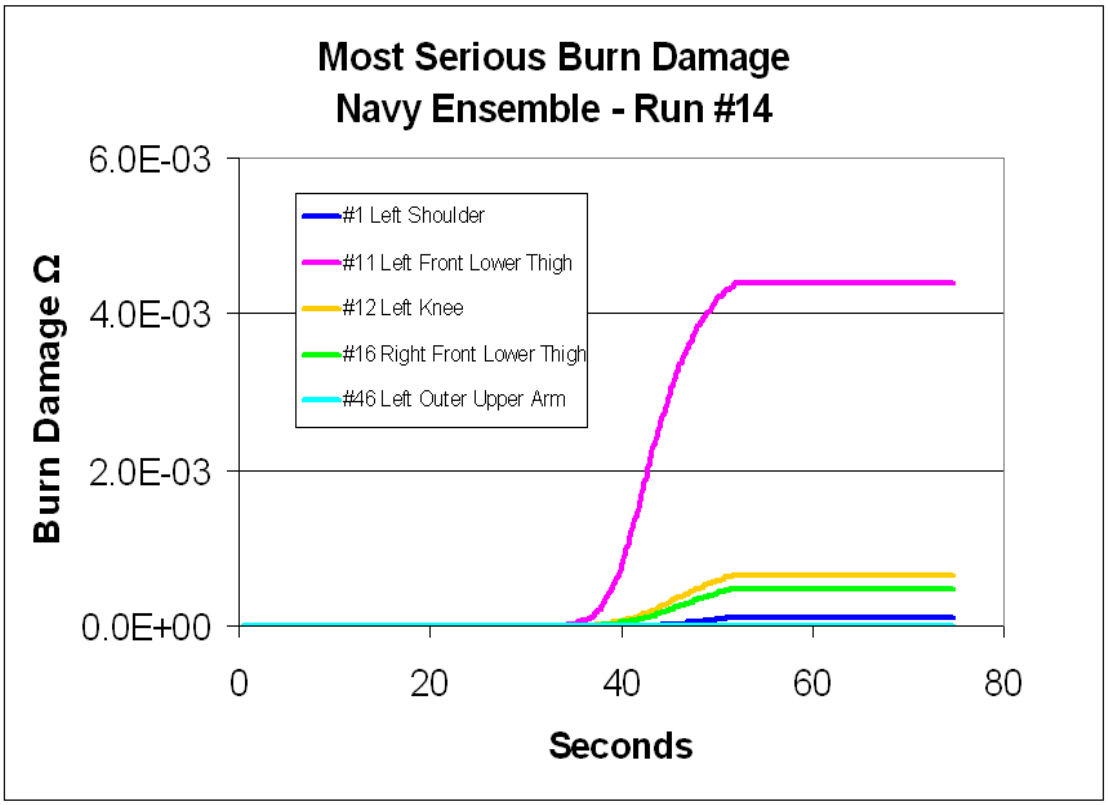

Figure 4-41: Navy Ensemble Ten Second Exposure Run 2

The final test on the navy ensemble was conducted by repeating the original doorway exposure. The results from this final test can be seen in Figure 4-42. According to this test, the second doorway exposure actually resulted in less energy exposure at the sensors than the initial doorway test. This could be a result of charring on the gear, or possibly uncontrollable changes to the laboratory environment. Regardless, after being exposed to multiple large fires, the ensemble did not deteriorate at any noticeable rate.

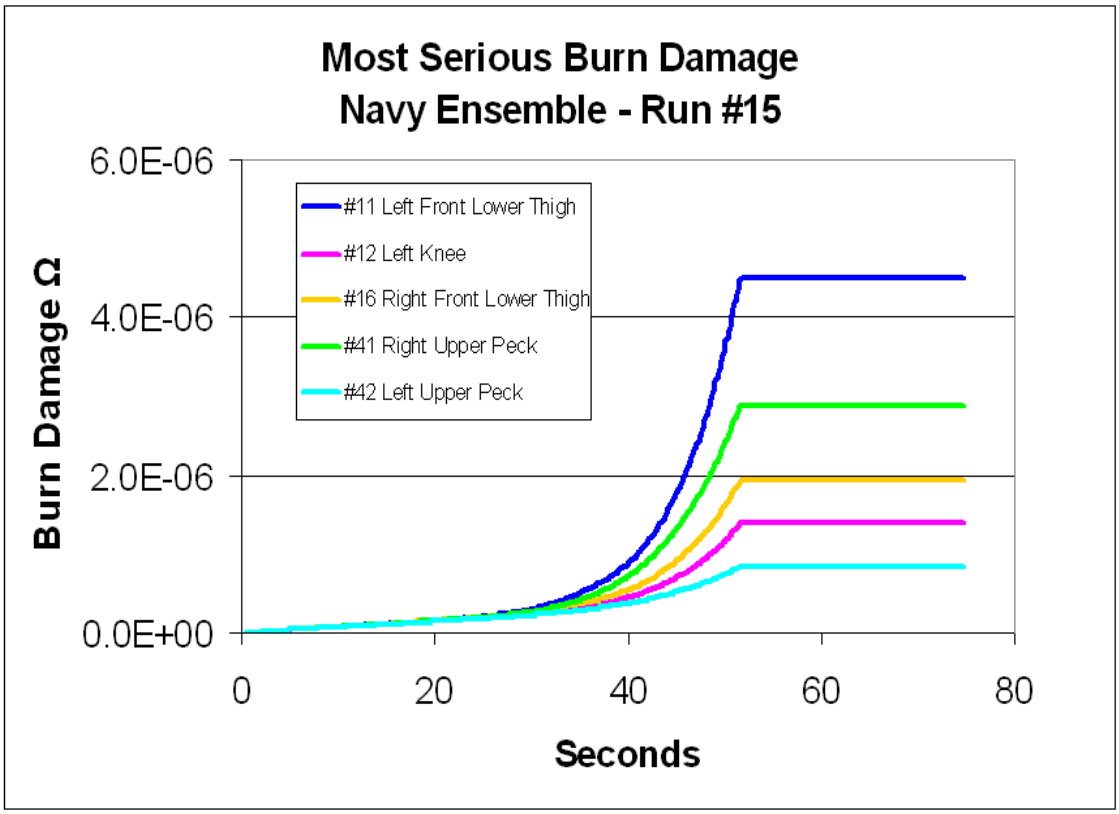

Figure 4-42: Navy Ensemble Doorway Exposure Run 2

After testing was completed on the ensemble, there were a few noticeable changes to the appearance of the protective gear. First, there was much charring in the leg region of the suit, and the helmet and facemask continued to acquire more and more soot. Also, one of the hoses on the SCBA that was exposed near the waist of the manikin melted, exposing the inner aluminum tubing. Since this piece of the apparatus was not designed for use by the person wearing the SCBA, this was not considered a failure. Also, it is possible that the use of this SCBA for so many fire tests caused degradation to the mechanism, which resulted in this failure during the test. Overall, the protective clothing was still in pretty good shape, considering the large fires that it had been exposed to. A picture of the gear post-testing can be seen in Figure 4-43.

Figure 4-43: Navy Ensemble Post-Test

5 Conclusions

5.1 Test Protocol

Based on the research collected, other fire fighter protective clothing tests, and our prototype testing, a sample test procedure was defined. The procedure generates comparable results to the ASTM F 1930 tests, exposing the manikin to equivalent total energy. The difference is that this test evaluates the entire fire fighter ensemble under more realistic fire conditions.

The defined testing procedure requires that all test runs be conducted with fire conditions in the room set to a 1.5 MW fire. Also, all test runs will include protecting the manikin from incident flux with the thermal shield until the fire has reached steady state. Finally, there must be sufficient time between tests for the manikin's sensors to cool back to near-ambient temperatures.

The tests are designed as increasingly severe tests, while also evaluating the ensembles deterioration after multiple exposures. The first test involves moving the manikin into the doorway plane and collecting heat flux data for 30 seconds. The manikin was exposed to 510 kJ/m^2 (as calculated in Section 3.5) which is equivalent to the six second exposure at 84 kW/m^2 Thermo-Man test. As the least energy exposure, and a purely radiative exposure, this test run is the baseline test for determining ensemble deterioration.

The next two runs are procedurally equivalent, ensuring that the test is both repeatable while also monitoring some level of material deterioration. This test includes moving the clothed manikin through the burn room at a rate of 0.27 m/s calculated in

Section 3.5. This test run also exposes the manikin to 510 kJ/m^2; however, it exposes both the front and the back of the manikin equivalently. This test offers an opportunity for the impact of direct flame impingement to be quantified.

The next two tests are conducted similar to the previous two, but with a slower traversal speed. The speed is now reduced to 0.16 m/s, making it a more severe test. This traversal rate exposes the manikin to 840 kJ/m^2, equivalent to a ten second Thermo-Man exposure at 84 kW/m^2.

The final test on the manikin is a repeat of the initial run where the manikin stopped in the doorway plane for 30 seconds. This test is included for comparison purposes to the first doorway test. Since the constant fire size of 1.5 MW emits a constant amount of energy to the doorway, this run evaluates ensemble deterioration while, in theory, holding all other variables constant. If the incident fluxes on the manikin's sensors are higher in this second doorway evaluation, then it can be concluded that ensemble deterioration has occurred.

This test evaluates fire fighter protective ensembles in more real-world fire scenarios compared to the ASTM F 1930 tests. Current fire fighter clothing tests utilize jet flame exposures that are rarely experienced by structural fire fighters, and do not test the full protective gear. This test allows for multiple aspects of ensemble protection to be evaluated, including radiative protection, flammability defense, and material deterioration over multiple fire exposures. The flame source used by this protocol is more characteristic of that produced in structural fires, and provides an accurate basis to test fire fighter ensembles. All these aspects are important when considering the intensity and quantity of exposures that fire fighters will encounter while relying on their gear to

protect them from skin burns. Also, if there is any life threatening equipment failures occur (i.e. material ignites or melts in areas with skin exposure, SCBA hoses melt or rupture, etc.), the ensemble will be considered a failure.

This study recommends that an ensemble fails if it allows the user to suffer ten percent or more of their total body area with second degree burns. Criteria were chosen based on the medical professions definition of a life threatening burn. Burn victims with ten percent second degree burns are immediately transferred to a specialized burn unit. This study acknowledges that medical treatment may be necessary for minor burns after extreme exposure such as in our test, but considers the severe case as unacceptable (refer to Section 2.7).

5.2 Prototype Ensemble Test Evaluation

The test protocol was applied to three different protective ensembles. Australian Ensemble 1 and the Navy jumpsuit passed the test as predicted, because the compositions were of advanced materials and new technologies. The second Australian ensemble (Australian Ensemble 2) was comprised of wool and FR cotton, and failed the test; resulting in over 20% of the TBA to suffer from second degree burns. The results were consistent with our expectations based on the composition of the ensembles.

5.3 General Recommendations

A list has been compiled of recommendations for future updates to the laboratory before resuming testing. The first recommended task would be to purchase a new computer to run the data acquisition hardware. Over the course of the project, four computers were used to run the equipment and did not have sufficient processor speed to

collect the required data. The suggestion would be to purchase a new laptop for the purpose of running LabView and gathering data. Once the data is obtained, the laptop could be brought back and stored at WPI to avoid damage from weather exposure.

Once a new computer is purchased, the next project group should look into constructing more copper slug sensors for the manikin. Currently there are 42 sensors on the manikin that work reliably. It is suggested that more accurate sensors be developed or purchased and then evenly distributed throughout the body. Defining the exact area of the body that each sensor covers is also necessary. To accommodate more sensors, a new data acquisition system should be designed, or at least a new connection card for the data acquisition board should be purchased. The existing card has ten broken connections, which reduce the amount of wires that can be run from the manikin to the data acquisition hardware.

Maximum fire size was not achieved due to restrictions in the flow. Based on the manufacturer's recommendation, the flow controller should be returned for a cleaning and repair because, in its current state, the flow rate is being limited to 60 percent of its potential.

Currently, the pilot flame is often extinguished before propane ignition. This is an indication that ignition procedures are in need of revision. Possible solutions include a propane pilot light or purging the system of nitrogen prior to ignition.

The research that has been compiled is just the beginning of the development of more realistic fire fighter protective clothing tests. It is suggested that the recommended test procedure be used to evaluate more brands of fire fighter clothing. Research should

be completed to determine if this developed test protocol could someday become a required standard for all fire fighter clothing companies.

6 References

American Burn Association. "Burn Unit Referral Criteria." Ameriburn.org. 1999. http://www.ameriburn.org/BurnUnitReferral.pdf. 10 April 2006.

Barter et al, "An Improved Mannequin Test", Major Qualifying Project, Worcester Polytechnic Institute, 2004.

Beyler, PhD., Craig L., et al. "Predicting 1st and 2nd Degree Skin Burns from Thermal Radiation." *Engineering Guide*. Society of Fire Protection Engineers, 2000.

Bradbury et al, "Traversing Mechanism for Clothing Flammability Test", Major Qualifying Project, Worcester Polytechnic Institute, 2001.

DuPont. Technical Brief: Nomex IIIA©. Richmond: DuPont, 2006.

Fay, Terry S., "Development of an Improved Fabric Flammability Test", M.S. Thesis, Worcester Polytechnic Institute, 2002.

Fire-Dex. 2006. Fire-Dex, Inc. 19 Mar. 2006. http://fire-dex.com/.

Gagnon, Brian D., "Evaluation of New Test Methods for Fire Fighting Clothing", M.S. Thesis, Worcester Polytechnic Institute, 2000.

Globe Holding Company, LLC. Globe Firefighter Suits. Available: http://www.globefiresuits.com/. 25 Mar. 2006.

Leblanc, David. Fire Environments Typical of Navy Ships. MS Thesis, Worcester Polytechnic Institute, 1998.

Lion Apparel. Lion Apparel, Inc. Available: http://www.lionapparel.com/index.html. 23 Mar. 2006.

Mell, William E. and Lawson, J. Randall. A Heat Transfer Model for Fire Fighter's Protective Clothing. Gaithersburg: National Institute of Standards and Technology, 1999.

Naradzay MD, Jerome et al. "Burns, Thermal." eMedicine.com. eMedicine. http://www.emedicine.com/emerg/topic72.htm. 13 April 2006.

NFPA 1971-Protective Ensemble for Structural Fire Fighting, 2000 Edition. National Fire Protection Agency, Quincy, MA.

NFPA 2112- Standard on Flame-Resistant Garments for Protection of Industrial Personnel Against Flash Fire 2001 Edition. National Fire Protection Agency, Quincy, MA.

Sipe, Joel E., "Development of an Instrumented Dynamic Mannequin to Rate the Protection Provided by Protective Clothing", MS Thesis, Worcester Polytechnic Institute, 2004.

Southern Mills, Inc. Southern Mills. Available: http://www.southernmills.com/. 23 Mar. 2006.

Woodward, Andrew B., "Fire Scenarios for an Improved Fabric Flammability Test", M.S. Thesis, Worcester Polytechnic Institute, 2003.

Wholesale Fire and Rescue Ltd. WFR. Available: http://www.wfrfire.com/. 20 Mar. 2006.

Appendix A: Heat Transfer through Fire Fighter Clothing

Radiant heat transfer or direct flame contact causes heat transfer through protective clothing. This energy will eventually reach the skin, resulting possibly in burns or injury of different severities. The heat transfer upon and through the ensemble will involve conduction, convection, and thermal radiation. (Mell and Lawson, 10)

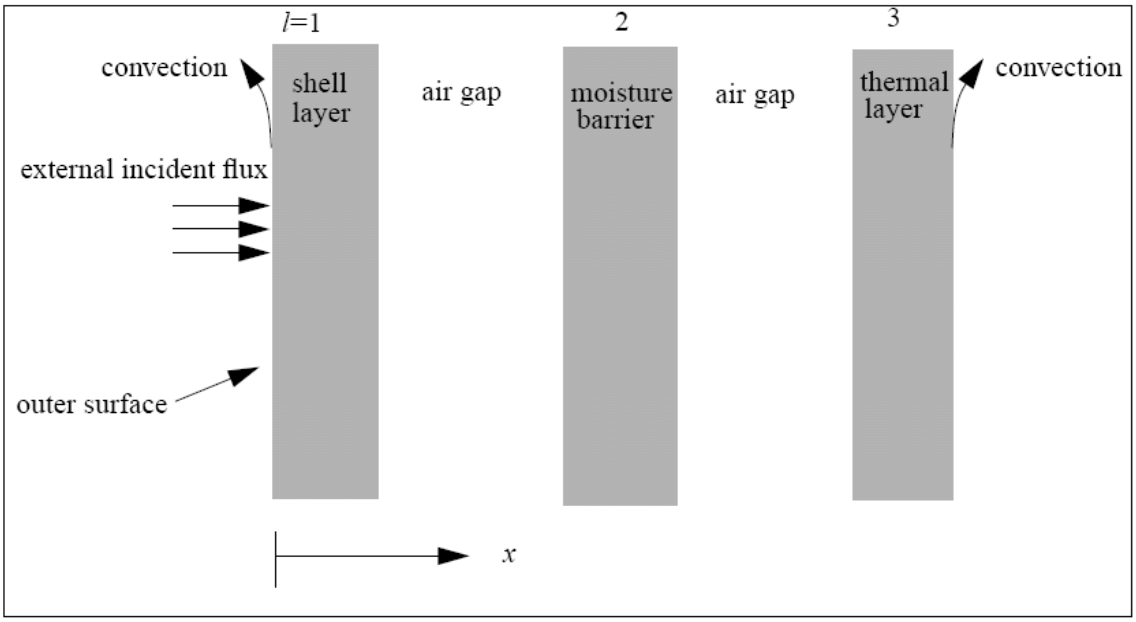

Figure 0-1: Cross-section of a typical three layered fire fighter ensemble in ambient conditions. (Mell and Lawson, 10)

For simplicity, it is assumed that convection occurs only on the outside of garment, therefore entering through the boundary conditions of the heat transfer model. A planar, one dimensional approach was used to model the energy transfer. The first step in developing the model is to set up the heat transfer equation (Equation 1).

$$\rho c_p \frac{\partial T}{\partial t} = -\frac{\partial q_{CD}}{\partial x} - \frac{\partial q_R}{\partial x} + g$$

Equation 1: One-Dimensional Governing Equation for Conservation of Energy (Mell & Lawson, 11)

With the respected fluxes represent by:

$$q_{\mathrm{CD}} = -k\frac{\partial T}{\partial x}$$

Equation 2: Conduction Flux or Fourier Law (Mell and Lawson, 11)

$$q_{\mathrm{R}}$$

Equation 3: Radiation Flux (Mell and Lawson, 11)

Equation 1 must be solved for each air gap or material layer within the ensemble, and requires both initial and boundary conditions. In order to solve for temperature distribution through each layer, Equation 2 is solved in conjunction with the radiative heat transfer equation. (Mell and Lawson, 10)

$$\frac{1}{\kappa_\lambda}\frac{dI_\lambda(s,\theta,\phi)}{ds} + I_\lambda(s,\theta,\phi) = I_{\mathrm{b},\lambda}[T(s)]$$

s = The Path Length of the Radiation Beam in the $\hat{\Omega}$ Direction, θ and ϕ= Polar and Azimuthal Angles Locating the Beam of Radiation in a Spherical Coordinate System, $I_{\mathrm{b},\lambda}$= Blackbody Spectral Intensity, T= Temperature

Equation 4: Radiative Transfer Equation (Mell and Lawson, 11)

Equation 4 represents the radiative heat transfer equation for the spectral intensity I_λ. This equation has been simplified, assuming thermodynamic equilibrium, the absence of scattering, and the validity of Kirchoff's Law. The spectral intensity is then split into forward (positive x) and backward components, (I^+ and I^-). (Mell and Lawson, 11)

$$I_\lambda = I_\lambda(x,\hat{\Omega}) = I_\lambda^+(x,\hat{\Omega}) + I_\lambda^-(x,\hat{\Omega}) = I_\lambda^+(x)\delta(\beta-1) + I_\lambda^-(x)\delta(1+\beta)$$

Equation 5: Spectral Intensity (Mell and Lawson, 11)

Equation 5 is now solved for all material layers (assuming that air gaps are nonparticipating) in both the backward and forward components of the spectral intensity. (Mell and Lawson, 11)

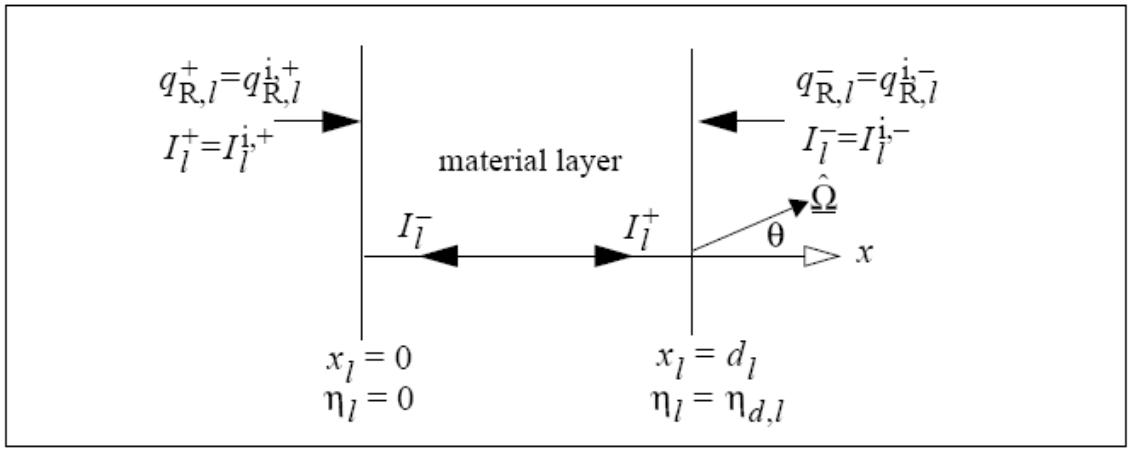

Figure 0-2: Thermal Radiation Model in an Arbitrary Material Layer (Mell and Lawson, 12)

The solution to Equation 6 is represented:

$$I^{+}_{\lambda}(x) = I^{i,+}e^{-\eta} + \int_0^{\eta} I_b e^{-(\eta-\eta')}d\eta',$$

$$I^{-}_{\lambda}(x) = I^{i,-}e^{-(\eta_d-\eta)} + \int_{\eta}^{\eta_d} I_b e^{-(\eta'-\eta)}d\eta',$$

Equation 6: Solution to the Radiative Heat Flux Model (Mell and Lawson, 12)

With:

$$\eta_{\lambda} = \int_0^{x} \kappa dx'$$

The net radiative heat flux can now be solved for by integrating Equation 6. (Mell and Lawson, 12)

$$q^{+}_{R}(\eta) = q^{i,+}_{R}e^{-\eta} + \sigma\int_0^{\eta} T^4(\eta')e^{-(\eta-\eta')}d\eta',$$

$$q^{-}_{R}(\eta) = q^{i,-}_{R}e^{-(\eta_d-\eta)} - \sigma\int_{\eta}^{\eta_d} T^4(\eta')e^{-(\eta'-\eta)}d\eta'$$

Equation 7: Net Radiative Heat Flux for Heat Transfer though Protective Clothing (Mell and Lawson, 12)

The first terms on the right-hand-side of Equation 7 represent the flux from radiation entering the layer. The second terms are representative of the flux due to self emission (Mell and Lawson, 12). In most cases it is assumed that the flux from self emission within a material is much smaller than the absorbed flux from external incident flux. This causes Equation 7 to reduce to the Beer-Lambert Law. (Mell and Lawson, 13)

$$q_{\mathrm{R},\,l} = q^{+}_{\mathrm{R},\,l} + q^{-}_{\mathrm{R},\,l} = q^{\mathrm{i},+}_{\mathrm{R},\,l} e^{-\eta_l} + q^{\mathrm{i},-}_{\mathrm{R},\,l} e^{\eta_l - \eta_{d,\,l}}$$

Equation 8: Beer-Lambert Law (Mell and Lawson, 13)

The absorptivity (α), transmissivity (τ), and reflectivity (r) of a material can be related by:

$$\alpha + r + \tau = 1$$

By assuming a constant absorptivity coefficient within a layer, the transmissivity and reflectivity can be determined. (Mell and Lawson, 13)

$$\tau_l = \frac{q^{+}_{\mathrm{R},\,l}(\eta_{\mathrm{d},\,l})}{q_{\mathrm{in}}} = \frac{(1 - r_l) q_{\mathrm{in}} e^{-\kappa_l d_l}}{q_{\mathrm{in}}}$$

q_{in} = Radiative Flux Entering the Layer Material

Equation 9: Transmissivity of the Fabric Layer (Mell and Lawson, 13)

Equation 9 results in the solution for the absorption coefficient of the ensemble layer:

$$\kappa_l = \frac{1}{d_l} \ln\left(\frac{1 - r_l}{\tau_l}\right)$$

Equation 10: Absorption Coefficient of Material Layer (Mell and Lawson, 13)

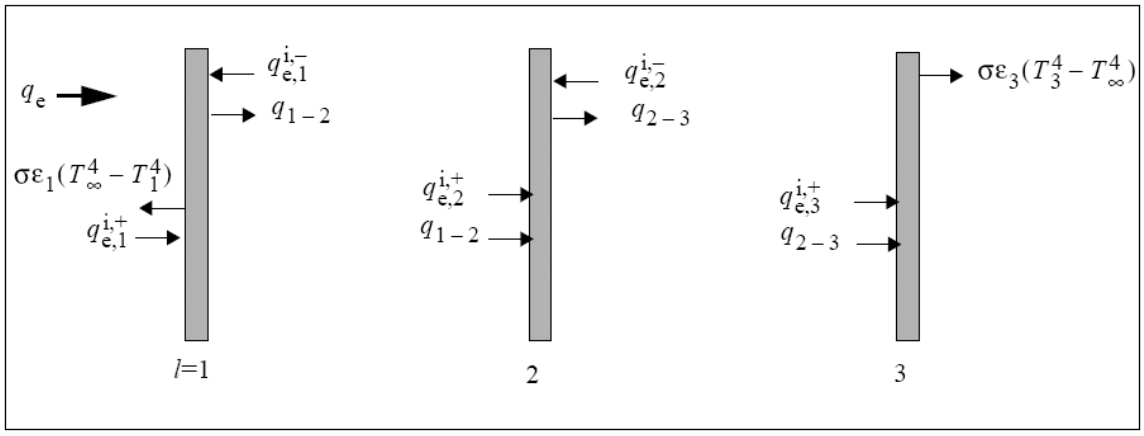

Figure 0-3: Radiant heat fluxes through the Fire Fighter Clothing Surrounded by Ambient Air (Mell and Lawson, 14)

Each material layer encounters the following heat flux:

Fabric Layer 1

$$q^{i,+}_{e,1} = q_e(1-r_1)$$

$$q^{i,-}_{e,1} = -r_2 q^{+}_{R,1}(\eta_{d,1}) = -q_e r_2(1-r_1)e^{-\eta_{d,1}}$$

Fabric Layer 2

$$q^{i,+}_{e,2} = (1-r_2)q^{+}_{R,1}(\eta_{d,1}) = q_e(1-r_2)(1-r_1)e^{-\eta_{d,1}}$$

$$q^{i,-}_{e,2} = -r_3 q^{+}_{R,2}(\eta_{d,2}) = -q_e r_3(1-r_2)(1-r_1)e^{-(\eta_{d,1}+\eta_{d,2})}$$

Fabric Layer 3

$$q^{i,+}_{e,3} = (1-r_3)q^{+}_{R,2}(\eta_{d,2}) = q_e(1-r_3)(1-r_2)(1-r_1)e^{-(\eta_{d,1}+\eta_{d,2})}$$

$$q^{i,-}_{e,3} = 0$$

The resulting heat flux on the right hand side of the material can be used to predict time to skin burns. This information is beneficial in determining protective gear performance and will aid in the development of future fire fighter clothing.

Appendix B: Sipe 2004 Sensor Energy Balance

(Provided by J. Sipe 2004 Thesis)

3.2.2. Sensor Design

The design that was used for the sensors is shown in figure 19 along with the energy balance for a radiant exposure. The sensor is basically a copper disk about the size of a penny mounted in the thermoset polymer sensor body from the existing Navy mannequin sensors. The front faces of the sensors were machined on a lathe to add a cylindrical hole to fit the disk. The disk is 1/16" (1.6 mm) thick and ¾" (19 mm) in diameter. The disks are machined from Copper 110 alloy (ρ=8910 kg/m^3, c_p=0.385 kJ/kg). There is a ¼" air gap behind the sensor insulating the back face.

Figure 19- New Copper Slug Sensor Design

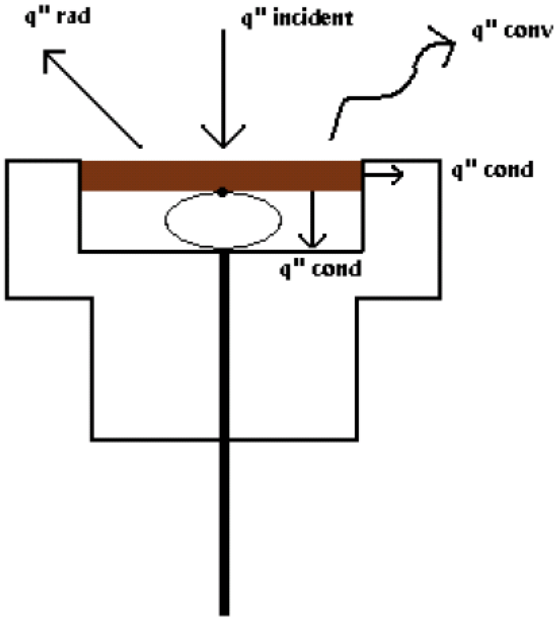

Disk temperature is measured by a 30 gauge type T thermocouple. The thermocouple bead is glued to the back of the mannequin and the glue has been shown to be durable to temperatures up to 100 deg C. Alternative methods of attaching the bead could include intrinsically welding it to the back face, or possibly soldering. Attempts were made to weld the wires to the disk, but the extremely thin diameter of the wire (0.254 mm)(Omega, 2000) prevented a good weld from being made. Solder was judged to add too much mass to the disk and would therefore add thermal inertia and cause the disk to act as if it had a greater thickness.

3.2.3. Sensor Operation

The operation of the sensors is outlined in the following energy balance. If a control volume is placed surrounding the disk. Then conservation of energy tells us that:

$$\varepsilon \dot{q}''_{incident} - \dot{q}''_{conv} - \dot{q}''_{rad} - \dot{q}''_{cond} - \dot{q}''_{storage} = 0 \qquad \text{(Eq. 16)}$$

$$\dot{q}''_{storage} = \rho c_p dL \frac{dT}{dt} \qquad \text{(Eq. 17)}$$

Eq. 16 can be re-arranged to solve for the incident heat flux:

$$\dot{q}''_{incident} = \frac{1}{\varepsilon}\left[\rho c_p dL \frac{dT}{dt} + \dot{q}''_{conv} + \dot{q}''_{rad} + \dot{q}''_{cond}\right] \qquad \text{(Eq. 18)}$$

The convective and radiative losses can be defined as a Newtonian cooling term and a function of temperature to the fourth power respectively:

$$\dot{q}''_{conv} = h(T(t) - T_\infty) \qquad \text{(Eq. 19)}$$

$$\dot{q}''_{rad} = \varepsilon\sigma\left(T(t)^4 - T_\infty{}^4\right) \qquad \text{(Eq. 20)}$$

The conductive losses can actually be broken into two distinct components, as shown in figure 13. There will be a radial and an axial conductive loss. Assuming that there is no contact resistance, these will be governed by equation 20.

$$\dot{q}''_{cond} = kL_{gap}\left(T(t) - T_{air}\right) \qquad \text{(Eq. 21)}$$

This assumes that there is no free convection occurring in the air gap. To justify this assumption a Grashof number can be calculated. Grimes gives a minimum Grashof number of 8000 as the threshold for free convection for vertically inclined surfaces, and a value of 2000 for horizontal surfaces (Grimes, 1993). If a Grashof number is defined as:

$$Gr = \frac{\rho^2 g \beta \Delta T x^3}{\mu^2} \qquad \text{(Eq. 22)}$$

where:

ρ = ambient air density (kg/m^3)

g = acceleration of gravity (m/s^2)

$\beta = T^{-1}$ (K^{-1})

$\Delta T = T_{disk} - T_{\infty}$

x = air gap thickness (m)

μ = viscosity of air

and the following properties are used for the air gap:

$\rho = 0.88$ kg/m^3

$g = 9.8$ m/s^2

$\beta = 1/273$ K^{-1}

$\Delta T = 127$ K

$x = 0.00635$ m

$\mu = 2.286 * 10^{-6}$

then the Grashof number can be calculated to be 1740. This is below the values of 8000 and 2000 at which free convection will begin on a vertical or a horizontal surface respectively. This indicates that the assumption of conduction into that air is a justified one. Air has a thermal conductivity of k = 0.0033W/m*K at a temperature of 400 K, higher than the disk is expected to reach. At this temperature the conductive heat flux into the air gap will be 0.0266 W/m^2. Since this is several orders of magnitude lower than the incident fluxes being measured it will be neglected for this analysis. The radial conduction values will be higher than the axial conduction values, but they are assumed to be negligible as well. The reason that they are not calculated is the changing temperature of the sensor body. There will be a temperature gradient in the thermoset polymer so the radial conduction will vary not only with time, but axial location. This spatial and temporal dependence is outside the scope of this simple energy balance, and for practical reasons it is ignored. The validity of this assumption is addressed later.

Appendix C: Manikin Suspension Models

Ideation/Invention:

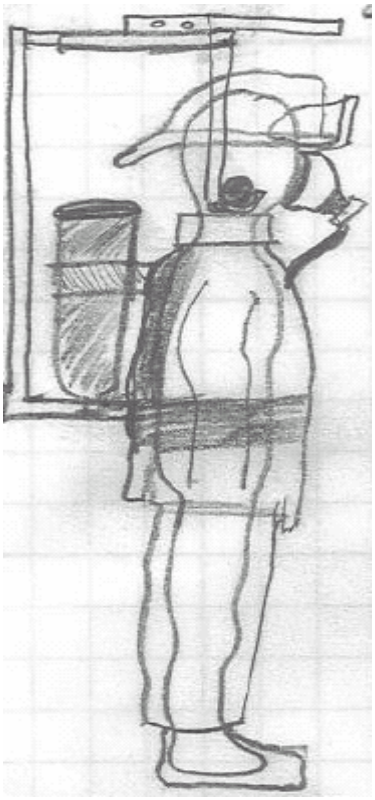

Square Head – U-shaped Back (MODEL 1):

This design is an expansion of the current suspension design. In it, the head supports are both widened and lowered to accommodate the inclusion of a helmet during testing procedures. The bar behind the manikin was also extended to allow for self-contained breathing apparatus, and pushes directly the SCBA harness, which would be applying pressure to the manikin anyway.

Pros

This model is quite similar to the current design, allowing for easy installation and machining. The U-shaped bar will allow for sufficient space for SCBA packs to be included in full ensemble tests. The bar will press against the pack at the SCBA belt such that minimal inference to the sensors will occur.

Cons

The U-shaped support bar may limit the size and shape of the SCBA units tested. Varying geometry of the SCBA packs could not guarantee that the support bar will hit at the belt, causing unwanted pressure points.

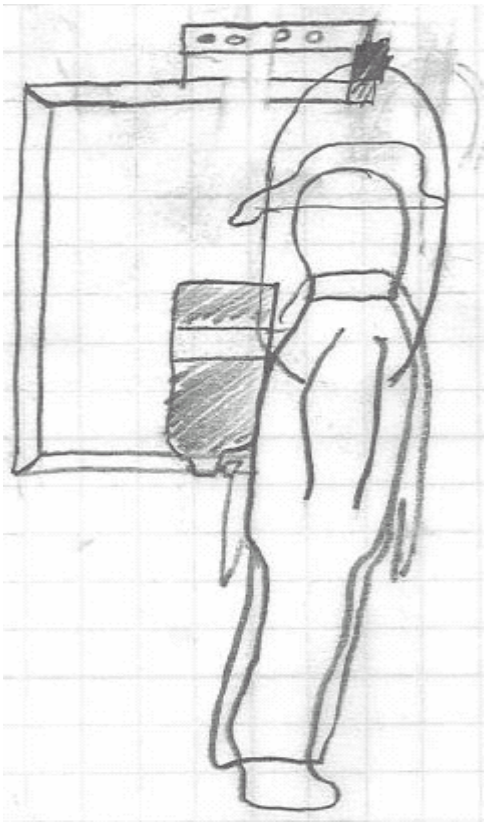

Chain Under Arms (MODEL 2):

This design uses two chains to support the manikin from under its arms. The chains run from the chain-mechanism down below the armpits, while a bar runs vertically down the manikin's back to keep it from swaying when moving.

Pros

This design would allow for minimal suspension interference with the ensemble pieces. Helmets and SCBA packs of various geometry could be tested with no obstruction from the under arm supports. This design would also be cost affective and quickly manufactured.

Cons

The weak connections between the arms and the shoulders of the manikin could easily fail during testing. Significant pressure points would also be caused by this type of suspension system.

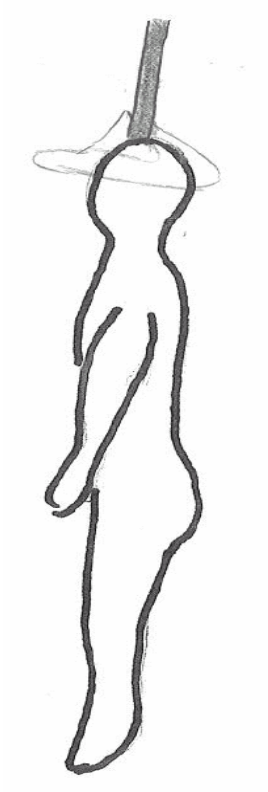

Hole in the Head (MODEL 3):

This design requires modification of the manikin, and any helmet that may be tested. It involves drilling a hole vertically down into the head of the manikin and inserting a rod. This rod would then connect directly to the support track. A helmet would also have to have this whole in it to be tested.

Pros

This model would allow excellent versatility for testing a wide variety of gear with minimal suspension interference. Dressing and maintaining the manikin would be effortless because all portions of the manikin are easily accessible.

Cons

The process of drilling a hole through the head of the manikin and every helmet tested would be incredibly difficult and damaging to test results. The head of the manikin may not provide sufficient strength to support the manikin and all the test gear.

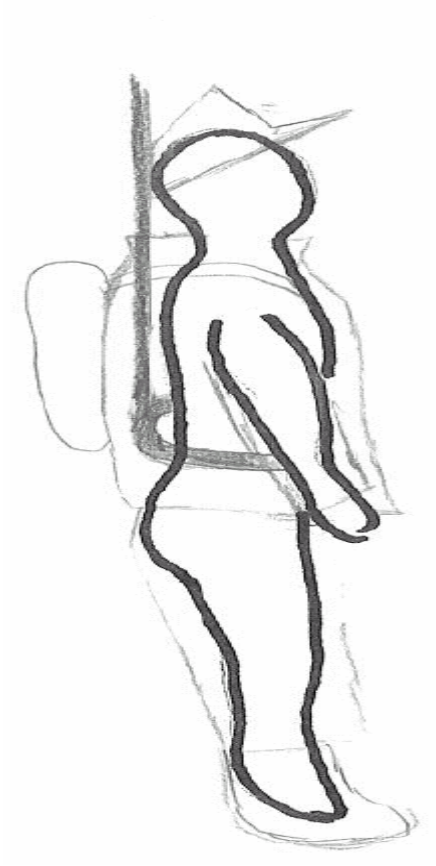

Interior Belt Support (MODEL 4):

For this mechanism, a bar would run vertically down from the track through the collar of the coat and attach directly to the manikin's hip-area. Here, a metal clamp would be used to wrap around the torso and securely hold the manikin in place.

Pros

This design places the support bar directly on the back of the manikin, under the clothing. This will allow for a wide variety of SCBA units to be tested with absolutely no interference from the suspension. The torso clamp will also provide sufficient support for the manikin and all of the testing gear.

Cons

The back support and torso clamp would create many pressure points and interfere with testing results. The location of the vertical support bar would not allow for helmet applications. Machining and the materials involved in this design would be very expensive and time consuming.

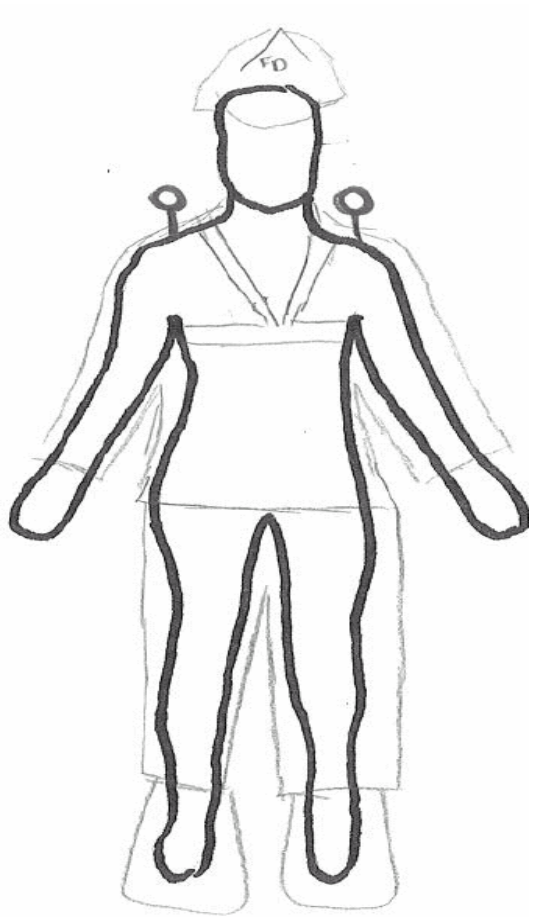

Shoulder Eye Hooks (MODEL 5):

Eye-hooks would be installed on the shoulders of the manikin, and cables would run from the track to hang it from in this design. This design would require modifications to the coat and, possible, the SCBA being tested.

Pros

The machining and installation of this design would be simple and cost affective. SCBA packs and helmets could be tested with minimal interference from suspension components. This design does not cause any unnecessary pressure points.

Cons

The modifications to the manikin, testing gear, and SCBA straps would be time consuming and my affect test results. This design does not provide a support feature to prevent the manikin from swaying during test situations.

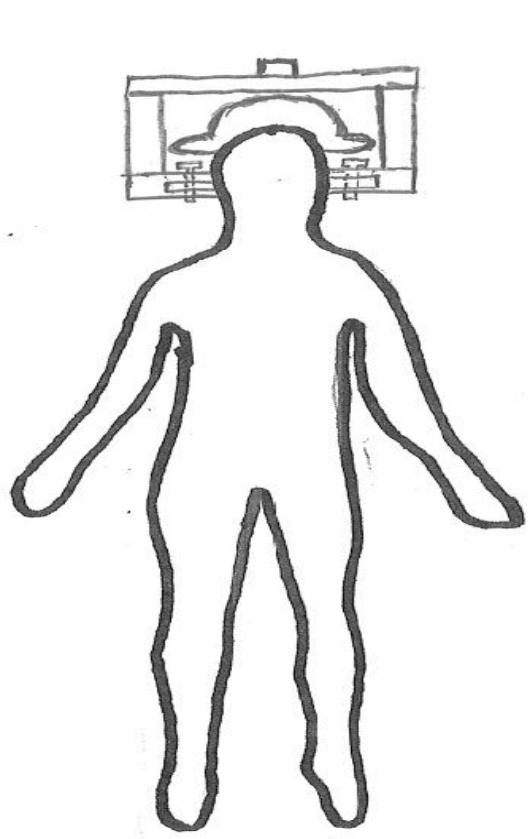

Bolted Hooks (MODEL 6):

Here, the manikin is supported with an expanded square structure holding up the rod in the neck of the manikin, very similar to the first design. Two vertical holes would then be drilled through the rod and would line up with similar wholes in the hooks. A bolt would be used to secure the bolt in place and secure it against lateral movement of the manikin.

Pros

This suspension both prevents sway and supports the manikin, without a back piece. The head unit allows for helmets and SCBA units of varying geometry to be tested. The construction and installation of this unit would be cost affective and simple.

Cons

The bolt and hook portion of this unit would be under great static and dynamic loading, and my not be able to support the manikin and all the gear.

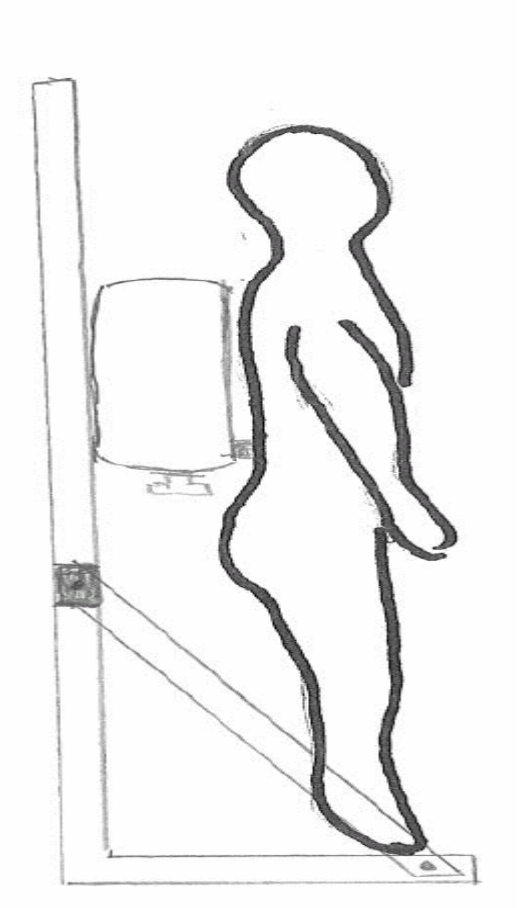

Platform Support (MODEL 7):

For this mechanism, a platform would hang from the ceiling and the manikin would stand in place on it. It appears that the platform may inhibit the fire test by blocking the flames from the manikin.

Pros

This suspension mechanism would allow for minimal interference to occur between the suspension and full ensemble components.

Cons

This design would interfere with the processes involved in ensemble testing. A large amount of materials and manufacturing would be required. Additional components would need to be included in order to assure sufficient support for the manikin and testing gear.

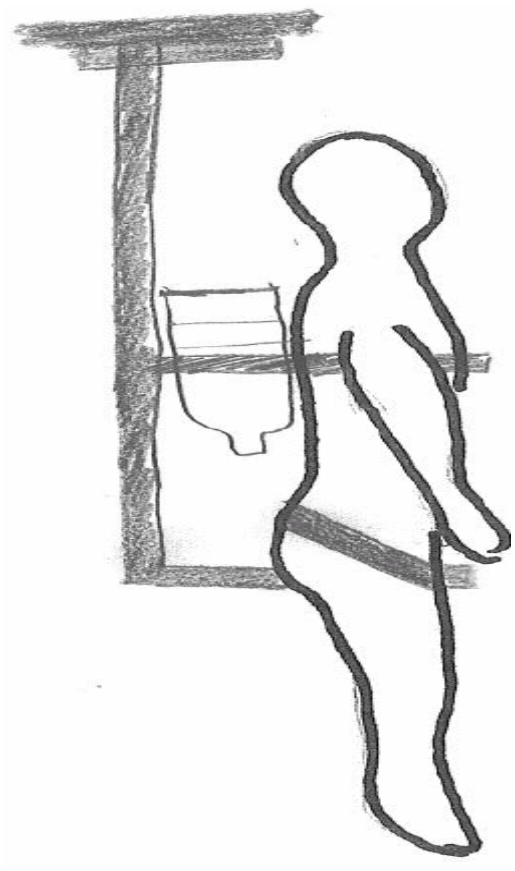

Groin Support (MODEL 8):

A rod would hang from the track, and wrap under the manikin's torso, with belt-like ties holding the manikin in place on the "rack". Another belt-like tie would be necessary across the upper torso to keep the manikin on the structure.

Pros

This model would provide a large amount of support to the manikin while also preventing sway.

Cons

The design of the mechanism causes multiple pressure points on the manikin's back and torso. The vertical rod and seat would interfere greatly with full ensemble components. A large amount of material and time would be required for this project.

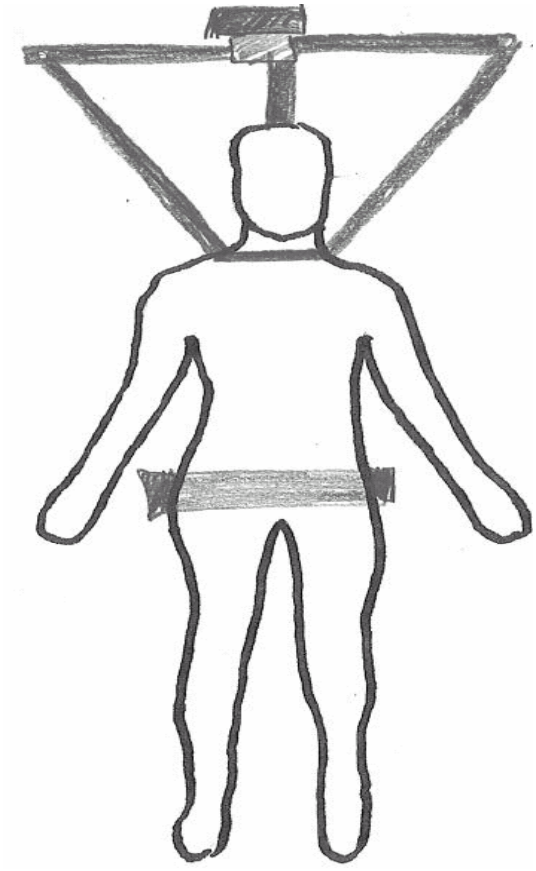

The Noose (MODEL 9):

A cable would hang from the track, and wrap around the outside of the hood on a clothed manikin. It would tighten around the neck and support the manikin in place. Some sort of bar would be needed to keep the manikin in its vertical orientation during movement; however.

Pros

This design is simple and could quickly be manufactured and installed.

Cons

The head of the manikin may not be able to support the load experienced during testing. This design will not affectively prevent the manikin from swaying while in motion.

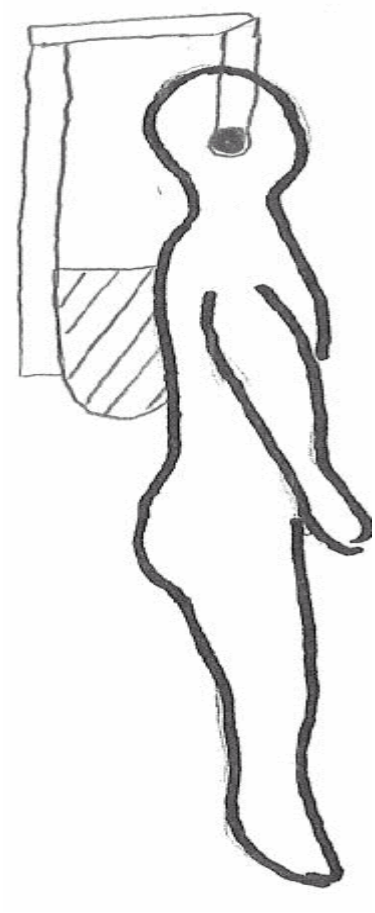

Square Head – Straight Rear Bar (MODEL 10):

This design is a modification of design one where the back rod only reaches down to the back of the SCBA tank. Here, it stabilizes the tank on the manikin, and therefore stabilizing the manikin.

Pros

This design is similar to the current one, with extensions to accommodate for full ensemble testing. Sufficient space would be allowed for both SCBA units and helmet applications. The vertical support will press directly against the SCBA bottle to prevent sway while minimizing pressure points.

Cons

The vertical support bar may not accommodate all SCBA geometries, causing interference during testing.

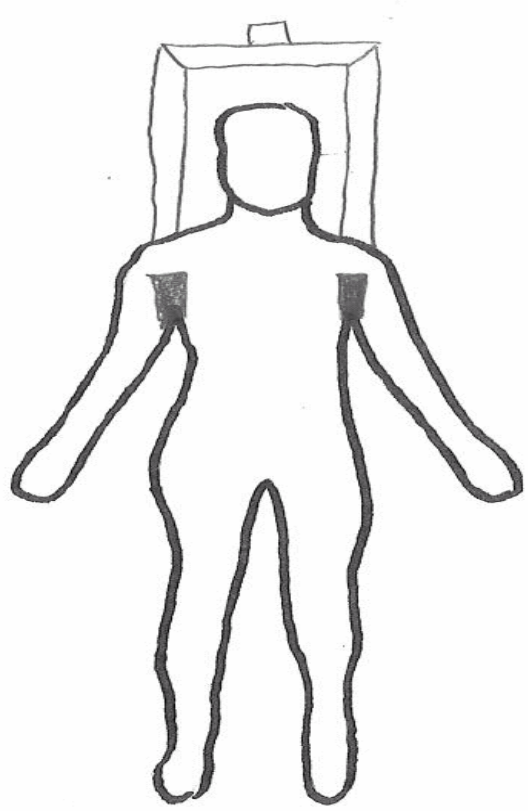

Under Arm Hooks (MODEL 11):
Two large hooks would drop from the track in the ceiling and under the manikin's arms. These larger hooks would both support the manikin vertically, as well as stabilize it during lateral movements.

Pros
The hooks included in this mechanism will allow the back portion of the manikin to be fully exposed, this would allow for testing of SCBA units.

Cons
The shoulders of the manikin may not be able to handle the load experienced during testing. The hooks would likely not be able to prevent sway of the manikin will in motion.

Appendix D: Suspension Calculations

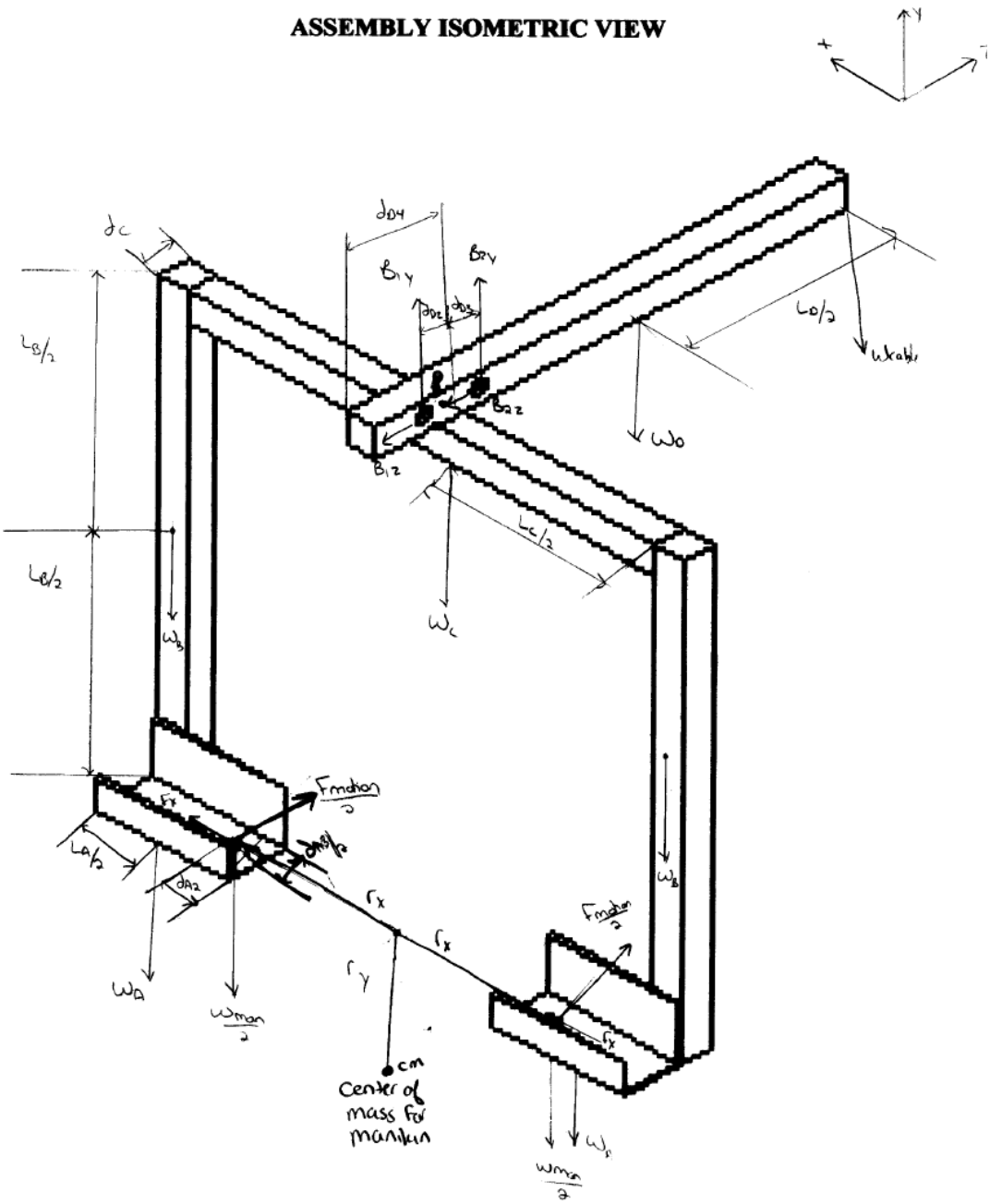

BAR A ISOMETRIC VIEW

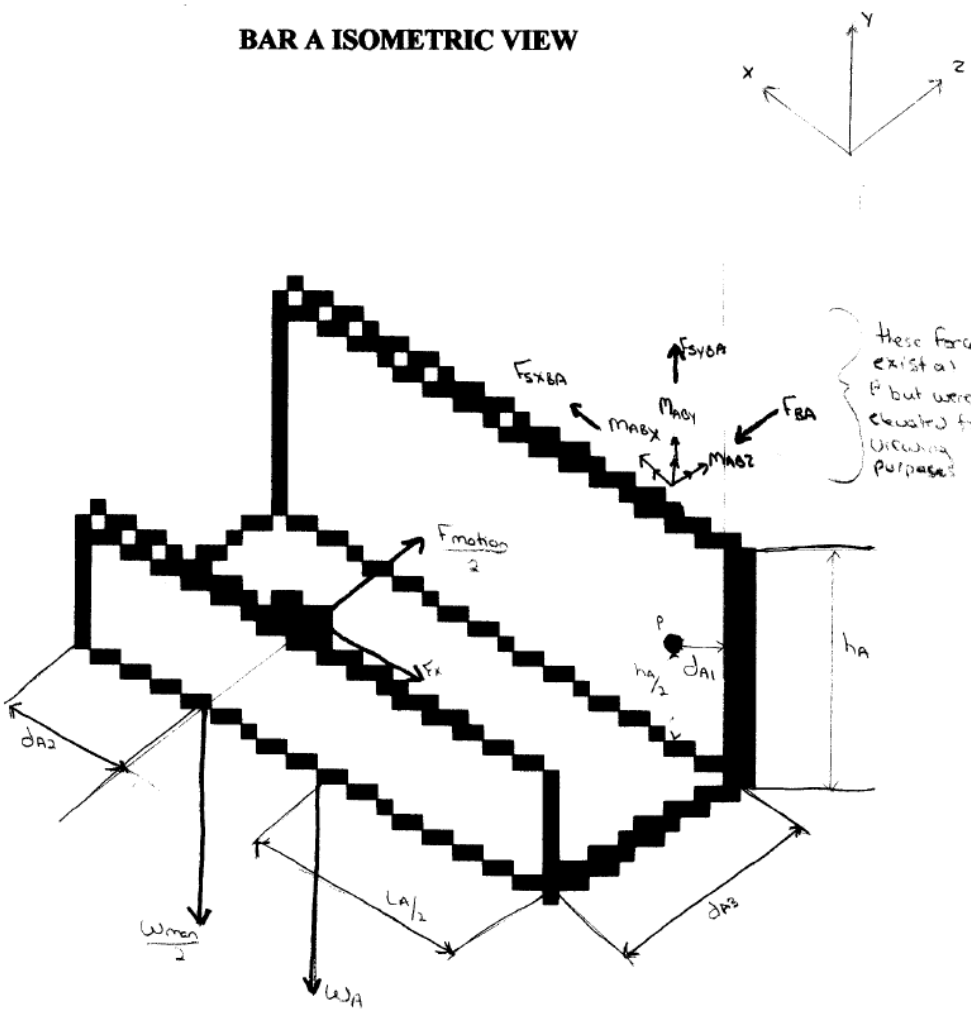

BAR B ISOMETRIC VIEW

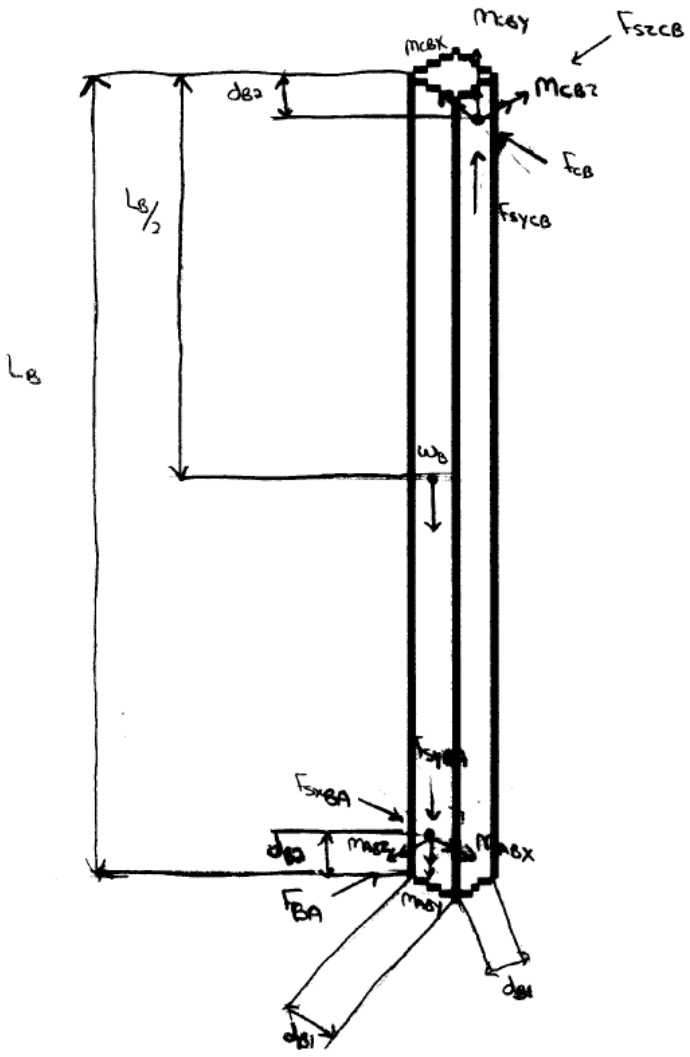

BAR C ISOMETRIC VIEW

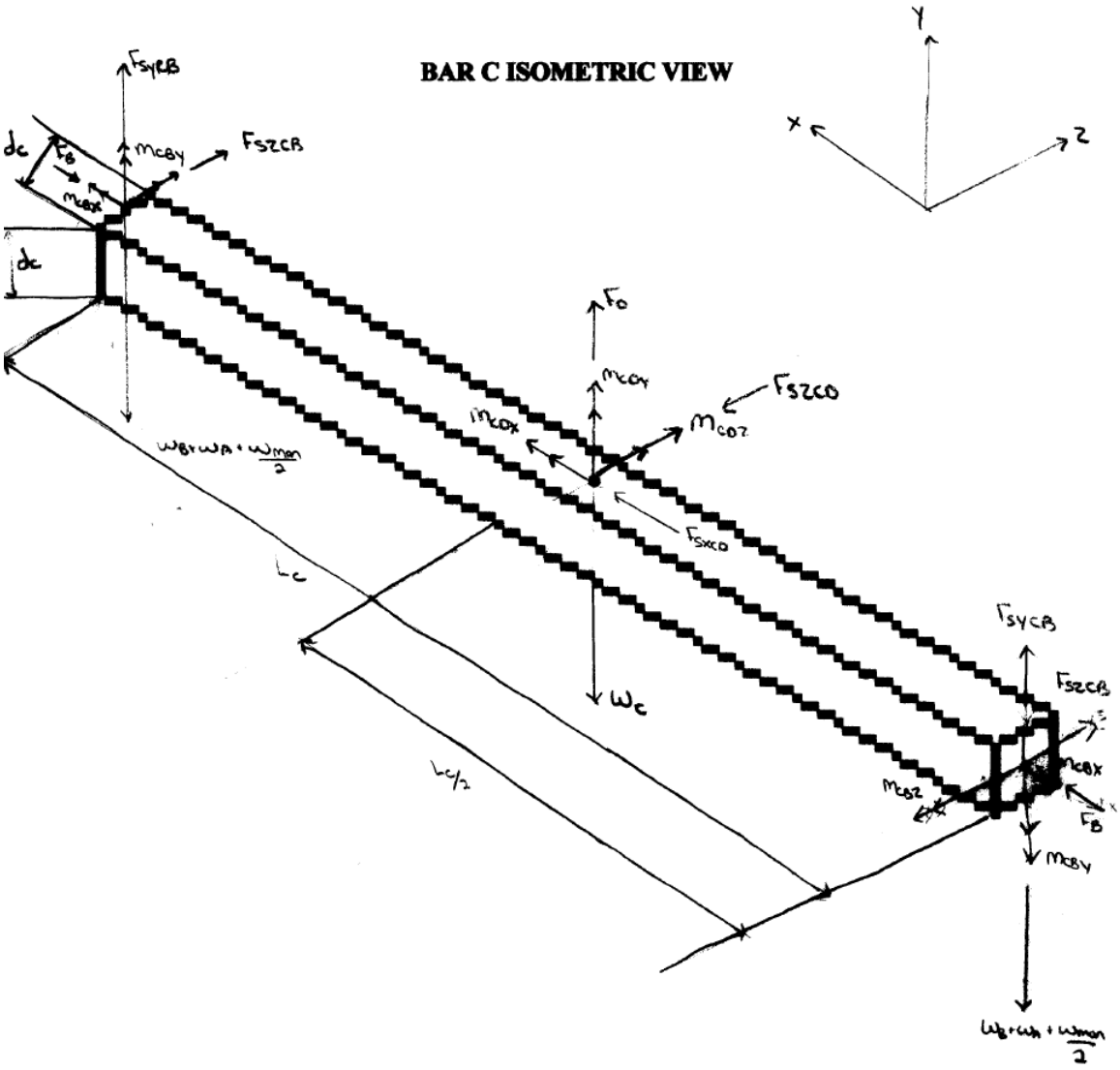

BAR D ISOMETRIC VIEW

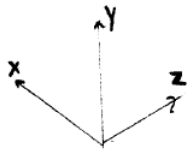

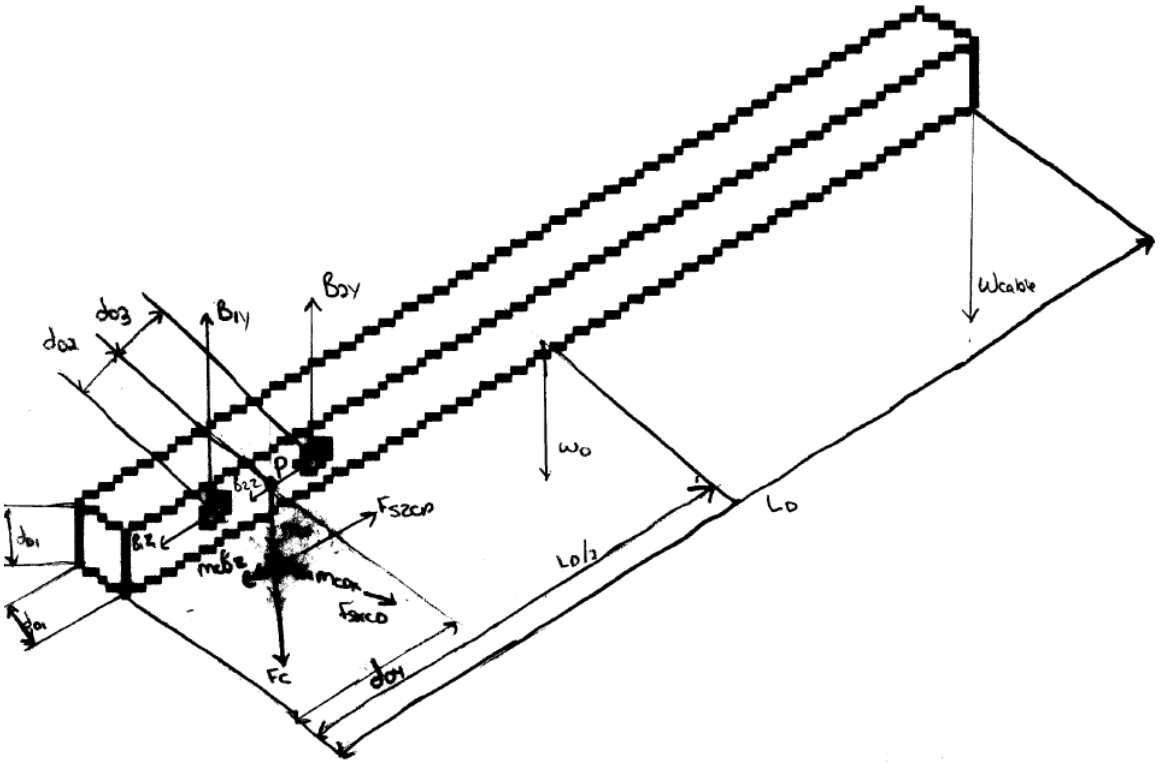

Point P is located at the "z" coordinate shown but is on the under-side of bar D (on xz plane) at $X = d_{D1}/2$

Suspension System Force, Moment, and Stress Calculations

The following Maple program calculates the forces, moments, and stresses acting on the suspension system. This was done prior to building the suspension system in order to ensure that our design could withstand the forces to be applied on it. The stresses on our welds (tau_moment) did not exceed the allowable stress for a steel weld. Please refer to the assembly diagrams for illustration of the terms.

Maple program:

List Known Quantities
First enter the known masses of the manikin and the gear. Then add those together (m_man) for the total weight of the manikin and gear.

```
> m_manikin:=51;
```

$$m\_manikin := 51$$

```
> m_gear:=70;
```

$$m\_gear := 70$$

```
> m_man:=m_manikin+m_gear;
```

$$m\_man := 121$$

```
> m_cable:=15;
```

$$m\_cable := 15$$

Now list the properties of the steel (thickness and density) and other knowns (gravity)

```
> thickness_steel:=(1/8);
```

$$thickness\_steel := \frac{1}{8}$$

```
> density_steel:=0.289;
```

$$density\_steel := .289$$

```
> width_bar_a:=2;
```

$$width\_bar\_a := 2$$

```
> width_bars:=1;
```

$$width\_bars := 1$$

```
> gravity:=32.2;
```

$$gravity := 32.2$$

```
> acc_man:=6.34;
```

$$acc\_man := 6.34$$

> **diameter_bolta:=.25;**

$$diameter\_bolta := .25$$

Weld yield strength in psi using E60XX steel filler material

> **sigma_steel:=50000;**

$$sigma\_steel := 50000$$

List known lengths of the bars.

> **L_a:=4.5;**

$$L\_a := 4.5$$

> **d_a1:=1/2;**

$$d\_a1 := \frac{1}{2}$$

> **d_a2:=1;**

$$d\_a2 := 1$$

> **d_a3:=2;**

$$d\_a3 := 2$$

> **h_a:=2;**

$$h\_a := 2$$

> **L_b:=16;**

$$L\_b := 16$$

> **d_b1:=1;**

$$d\_b1 := 1$$

> **d_b2:=1;**

$$d\_b2 := 1$$

> **L_c:=16;**

$$L\_c := 16$$

> **d_c:=1;**

$$d\_c := 1$$

> **L_d:=16;**

$$L\_d := 16$$

> **d_d1:=1;**

$$d\_d1 := 1$$

> **d_d2:=.9375;**

$$d\_d2 := .9375$$

> **d_d3:=.9375;**

$$d\_d3 := .9375$$

```
> d_d4:=2.5625;
```

$$d\_d4 := 2.5625$$

```
> r_x:=6.5;
```

$$r\_x := 6.5$$

```
> r_y:=32;
```

$$r\_y := 32$$

```
> Length_weld_AB:=1;
```

$$Length\_weld\_AB := 1$$

```
> width_weld_AB:=2;
```

$$width\_weld\_AB := 2$$

```
> Length_welds:=1;
```

$$Length\_welds := 1$$

```
> width_welds:=1;
```

$$width\_welds := 1$$

Calculate the area of steel in a one inch square bar and a 2 inch square bar. (open for calculations)

```
> area_one:=1*1-((3/4)*(3/4));
```

$$area\_one := \frac{7}{16}$$

```
> area_two:=2*2-((14/8)*(14/8));
```

$$area\_two := \frac{15}{16}$$

Calculate the mass of the bars with density x length x area.

```
> mass_bar_a:=density_steel*L_a*(area_two/2);
```

$$mass\_bar\_a := .6096093750$$

```
> mass_bar_b:=density_steel*L_b*area_one;
```

$$mass\_bar\_b := 2.023000000$$

```
> mass_bar_c:=density_steel*L_c*area_one;
```

$$mass\_bar\_c := 2.023000000$$

```
> mass_bar_d:=density_steel*L_d*area_one;
```

$$mass\_bar\_d := 2.023000000$$

```
>mass_all:=m_man+2*mass_bar_a+2*mass_bar_b+mass_bar_c+mass_bar_d+m_cable;
```

$$mass\_all := 145.3112188$$

Calculate the Force due to gravity of these bars.

```
> W_a:=mass_bar_a*gravity;
```
$$W\_a := 19.62942188$$

```
> W_b:=mass_bar_b*gravity;
```
$$W\_b := 65.14060000$$

```
> W_c:=mass_bar_c*gravity;
```
$$W\_c := 65.14060000$$

```
> W_d:=mass_bar_d*gravity;
```
$$W\_d := 65.14060000$$

```
> W_man:=m_man*gravity;
```
$$W\_man := 3896.2$$

```
> W_all:=mass_all*gravity;
```
$$W\_all := 4679.021245$$

```
> W_cable:=m_cable*gravity;
```
$$W\_cable := 483.0$$

Torque caused by the manikin

```
> F_motion:=m_man*acc_man;
```
$$F\_motion := 767.14$$

```
> Tx:=F_motion*r_y;
```
$$Tx := 24548.48$$

```
> Ty:=F_motion*r_x;
```
$$Ty := 4986.410$$

```
> Tz:=W_man*r_x;
```
$$Tz := 25325.30$$

Free Body Diagrams for whole Assembly

```
> B2y:=(-(W_man+2*W_a+2*W_b+W_c)*(d_d2)-W_d*(L_d/2-
d_d4+d_d2)-W_cable*(L_d-d_d4+d_d2))/(-(d_d2+d_d3));
```
$$B2y := 5989.918363$$

```
> B1y:=W_man+2*W_a+2*W_b+W_c+W_d+W_cable-B2y;
```
$$B1y := -1310.897119$$

```
> B1z:=F_motion-B2z;
```
$$B1z := 767.14 - B2z$$

```
> Mpx:=B2y*d_D3-B1y*d_d2+2*W_a*(d_a3+d_c/2)-(W_d*L_d/2-
d_d4)-W_cable*(L_D-d_d4);
```
$$Mpx := 5989.918363\ d\_D3 + 2046.238358 - 483.0\ L\_D$$

```
> M_B1_x:=0;
```
$$M\_B1\_x := 0$$

BAR A (open below for calculations)

Free Body Diagram Calculations for Bar A (the "hook") using a weld area of 1 inch.

```
> F_sy_BA:=W_a+W_man/2;
```
$$F\_sy\_BA := 1967.729422$$

```
> F_BA:=F_motion/2;
```
$$F\_BA := 383.5700000$$

```
> F_sx_BA:=F_x;
```
$$F\_sx\_BA := 0$$

```
> F_x:=0;
```
$$F\_x := 0$$

```
> shear_stress_BA:=F_sy_BA/(area_two);
```
$$shear\_stress\_BA := 2098.911384$$

Moment Calculations for A

```
> M_ABy:=-1*(-F_x*d_a3+F_motion/2*(L_a-d_a2-d_a1));
```
$$M\_ABy := -1150.710000$$

```
> M_ABx:=-1*((-W_man/2)*(-d_a2/2)-(W_a)*(-
d_a3/2)+F_motion/2*(-h_a/2));
```
$$M\_ABx := -610.1094219$$

```
> M_ABz:=-1*(F_x*(-h_a/2)-(W_man/2)*(L_a-d_a2-d_a1)-
W_a*((L_a/2)-d_a1));
```
$$M\_ABz := 5878.651488$$

```
> J_AB:=((Length_weld_AB+width_weld_AB)^3)/6;
```
$$J\_AB := \frac{9}{2}$$

Tau moment is in psi

```
> tau_moment_ABz:=M_ABz*(Length_weld_AB/2)/J_AB;
```
$$tau\_moment\_ABz := 653.1834985$$

```
> tau_moment_ABy:=M_ABy*(Length_weld_AB/2)/J_AB;
```
$$tau\_moment\_ABy := -127.8566666$$

```
> tau_moment_ABx:=M_ABx*(Length_weld_AB/2)/J_AB;
```
$$tau\_moment\_ABx := -67.78993575$$

BAR B (open below for calculations)

Free Body Diagram Calculations on Bar B (one of two vertical bars on either side of manikin's head) using a weld area equal to that of the steel bar end area.

```
> F_sy_CB:=F_sy_BA+W_b;
```
$$F\_sy\_CB := 2032.870022$$

```
> F_sz_CB:=F_BA;
```

$$F\_sz\_CB := 383.5700000$$

```
> F_CB:=F_sx_BA;
```

$$F\_CB := 0$$

```
> F_s_AB:=-F_s_BA;
```

$$F\_s\_AB := -F\_s\_BA$$

```
> shear_stress_CB:=F_sx_CB/area_one;
```

$$shear\_stress\_CB := 4646.560050$$

Moment Calculations for B

```
> M_CBz:=-1*(M_ABz-F_sx_BA*(-(L_b-2*d_b2))-W_b*(-d_b1/2)-
F_sy_BA*(-d_b1/2));
```

$$M\_CBz := -6895.086499$$

```
> M_CBx:=-1*(-F_sy_BA*(-d_b1)-W_b*(-d_b1)+F_BA*(-1*(L_b-
2*d_b2))+M_ABx);
```

$$M\_CBx := 3947.219400$$

```
> M_CBy:=-1*(F_BA*(-d_b1/2)-F_sx_BA*(-d_b1/2)+M_ABy);
```

$$M\_CBy := 1342.495000$$

```
> J_BC:=((Length_welds+width_welds)^3)/6;
```

$$J\_BC := \frac{4}{3}$$

```
> tau_momBCz:=M_CBz*(Length_welds/2)/J_BC;
```

$$tau\_momBCz := -2585.657437$$

```
> tau_momBCy:=M_CBy*(Length_welds/2)/J_BC;
```

$$tau\_momBCy := 503.4356250$$

```
> tau_momBCx:=M_CBx*(Length_welds/2)/J_BC;
```

$$tau\_momBCx := 1480.207275$$

BAR C(open below for calculations)

Free Body Diagram Static Calculations on Bar C (connects the 2 B bars).

```
> F_D:=W_c+2*(W_b+W_a)+W_man-2*F_sy_CB;
```

$$F\_D := 65.140600$$

```
> normal_stress_DC:=F_D/area_one;
```

$$normal\_stress\_DC := 148.8928000$$

```
> F_sx_CD:=F_B-F_B;
```

$$F\_sx\_CD := 0$$

```
> F_sz_CD:=F_sz_CB-F_sz_CB;
```

$$F\_sz\_CD := 0$$

Moment Calculations for C, in the middle of bar C (on weld to D)

```
> M_CD_z:=0;
```

$$M\_CD\_z := 0$$

```
> M_CD_y:=0;
```

$$M\_CD\_y := 0$$

```
> M_CD_x:=2*F_sz_CB*(-d_c/2);
```

$$M\_CD\_x := -383.5700000$$

```
> J_CD:=((Length_welds+width_welds)^3)/6;
```

$$J\_CD := \frac{4}{3}$$

```
> tau_momCDz:=M_cz*(Length_welds/2)/J_CD;
```

$$tau\_momCDz := 0$$

```
> tau_momCDy:=M_cy*(Length_welds/2)/J_CD;
```

$$tau\_momCDy := 0$$

```
> tau_momCDx:=M_cx*(Length_welds/2)/J_CD;
```

$$tau\_momCDx := 6472.743750$$

BAR D (open below for calculations)

Free Body Diagram Static Calculations for Bar D (connects C to the track mechanism and the back bar).

```
> B1y:=W_d+W_cable-B2y+(2*W_a)+(2*W_b)+W_c+W_man;
```

$$B1y := -1310.897119$$

Moment Calculations on D

```
> M_px:=(B1y*(-d_d2)-W_d*((L_d/2)-d_d4)-W_cable*(L_d-
d_d4)+B2y*d_d3+M_cx)*(-1);
>
```

$$M\_px := -17260.65000$$

```
> M_pz:=0;
```

$$M\_pz := 0$$

```
> M_py:=0;
```

$$M\_py := 0$$

```
> J_DC:=((Length_welds+width_welds)^3)/6;
```

$$J\_DC := \frac{4}{3}$$

```
> tau_momDC:=M_px*(Length_welds/2)/J_DC;
```

$$tau\_momDC := -6472.743750$$

Appendix E: Preliminary Tests

Traditional United States Fire Fighter Ensemble

The first set of fire fighter protective clothing that was tested involved used, previously donated clothing from local fire departments. The ensemble included a brown Janesville jacket with orange trim, a set of yellow bunker pants, the used self-contained breathing apparatus that was donated by the Massachusetts Fire Academy, and the hood that was previously on the manikin. The manikin was also dressed with a pair of rubber boots to prevent damage to the feet. The ensemble can be seen in Figure 0-1 on the manikin in preparation for testing.

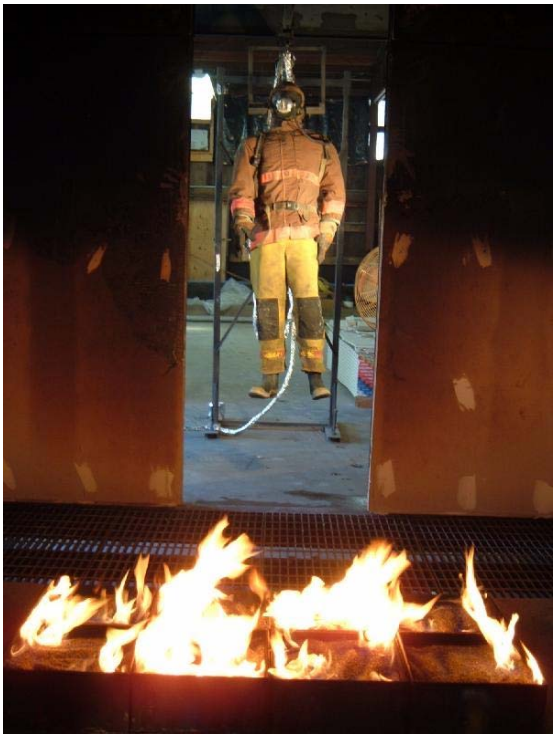

Figure 0-1: Traditional Fire Fighter Ensemble

As this was the first ensemble tested, the test protocol was created impromptu in order to observe what would happen to the manikin during various exposures. The first run conducted involved bringing the manikin to the doorway plane and holding it there

for 30 seconds. Estimated skin burns were calculated for the five most severely heated sensors, and the burn damage parameter can be seen in Figure 0-2. The graph below demonstrates the burn parameter calculated by Henrique's Burn Integral. It is based on the temperature change of the basal layer of the skin. This temperature was calculated by using the finite difference method to calculate the temperature of the skin at various depths. The burn parameter value representing the threshold for second degree burns is 1.0. As is demonstrated by the graph, the worst burn damage during this scenario is nearly five orders of magnitude less than this value.

Figure 0-2: Traditional Ensemble Run #1 Burn Damage

The next trial included four runs at 0.922 m/s. During the first of these four runs, the data collected demonstrated one fast increase and decrease in heat flux, around the time that the manikin was in the center of the room. The energy absorbed by all the sensors during this run can be seen in Figure 0-3. Notice the large jump in energy around 15 seconds. It is interesting that multiple sensors reacted during this time period, but the large increase could not be explained.

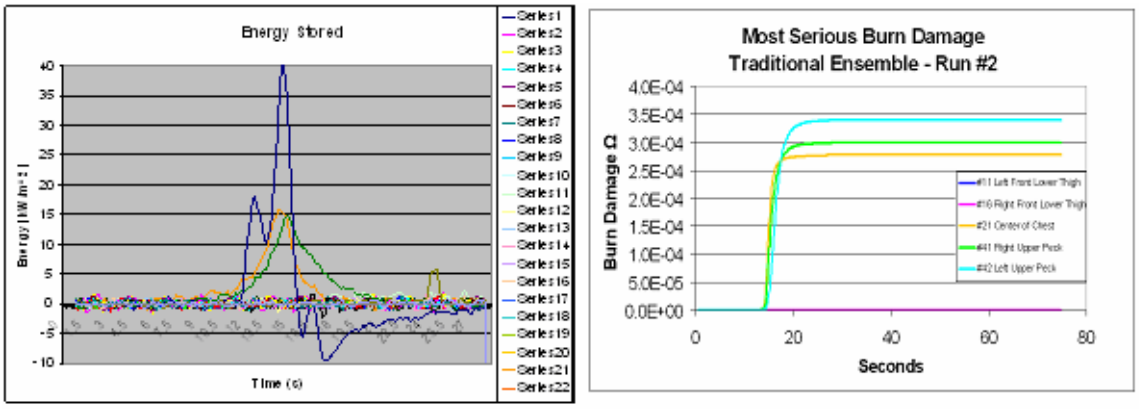

Figure 0-3: Traditional Ensemble Energy Stored

This large increase prompted the repeat runs at this speed. The stored energy and burn damage parameters for the third run can be seen in Figure 0-4. The energy stored chart demonstrates the amount of energy (in kW/m^2) that was stored in the copper disk. This is the value that is used as the incident heat flux on the sensor, as convective losses can be ignored while the manikin is clothed. The burn damage parameter for this run was approximately one thousandth of the values collected during the previous run. The parameters for the worst sensors were similar to run number three, and can be seen in Figure 0-5.

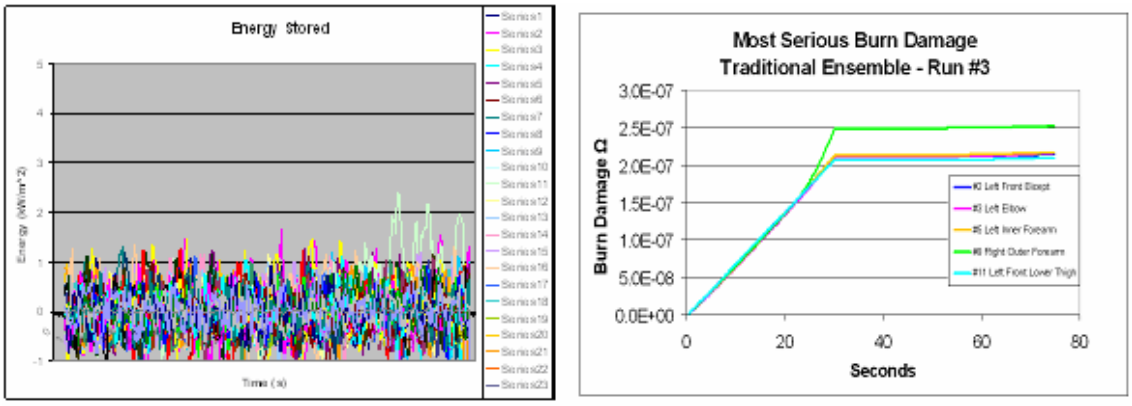

Figure 0-4: Traditional Ensemble Run #3 Stored Energy and Burn Damage

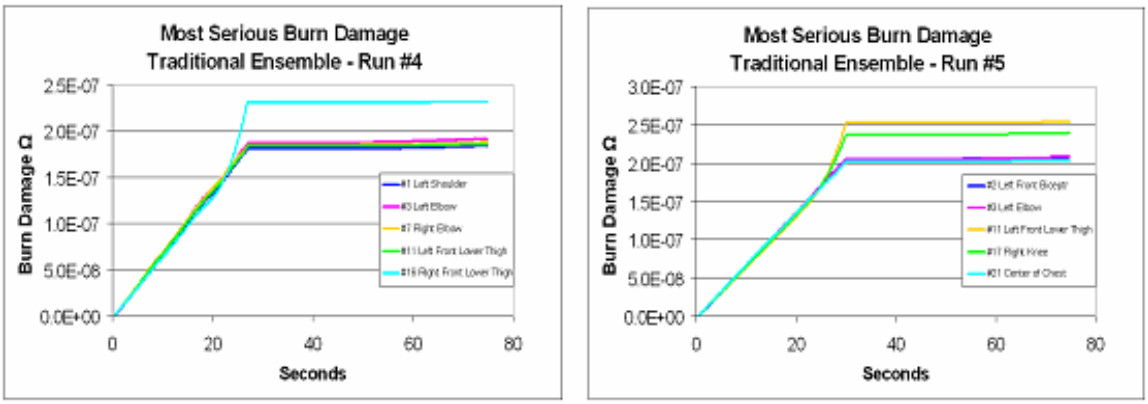

Figure 0-5: Traditional Ensemble Runs #4 and 5 Burn Damage

Runs six and seven were conducted at speeds of 0.89 m/s and 0.58 m/s. The results from these runs were similar to those of the previous three evolutions, and can be seen in Figure 0-6. Run seven had one outlier that was very high, sensor eleven which appears to record large heat fluxes often, and may be an erroneous sensor. Also, note that the burn damage for run seven is slightly more intense than run six, which would be expected due to the longer exposure time.

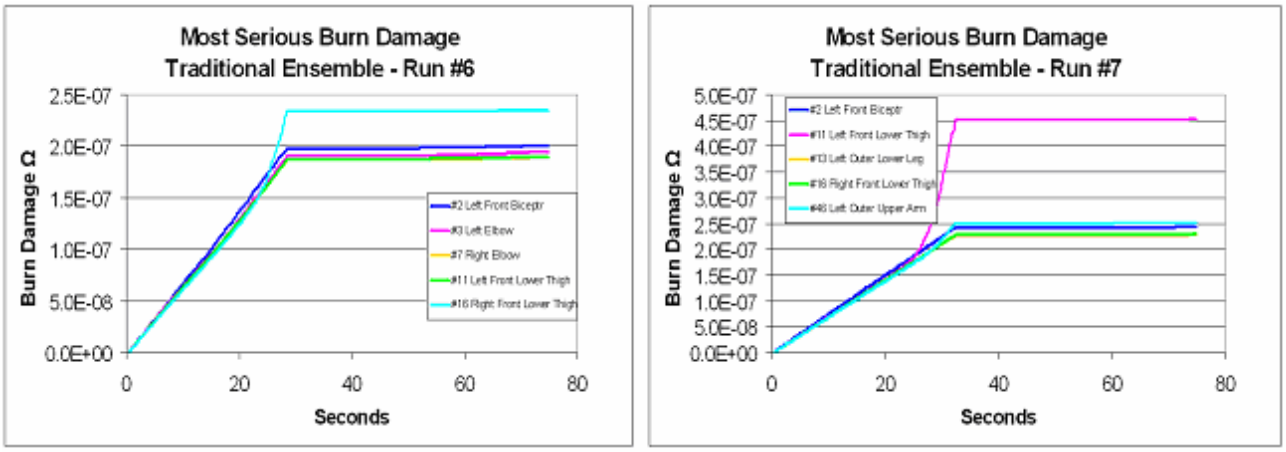

Figure 0-6: Traditional Ensemble Runs #6 and 7 Burn Damage

The final run that was conducted with this ensemble involved running the manikin through the room at a speed of 0.36 m/s. This run exposed the manikin to the largest amount of energy and would, in theory, have the highest burn damage parameters. The calculated burn damage parameters for the most severe five sensors are shown in Figure

0-7. As you can see, the most impacted sensor recorded a burn parameter of over 0.00001, just under two orders of magnitude higher than the next fastest run.

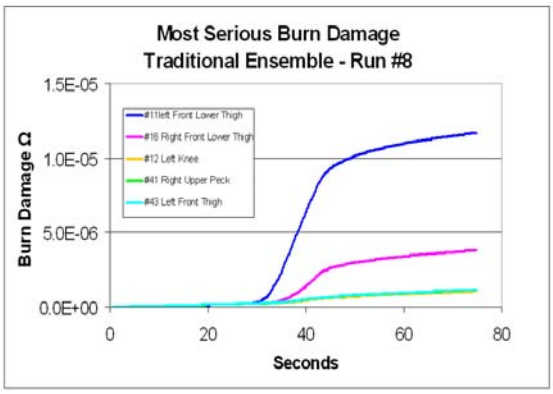

Figure 0-7: Traditional Ensemble Run #8 Burn Damage

Figure 0-8 is a photograph of the Traditional Ensemble's pants, boots, and SCBA after testing was completed. As you can see, there was some slight melting of the bottom of the boots and the reflective trim. Other than that, the majority of the char on the clothing and any other damage was attributed to past wear and tear since these garments were previously used in fire fighting operations.

Figure 0-8: Traditional Ensemble After Testing was Complete

From the results of these runs, it is shown that the burn damage does get progressively worse as the speed decreases, but it also shows that the doorway run has higher burns than the equivalent test with the manikin traversing the fire.

United States Navy Ensemble

Next, tests were conducted using the United States Navy's newest single piece suit in conjunction with a new Scott Health and Safety SCBA, rubber boots, and United States Navy helmet and gloves (Figure 0-9). As this was the second set of tests conducted in the facility, some changes were made to the test protocol as deemed appropriate from the results of the Traditional Ensemble. For this test, seven runs were conducted. The first, similar to the previous set of tests was a doorway test. The next two tests were conducted at the faster speed setting, followed by two slower tests. Then, the doorway test was repeated. The evaluation was completed by conducting a test at the slowest traversal speed setting.

Figure 0-9: United States Navy Ensemble on Manikin

The first run in this test was conducted with the 1.5 MW fire and the manikin being held in the doorway for 30 seconds. Figure 0-10 demonstrates the burn damage

associated with the doorway test. Note that the threshold for a second-degree burn is 1.0, approximately three orders of magnitude greater than the most severe sensor.

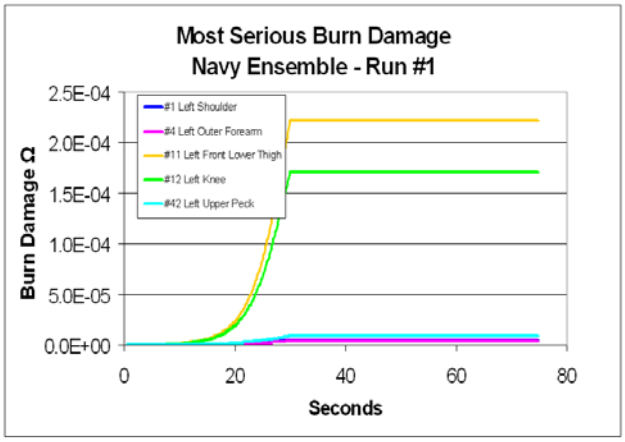

Figure 0-10: Navy Ensemble Run #1 Burn Damage

The next two runs involved traversing the manikin through the room at a speed of 0.922 m/s. Between each run, the manikin's sensors were cooled to near-ambient conditions. Figure 0-11 demonstrates similar results from the two test runs. It is apparent that the burns acquired during the latter test are slightly ($3*10^8$) greater than those from the previous; however this difference is so small that it could be caused by any number of variables. It is not a sufficient difference to conclude that the suit has deteriorated at all, and the calculated values are still well below that of the burn parameter thresholds.

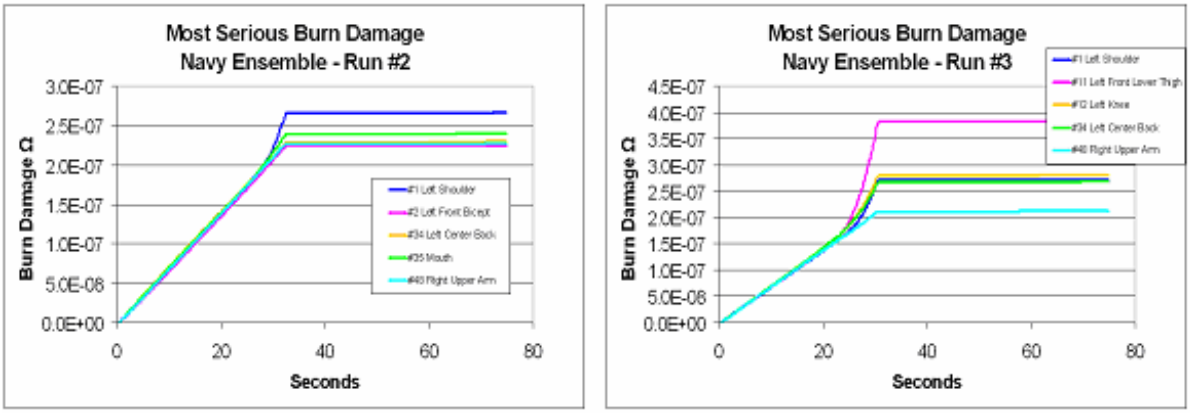

Figure 0-11: Navy Ensemble Runs #2 and 3 Burn Damage

The next two runs were completed with a manikin speed of 0.58 m/s. The burn data for these test runs can be seen in Figure 0-12. There is slightly more deviation between these two results, but because the values are of such small magnitude, the deviation does not indicate any real differences between the tests. Once again, the values are well below the 1.0 threshold value.

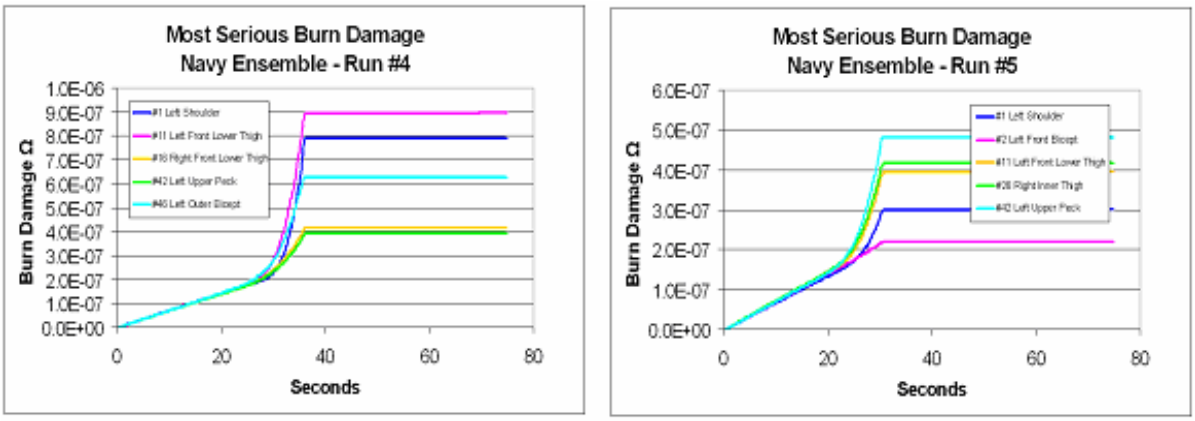

Figure 0-12: Navy Ensemble Runs #4 and 5 Burn Damage

The sixth run was conducted with the manikin held in the doorway plane. Figure 0-13 demonstrates the sensors with the largest heat impact compared to the burn damage incurred on the first evolution of the test. There appears to be a larger difference between these two data sets, at least for the sensors with the highest exposure. It is also important to note that the same sensors are at the most elevated values; however, the magnitudes differ by four times for the left front lower thigh, and nearly two times for the left knee. This may be an indication of material deterioration. However, once again it is probably not a cause for concern since the values are still multiple orders of magnitude lower than the burn thresholds.

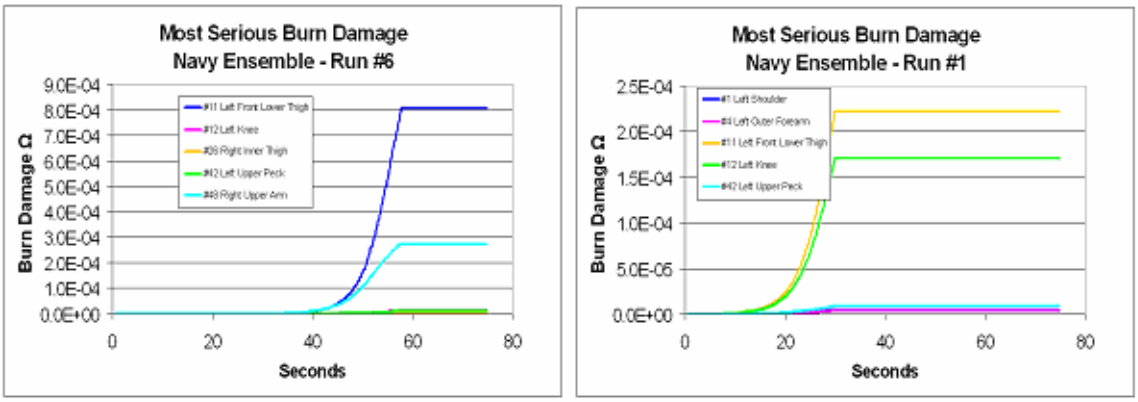

Figure 0-13 Navy Ensemble Run #6 Compared to Run #1

The final evolution of the test involved the manikin traversing the fire at a rate of 0.36 m/s. During this test, it would be expected that the values would be lower than all the other tests; however, in the end there appears to be less burn damage incurred (See Figure 0-14). The reasoning for this effect is unknown at this time.

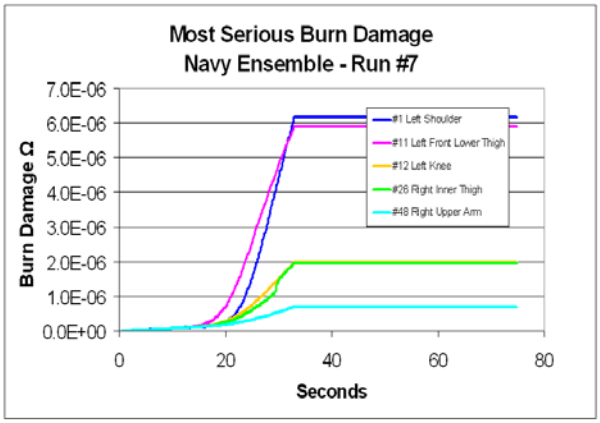

Figure 0-14: Navy Ensemble Run #7 Burn Damage

All these values were expected, based on the performance of the traditional fire ensemble. It was noted that the doorway incident flux caused higher burn damage than the traversing manikin's exposed energy; however, this result remains unexplained.

After each test was completed, the gear was inspected for any deformities. Figure 0-15 demonstrates two such deformities that occurred after the initial doorway test. In the picture to the left in Figure 0-15, the neck fabric was changed from black to a red tinge due to the extreme heat. Also, within the circle to the right is the beginning of the

degradation of the helmet face shield. This was not considered an ensemble failure because the face shield is a secondary source of protection designed to protect the SCBA face piece, not the wearer directly.

Figure 0-15: Navy Ensemble Neck Discoloration and Helmet Deformity after Initial Doorway Test

Australian Structural Ensemble 1

The third ensemble tested in the laboratory was the Country Fire Authority of Victoria, Australia's most recent ensemble that was donated as an update to the other Australian ensemble tested. This ensemble was comprised of a matching set of green colored three layer coat and pants. Also tested on this ensemble were the boots gloves and helmet that arrived with the original ensemble and the Scott Health and Safety SCBA unit. The hood used for this test was the original manikin hood. The procedure for this test was identical to the procedure used during the United States Navy Ensemble test.

The first run, with the manikin held in the doorway plane for 30 s, recorded the following burn parameters seen in Figure 0-16. Note that the majority of the top five sensors are located on the left and right thighs. Once again, these values are multiple orders of magnitude less than the second degree burn threshold of 1.0.

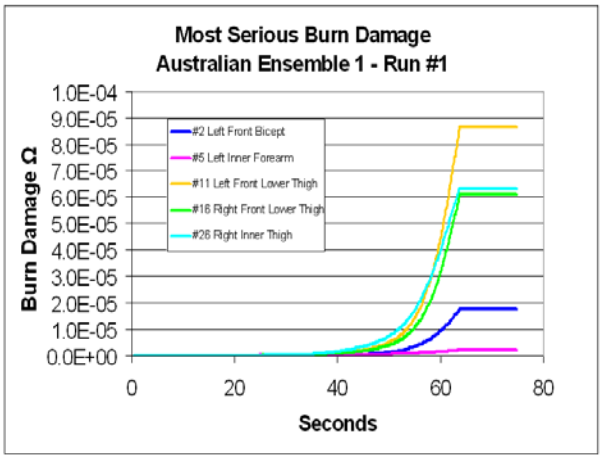

Figure 0-16: Australian Ensemble 1 Run #1 Burn Damage

The next two runs recorded data recorded in Figure 0-17. As can be seen, the burn damage for the majority of the sensors remained constant over the two runs indicating initially that this ensemble has strong resistance to deterioration due to incident heat flux and fire.

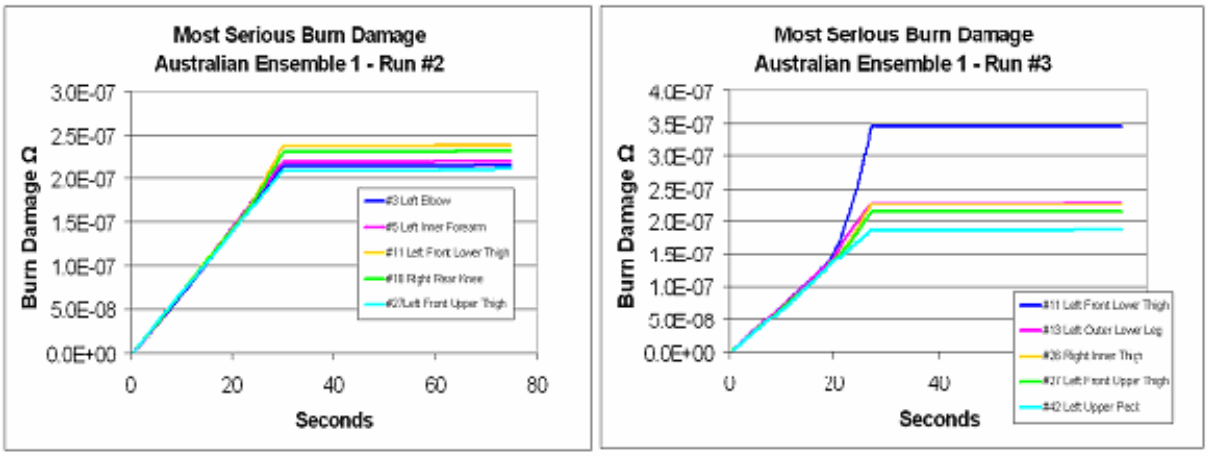

Figure 0-17: Australian Ensemble 1 Runs #2 and 3 Burn Damage

The next two runs were completed at the slower speed setting, and resulted in the following data collection (see Figure 0-18). There is a higher distribution among the highest impacted sensors in the latter run; however, of the five top sensors, the average burn parameter is approximately the same. Once again, this goes to show the repeatability of the test. All values are still well below the 1.0 threshold for second-degree burns.

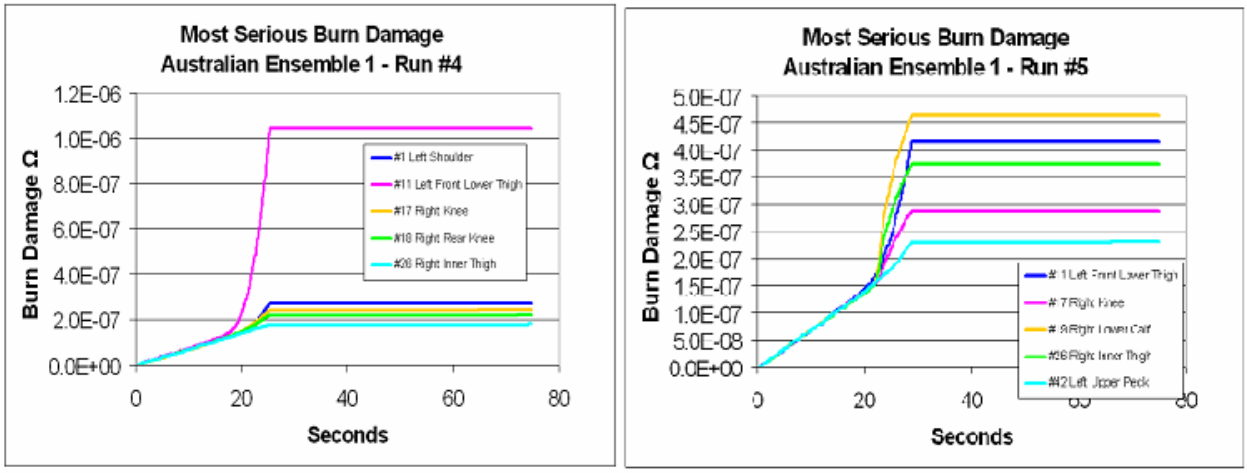

Figure 0-18: Australian Ensemble 1 Runs #4 and 5 Burn Damage

The sixth run is the repeat of the doorway test. The burn parameter values for the top five sensors are graphed in Figure 0-19. As you can see, the burn damage parameter is about an order of magnitude higher in this evolution than it was in the previous two runs. This is consistent with the previous data collected on the Traditional Ensemble and the Navy Ensemble. The difference lies in the decreased burn parameter as compared to the initial doorway test by over an order of magnitude. The only explanation for this type of difference must be uncontrollable variable changes such as wind conditions, or an unknown restriction on the fire.

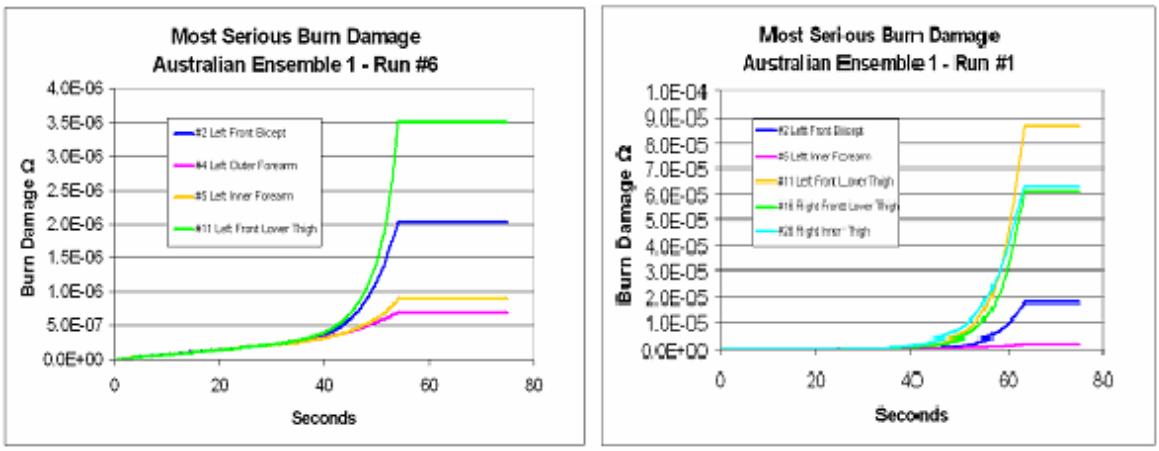

Figure 0-19: Australian Ensemble Run #6 Burn Damage Compared to Run #1

Finally, the last test run that was conducted on Australian Ensemble 1 was the slowest-speed setting run. The burn parameters calculated from the data collected during this run can be seen in Figure 0-20. These values are more characteristic of what one would expect for such a slow traversal of the fire, although the values are still slightly lower than the initial doorway test. Other than that data, these values are the highest burn parameters for this ensemble. The threshold for second-degree burns is still four-thousand times the highest burn potential that could be obtained from these ensembles.

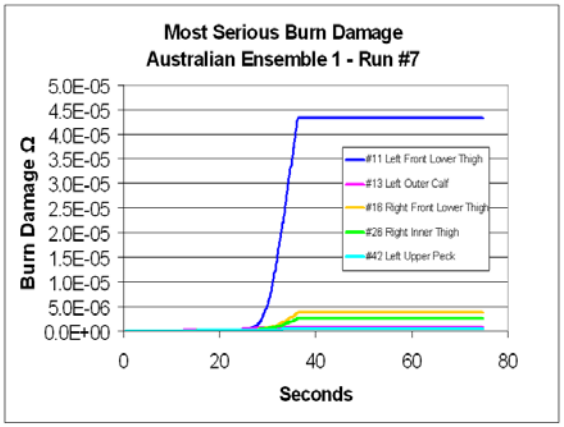

Figure 0-20: Australian Ensemble 1 Run# 7 Burn Damage

Figure 0-21: Australian Ensemble 1 Post-Test

After the tests were completed on the first Australian Ensemble, the legs appeared singed, but still intact. Also, the reflective trim on the ensemble had melted in a few places. The helmet was fully intact, but slightly sooty, and the gloves appeared to turn brownish-black in the fire, but were still intact. The boots had very slight melting on the soles, but seemed to hold up very well during the testing. After these tests, there was no evidence of any life threatening equipment failures.